Integrating mechanical behaviour of non-ideal features in prismatic polyhedra based tolerance analysis

Carlos Andrés Restrepo García

THÈSE PRÉSENTÉE

POUR OBTENIR LE GRADE DE

DOCTEUR

DE L'UNIVERSITÉ DE BORDEAUX

ÉCOLE DOCTORALE DES SCIENCES PHYSIQUES ET DE L'INGÉNIEUR

SPÉCIALITÉ: MÉCANIQUE ET INGÉNIERIE

Par **Carlos Andrés RESTREPO GARCÍA**

INTÉGRATION DU COMPORTEMENT MÉCANIQUE DES ÉLÉMENTS NON IDÉAUX EN ANALYSE DE TOLÉRANCES PAR DES POLYÈDRES PRISMATIQUES

INTEGRATING MECHANICAL BEHAVIOR OF NON-IDEAL FEATURES IN PRISMATIC POLYHEDRA BASED TOLERANCE ANALYSIS

Sous la direction de : **Denis TEISSANDIER**
Et la co-direction de : **Nabil ANWER**

Soutenue le 12 novembre 2024

Membres du jury :

M. LINARES, Jean-Marc	Professeur des Universités	Aix-Marseille Université	Président du Jury
M. DANTAN, Jean-Yves	Professeur des Universités	ENSAM Metz	Rapporteur
M. SCHLEICH, Benjamin	Professor Doktoringenieur Habilitation	Technische Universitat Darmstadt	Rapporteur
M. TEISSANDIER, Denis	Professeur des Universités	Université de Bordeaux	Directeur de thèse
M. ANWER, Nabil	Professeur des Universités	Université Paris Saclay	Co-directeur de thèse
M. LEDOUX, Yann	Maître des conférences (HDR)	Université de Bordeaux	Invité
M. DELOS, Vincent	Ingénieur de Recherche (HDR)	Université de Bordeaux	Invité

A mi amada familia, por su compañía en la distancia.
A mis queridos amigos, porque son luz en mi vida.

Acknowledgements

First, I want to acknowledge the distinguished members of the jury of this thesis, Pr. Dantan, Schleich and Linares for the valuable comments on this manuscript, as well as for the interesting discussion during my dissertation.

To my supervising team, this was really a joint work. Thanks for your dedication to this project, your support meant a lot, specially during the tough first months. Thanks, Denis, for your patience and generosity, with those qualities, and many others, you have shown me the type of professor I would like to resemble. Your sense of duty and justice inspire me. I very much enjoyed our conversations and I deeply appreciate your hard-working pushy attitude while keeping always a respectful and kind consideration for others. Thanks, Nabil, for your mind-blowing diligence, the moments we spent together allowed me to admire your sharp intelligence and your eloquent and straightforward discourse. I felt grateful in repeated occasions for the insights the came after our discussions. Thanks, Yann, for pushing me so I could exceed myself. I really enjoyed your sense of humor, it warmed our discussions. Thanks, Vincent, for your support all along this project. It was nice to have somebody to come to when I had questions related to informatics, or even just to have interesting discussions about culture and languages. Thanks, Laurent, for your contibutions and time dedicated to this project.

Thanks to all my friends, I am filled with gratitude every time I think the amazing group of people I got to share with in Bordeaux and in Paris. Thanks for the Thursdays evenings around a beer or a coffee. Thanks for always wanting to keep in touch even when we were apart. Thanks for the birthday presents and the parties and trips we share. All of those made these years really worth it.

Thanks to my lulito for being my emotional support and the reason I am excited about the future. We know what we had to go through during this period in our lives, and we came our stronger and feeling more connected that ever. Love you.

Y gracias a mis padres y mis hermanos por siempre estar presentes en mi vida, por celebrarme y acompañarme en las decisiones que tomo. Ustedes son el núcleo, el lugar al que vuelvo a recargarme. Esto es por ustedes. Los amo.

Résumé

Les architectures des produits sont aujourd'hui plus complexes en raison du besoin du marché de produits personnalisés et optimisés, des progrès technologiques dans les machines de fabrication et les dispositifs d'inspection, et de l'utilisation des données dans la modélisation et la simulation des pièces. Les progrès des capacités de fabrication et de mesure en réponse aux besoins du marché ne se traduisent pas immédiatement par des modèles plus précis. En fait, la prise en compte des défauts géométriques et de la variabilité dans le processus de conception est encore très limitée, cela est dû en partie aux limites des modèles mathématiques et de leurs hypothèses subjacentes. La première contribution de ce travail porte sur la caractérisation de la variabilité géométrique en tolérancement. La première partie de ce travail concerne les modèles de représentation de forme et plus particulièrement l'adoption du paradigme de forme du modèle de peau (skin model) dans le contexte de gestion des tolérances en utilisant la méthode polyédrique. Les instances du modèle de peau sont plus représentatives des pièces réelles individuelles que les modèles CAO traditionnels. Pour simuler un comportement plus réaliste des assemblages, la deuxième partie présente une nouvelle approche de simulation de contact rigide à l'aide de polyèdres. L'approche intègre les conditions aux limites de charge qui permettent le contact entre les éléments potentiellement en contact en enrichissant la définition d'un opérande polyèdre prismatique pour la simulation du contact. Avec cette approche enrichie, pour un mécanisme donné, une quantification objective de l'impact de la non-prise en compte des défauts de forme peut être calculée en fonction d'une condition de chargement. Une approche pour la simulation des contacts en prenant en compte les déformations locales des pièces potentiellement en contact a également été développée pour la méthode polyédrique en tolérancement. Enfin, les algorithmes de simulation de contact et le générateur de instances de formes réalistes ont été implémentés dans un logiciel open source dans un environnement CAO.

Abstract

The architectures of new products are more complex nowadays due to the need of the market for customized and optimized products, the technological advancements in manufacturing machines and inspection devices, and the extensive use of data in the product's modeling and simulation. The evolution of manufacturing processes and the advanced measurement capabilities in response to the market needs do not translate immediately into more accurate products. Actually, there is a limited consideration of geometric defects and variability in the design process, this is partially due to the limitations of the mathematical models and their underlying hypothesis. The first contribution of this work is on the characterization of the geometric variability in tolerancing. The first part of this work concerns the shape representation models and specifically the adoption of the skin model shapes paradigm in the tolerance management context using the polyhedral-based method. The skin model instances are more representative of individual real parts than the traditional CAD models. To simulate more realistic behavior of assemblies, the second part presents a novel approach for simulation of rigid contact using polyhedra is presented. The approach integrates the load boundary conditions that allow the contact between matting features by enriching the definition of a prismatic polyhedron operand for contact simulation. With this enriched approach an objective quantification of the impact of disregarding form defects for a given mechanism can be computed given a loading condition. An approach for simulating features potentially in contact by taking into account the local deformations of potentially contacting parts has also been developed for the polyhedral method in tolerancing. Finally, the algorithms for the contact simulation and the generator of realistic shape representatives were implemented in an open source CAD compatible software.

Table of contents

List of figures

List of tables

Introduction

a Preamble

There is a pressing demand for cheaper, lighter, faster, and in general better performing mechanical systems. These systems have benefited from the advent of the data era improving their performance by including all sorts of prediction and analysis methods at different stages of the design process. Even with the aid of sophisticated algorithms and the high computer power available nowadays the contact management of features with geometric deviations constitutes a challenge in many engineering activities.

The management of the deviations on mechanical assemblies concerns all the stages of the product development and their neglect can seriously impact the conformance of the parts and the general functioning of the system. At the early stage of the product development, the consideration of geometric deviations is mainly performed at the tolerancing stage. Most of the mathematical models in tolerancing rely on the hypothesis of ideal features and rigid bodies which may result insufficient to guarantee specific assembly functions. Furthermore, the inclusion of the loading conditions in the simulation process is often done to check the respect of certain mechanical conditions but less to check the functional conditions which can also result in misleading results.

Tolerance analysis evaluates the respect of a condition that guarantees the prescribed functioning of a mechanical system given a set of tolerances. In order to evaluate the respect of a functional condition, the accumulation of tolerances or displacements has to be computed. Generally, this evaluation is carried out either by worst-case analysis or statistical approaches. When the worst-case analysis is used, the models are dealing mostly with the accumulation of tolerances; on the other hand, when statistical approaches are used, the tolerancing models deal with the accumulation of displacements from each part in an contact chain.

b Context and objectives

This research work is the result of a partnership between two research laboratories: I2M at university of Bordeaux, and LURPA laboratory at ENS Paris-Saclay university. The project was born to respond to the need of a more comprehensive approach to the geometric tolerancing.

The project has both research and development objectives. From a research point of view the objectives are:

- **At the part level**: characterize and represent the deviations of non-ideal features at different stages of the design process. That implies the implementation of methodology capable of guaranteeing the prediction and/or observation of geometric deviation on parts.
- **At the assembly level**: simulate the realistic behavior of assemblies by incorporating external loading conditions and local deformation to assess the functional conditions of assemblies.

From a development perspective the main objective is to develop freely downloadable software that can be integrated into existing CAD solutions. The tools will be developed both for individual parts and for assemblies and they will be shared in open source format.

c Research questions

The research questions concern the two main aspects of the work presented here. The first one is the integration of the non-ideal features in the polyhedral-based tolerance analysis. At a first stage, we are dealing with a representation problem. In this aspect, the questions are: what is a shape in the skin model and how can it be represented? How to incorporate form deviations into the polyhedral-based approach at the feature level? For the integration of the non-ideal features, it is important to ask: when could these deviated features be part of the tolerancing process using prismatic polyhedra? Also, what is the impact of neglecting these deviations in the tolerancing process?

The second aspect concerns the contact modeling. One of the main challenges is to integrate the mechanical behavior of the assembly, for that it is necessary to be able to include the notion of force, or its effects, in the tolerancing context. The questions that raises is what is a force in the dual space were a polyhedron exists? and how could it be represented?. Going further in the incorporation of the mechanical behavior, one could ask if it is feasible to describe the local deformation phenomena by exploiting the deviation space were the contact polyhedron lies? Also, would the incorporation of the mechanical behavior allow to explicitly model contact configurations difficult to model otherwise like unilateral fixed contacts?

In order to try to answer these questions, the following thesis structure is proposed.

d Structure of the thesis

Chapter 1 presents a comprehensive review of the tolerancing models and deviation methods for modeling non-ideal features. The main contribution of this chapter is the generalized polyhedral-based framework for the inclusion of form defects and simulation of contact with or without local deformation for tolerance analysis.

In chapter 2, an enriched definition of the polyhedral-based approach including the external loading is presented. The inclusion of the external loading as additional restrictions allows us to find the contact between ideal or non-ideal features in the rigid regime. The enrichment of the polyhedral-based approach allowed us to: i) model the sliding behavior of contacts when parallel contacts consume the mobilities of the system; ii) objectively quantify the impact of disregarding the form defects in the contact simulation.

In Chapter 3, a local deformation model based on erosion is presented. This chapter presents a further enrichment of the polyhedral-approach to model the local deformation. We showed that the plastic deformation of the nodes in the geometry can be translated in the deviation space as displacement of the contact restrictions, and that by exploiting the duality between the wrench and the twist we can include the dynamics of the deformation process from the deviation space.

Chapter 4 presents the incorporation of the generalized polyhedral-based framework in an open source CAT. The architecture and the data modeling of the system is presented to show how the integration of the general polyhedral-based framework in an open source CAT is achieved. With this chapter, authors hope to contribute to the development of comprehensive open source CAT tools for tolerance analysis.

The last part presents a brief synthesis of the work presented here along with the conclusions and perspectives of this thesis.

Chapter 1

Representation and simulation of digital mechanisms with geometric deviations

Digital representations of mechanical systems supports all the stages of the design, manufacturing and quality control of product development process. From CAD to manufacturing systems, passing through the simulation of the mechanical behavior of systems under different conditions and the verification of geometrical constraints, the digital representation of systems is omnipresent in mechanical engineering. When it comes to the representation of mechanisms, the basic idea is to start from the nominal definition of individual parts and then move up to sub-assemblies and to the general assembly. Many of the subsequent analysis are performed on the basis of such ideal model.

The ideal representation of mechanisms is adapted to model systems in which the geometric requirements are loose, or when the stresses in the system are not significantly impacted by small geometric deviations. Generally, as the complexity of a system increases, its geometric requirements become tighter, and its functionality more sensible to geometric deviations and form defects. The challenge of ensuring the functionality of complex systems relies on how accurately we are describing and representing the digital parts and their interactions. One way to address this challenge is by improving the numerical models that describe the complex interactions among components of a system under different environmental and loading conditions. A more compelling way to look at this problem is by considering the impact of geometric deviations in the mechanical behavior of a system.

The study presented in [91] showed that the misalignment between the hole-to-hole assemblies can lead up to 36 % decrease in the ultimate load and a 14 % decrease in the Key Fatigue indicator. This study showed experimentally that clearance and misalignment

between holes and bolts has direct impact in the mechanical strength of an assembly. Another study [74] assessed the impact of the surface integrity of the drilled holes on the fatigue behavior of an aluminum alloy assembly, but it did not include the effects of the small defects in the holes. The idea in these approaches is to quantify the impact of geometrical deviations in the mechanical strength of a system.

Another way to look at the problem is to consider the geometric specifications and deviations to assess their impact in a functional condition of a mechanism. The functional conditions can implicate intricate contact interactions among the components of an assembly, and they assure that the aggregation and compensation of geometrical deviations respect a certain requirement. This way of approaching the challenge of complex system interactions is studied in the field of tolerance analysis [46], and it is the vision adopted in this work. This chapter is organized as follows: Section I presents a review of the existing tolerancing models and their limitations; Section II explains at the lower level how shapes are described and represented, and it introduces the concept of Skin Model and Skin Model Shapes used in this work; Section IV presents the different data modeling languages for tolerancing; Section V presents the digital system used in tolerancing; and Section II presents a framework to model mechanisms with different detailed levels

I Tolerancing models

In tolerance management, the dimensional and geometric specification process is largely dependent on the knowledge of people, but it is being supported every time more by digital systems. Capture and transfer of the meaning of a specification from the text to a computer was, and still is, not an easy task. On the one hand, an unambiguous language for the specification of tolerances is needed. Standards for the specification of geometrical and tolerance in design have contributed to that purpose. The two main standards are the ISO GPS [68] and the ASME Y14.5 [19]. On the other hand, the correct interpretation of the specifications by a computer needs a formalization and an explicit representation of the semantics. In data models, the semantics is often informal and adapted only to a specific application. The ontologies formally specify agreed logical theories by defining domain rules that approximate the intended meaning of a conceptualization [130], and they can be generally used by any application that satisfies the domain rules.

A part of the tolerancing activities consist on setting limits and constraints to the dimensions and geometry of features, parts and assemblies. In this task two types of data

are needed: the geometry and topology of the parts and assemblies, and the tolerance data consisting basically of relationships between features of the same parts, between features of different parts, and functional conditions. The representation of the tolerance information needs two basic components: the tolerance model, referred to sometimes as interpretation model or mathematical model [96], it aims at interpreting the semantics of the tolerance information; and the data model that defines the tolerance data objects and their relationships.

The tolerance models aim at interpreting the information coming from the specifications. They are used from early design stages because they are the core of the tolerance analysis process that is part of the tolerance synthesis and optimization processes as it can be seen in Fig.1.1. The three main activities in tolerance management are: tolerance specification, in which the types of tolerances are defined; tolerance allocation that consist in assigning values to the previously defined tolerance specifications; and tolerance analysis, in which the tolerances are stacked-up to evaluate if the system is compliant with some functional requirements [34]. The data needed to carry out the tolerance management activities should be collected from early design stages. The client requirements need to be translated into technical ones, and from those geometric requirements are then extracted. In practice, all the data is not available and the translation of the requirements relies on subjective interpretations of people.

Tolerance synthesis and tolerance cost optimization make use of tolerance analysis in an iterative way. In the first, the results from tolerance specification, allocation and analysis are considered simultaneously in a synthesis step [39]. In the second, in most cases, the idea is to minimize the manufacturing cost by assuring the fulfillment of the functional requirements [61].

The models used in tolerance analysis can be understood from different perspectives. In the literature, the categories that arises the most frequently are: the type of method (parametric, sets of constraints), analysis type (worst case, statistical), dimensionality (1D, 2D, 3D), tolerance type (dimensional, geometric, form); and less frequently: tolerance zone interaction (representation of the interaction among several tolerances on one feature) and datum precedence [126, 8, 94, 34].

The authors in [90] proposed to classify the mathemathical methods that capture tolerance zones in offset, parametric space, algebraic, homogeneous transformation and user-defined

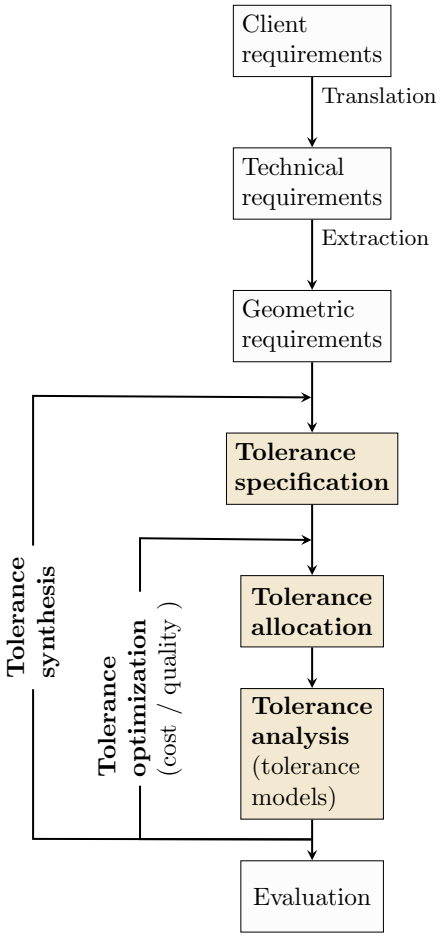

Fig. 1.1 Activities in tolerance management

offset zones methods.

a Parametric models in tolerance analysis

The conventional ± method for dimensional tolerancing consisted in setting a value to the upper and lower bounds of a dimension. The tolerance charts method [53], widely used in the industry, was based in this idea, and although consistent with the standards, it was limited to one-dimensional cases for both worst case and statistical analysis. The idea with the parametric methods for tolerance analysis was to use them easily in CAD/CAE/CAM environments, that is why sometimes they are referred to as models retrofitted for CAD [8].

Leaving the idea of dimensional tolerancing behind, one of the precursors on the implementation of parametric approaches by zones was Requicha [101] with his offset solid

model. Requicha used the Minkowski sum to construct the parametric offset zones for MMC (Maximal Material Condition) and LMC (Least Material Condition) solids [109]. Authors in [90] address various issues concerning this method, including the impossibility to study the tolerance zone interactions as specified in the standards.

The variational solid modeling appeared as a class of the offset modeling. The idea is to create variational objects from the nominal object that are interchangeable in an assembly and are functionally equivalent [112]. The variational model was born as a more wide concept of "applying variations to a computer model of a part or assembly of parts" [60]. It basically involved the idea of creating transformed instances of the nominal to account for different model variations.

Another parametric method commonly found in the literature is the vectorial tolerancing model. It describes a surface by its location, orientation, form and size [137]. The principle of degrees of freedom (DoF) serves at defining the location and orientation parameters of a surface. The authors in [83] described in a formal way the tolerance information of this method using EXPRESS (modeling language developed by STEP). The vectorial tolerancing model does not consider the dependencies between the limits of translation and rotation parameters, so several iterations are needed to conclude on a specific functional condition [17].

The Direct Linearization method (DLM) is a generalization of the vector loops method to include small kinematics adjustments [51]. It uses implicit relationships instead of explicit ones drawn from the assembly kinematic constraints and solved using Taylor's series expansion. The kinematic constraints can be of assembly or manufacture variables and they can be solved through worst-case or statistical analysis. This approach is suitable for computer automation and easy CAD integration.

The TTRS model (Technologically and Topologically Related Surfaces) [40] establishes that any part can be modeled through binary associations of surfaces forming a tree. Each one of the elementary surfaces belongs to a class that is characterized by its degrees of invariance and represented by *Minimum Geometric Datum Elements* (MGDE) with which the variations in a tolerance zone can be modeled. Researches that use TTRS consider the tolerances with the aid of tensors or screws along with some intrinsic parameters**??**. The interactions of orientation, location and form are not modeled. In [8], a review and

Model	Tolerancing type	Analysis	Dimension	Advantages	Disadvantages	Ref
Tolerance charts	Dimensional	Worst-case and statistical	1D	Easy to implement; intuitively	Only 1D dimensional tolerances	[53, 8]
Offset solids	Dimensional and geometric	Worst-case	3D	CAD compatible;	It is not able to deal with form tolerances; Not ISO compliant	[101]
Variational	Dimensional and geometric	Worst-case and statistical	3D	Stack-up functions involving networks	No tolerance zone interaction; Not ISO compliant	[30, 60]
Vector loops	Dimensional and geometric	Worst-case and statistical	3D	Form tolerances; Stack-up functions	No tolerance zone interaction; Not ISO compliant; Needs explicit function to describe relationships	[83, 137]
Direct Linearization	Dimensional and geometric	Worst-case and statistical	3D	No explicit functions needed; Convenient for CAD integration	No tolerance zone interaction	[51]
TTRS	Dimensional and geometric	Worst-case and statistical	3D	The tree structure is easy to implement in CAD; Systematic way to ensure that datums are consistent.	Interactions of orientation, location and form not modeled	[40, 11, 8]

Table 1.1 Parametric models in tolerance analysis

comparison of Tolerance-Maps, Deviation Domain and TTRS was done.

In his thesis work, Dumas [41] used the Small Displacement Torsor (SDT) [29] to model the parameters of a mechanism and he used Monte Carlo simulation coupled to an optimization technique to conduct tolerance analysis. Goka [55] used the SDT to model behavior of fixed, sliding and floating contacts with form defects and used the same resolution methods (FORM method) to evaluate the functional requirements.

In Table 1.1, the list of parametric methods is shown naming the main advantages and disadvantages. It is clear that the parametric methods evolved rapidly to work not only with

dimensional tolerances, but also with geometric ones. Parametric approaches are in general better suited for CAD integration since in many cases the objects are created as transformed copies of the nominal geometry, or they use explicit or implicit functions to describe the geometric variations. One of the main disadvantages when using these approaches is the impossibility of evaluating simultaneously the dimensional and rotational limits requiring more than one simulation to assess the respect of a functional condition.

b Methods based on sets of constraints

The approaches based on sets of constraints consider simultaneously all the admissible displacements of a feature inside a zone by representing them in an spatial way [17]. There are differences in the mathematical spaces in which the different methods work, and in the way the deviations are expressed.

In the T-maps approach [36], authors follow a barycentric coordinate formulation to get areal coordinates. The areal coordinates are used to describe a volume of points that represents all the possible variations of a feature in a tolerance zone. The T-maps has the advatage that the parallel configuration in assemblies are modeled through Mikonwski sums, allowing a linear relationship between the tolerancing and the respect of a functional condition, however, this is only possible in iso-static assemblies [82].

In the deviation domain model [54], the features and the allowed displacements from each point are described using the small displacement torsor (SDT), and then represented in a deviation domain. The deviations are represented in a configuration space that characterizes the small rotations and translations of a feature in is tolerance zone or the clearance between two mating features. The inequalities obtained using this method can sometimes not be linear, specially for non axi-symmetric cases, which makes it difficult to compute the Minkowski sum to obtained the stack up tolerances.

The polytope and polyhedral-based approaches share the representation of the bounded displacements, and the basic idea behind them is very similar to the one presented in the approach by domains. Again, a polytope can represent all the possible displacements of a feature in a zone [135, 17], and it can be: a) geometric, if the specification is between features belonging to the same part; b) of contact, if the specification is between features of different parts; or c) functional if it regards features involved in a functional condition [64]. The polytope lies in the subspace of the bounded displacements of the features and

it is obtained trough the intersection of a finite set of half-spaces written at each point of discretization of a feature. The prismatic polyhedral-based approach takes into account the degrees of invariance of a surface, or the degrees of freedom of a contact, and models them as the sum of some straight lines perpendicular to a polytope that represents the bounded displacements [16].

Model	**Tolerancing type**	**Analysis**	**Dimension**	**Advantages**	**Disadvantages**	**Ref**
T-Maps	Dimensional and geometric	Worst-case and statistical	3D	Compliant with standards; material conditions modeled; variations in size, form and orientation	No algorithm to obtain the sensitivity and percent contribution of tolerance; Difficulty to deal with over-constraint assemblies;No multiple stack up chains	[36, 8, 82]
Deviation domains	Dimensional and geometric	Worst-case and statistical	3D	Interaction of orientation, form and location; material conditions	Complex calculation of Minkowski sum for non linear inequalities	[54, 8, 82]
Polytopes	Dimensional and geometric	Worst-case and statistical	3D	Form tolerances; Stack-up functions; Tolerance zone interactions; over-constraint mechanisms	Added complexity in unilateral contact cases; Not kinematics explained.	[135, 17, 64]
Polyhedral-based	Dimensional and geometric	Worst-case and statistical	3D	Kinematic analysis explained; stack-up functions; Fast computation of operands	Difficult to implement in CAD; Added complexity in unilateral contact cases	[38]

Table 1.2 Methods based on set of constraints for tolerance analysis

Polytopes have been used in a multiphysical approach to include the thermomechanical specifications of two turbine architectures as shown in [93]. The polytope method can be used in both worst-case or statistical analysis, and it is suited, as the other methods based on set of constraints, for modeling overconstraint systems. In [57], the authors used this method to describe the assembly behavior of a flange with five pins considering the form defects.

The polyhedral-based approach in tolerancing improves the polytope method by describing not only the geometric and contact restrictions, but also the degrees of freedom of parts in contact. The authors in [38] showed that by using polyhedra, the complexity of the resulting operands and the computation time are significantly reduced, and it is fairly easy to describe the kinematics of a complex system using an approach based on this method.

Table 1.2 shows a synthesis of the presented literature, it shows the main advantages and disadvantages of each one of the methods. The methods based on set of constraints work at the feature-level (generally at the surface level) and then transfer the geometric deviations to the whole system. It is then important to understand how shapes are described and represented.

The parametric and set of constraints based models can be used to conduct worst-case and statistical tolerance analysis. It is often the case that the statistical analysis is used when the variation management is carried out by accumulating the displacements of each part. While worst-case is used when dealing with the tolerances stack-up. The main drawback from the models presented above is that often the form deviations are neglected when considering the individual parts. Sometimes, it is due to a impossibility to include them with used models (as it is often the case with basic parametric models). More often, it is because considering form deviations is complex and computational expensive.

The next section presents the models for the description and representation of shapes, and it discusses the concept of shape and its incorporation into the tolerance management process.

II Geometrical description and representation of shapes

A shape is generally understood as being a two or higher dimensional object constituted of points, lines, curves and/or surfaces. When we think of a shape we think of an object with a defined contour that occupies a space. Geometric topologists have constructed a theory of shape in which they study the properties of spaces and the family of maps from one space to another [27]. They use both levels of information: the geometric information for the characterization of specific instances of shapes, and the topological properties to abstract the invariant characteristics of the same.

Shape, as said by Requicha [103], has different levels of abstraction: the physical, the mathematical and the representation universe. It is important to separate the actual physical shape from its mathematical description and its digital representation. A digital shape is defined by Biasotti [24] as: "any multi-dimensional media that is primarily characterized by form or spatial extent in a space of two, three or higher dimension". From Kendall [70] we have that a shape is what is left after we have filtered out the contributions coming from translations, rotations and scaling.

Ever since the advent of computers, geometry and topology research on shape has been the object of study in many fields like Computer-Aided Design (CAD), computer vision and graphics, Computer Tomography (CT) scans, tolerance analysis, among others. When it comes to solid modelling, authors in [103, 110] worked on the representational issues in three-dimensional solid geometry and contributed to the characterization of what they called r-sets (regular sets), that are subsets of the three-dimensional Euclidean space that are bounded, closed, regular and semi-analytic. They also contributed to the definition of a representation scheme as a relation from a modeling space (M) to a representation space (R).

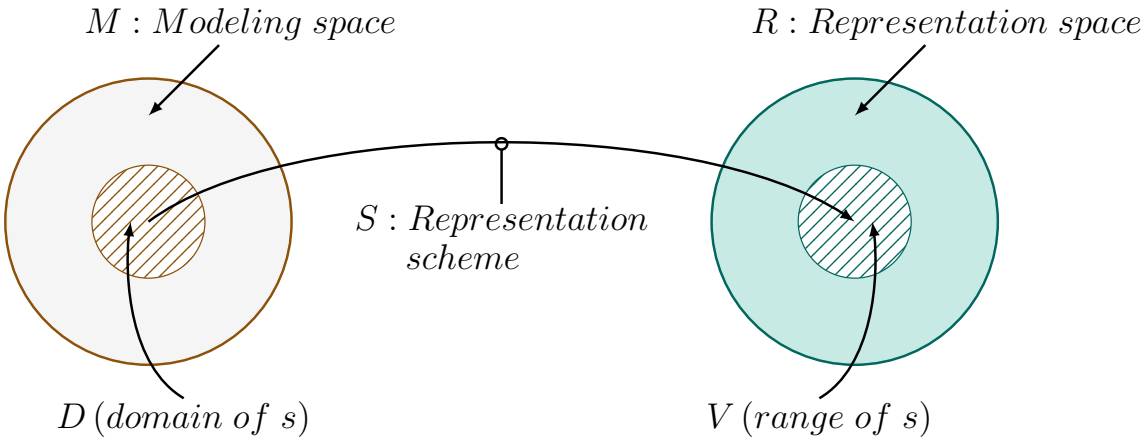

Fig. 1.2 Representation scheme adapted from [103]

In fig.1.2, we can see the domain and range of a representation scheme as defined by [103]. There are two spaces: a modeling space (M) whose elements are r-sets, and a representation space (R) that is a space of syntactically correct representations constructed by a grammar. The semantics of a representation is achieved by associating a geometric entity from M to a syntactically correct representation from R. A subset D from M is the domain of the representation scheme S, and the range of D under S is a subset V from the modeling

space.

An important distinction between representation and description of a shape has been made in the literature. In [87], the authors understands an object representation as "having enough information from which to reconstruct (an approximation to) the object, while a description only contains enough information to identify an object as a member of some class of objects"

In mechanical design, solid modeling is the basis of almost any other activity performed during the different design phases. Many activities rely on the explicit or implicit information designers can get from the digital models. The information that can be extracted from these models is largely dependent on the type of representation scheme used in the CAD software. The most common types of representation schemes used for solid modeling in mechanical design are the constructive and cell complex type. From the first, the Constructive Solid Geometry (CSG) is the most known and used. It is based on Boolean operations in geometric primitives to construct more complex ones. Almost every CAD software is based on a kernel that uses this representation, although today it coexists with other type of representations like the B-rep. The B-rep can be categorized as a cell complex representation [143]. It represents a solid by elements that bound its volume. In the core of this representation is the distinction between the topological and geometric information.

When it comes to the discrete representation of shapes, the mesh-based scheme is the most used in several engineering applications, especially for mechanical calculation, manufacturing and metrology. The polygonal mesh-based representations are based on points, edges and polygonal facets. The way these elements are arranged depends on the type of format used. The edge-based boundary representations preserve both the geometrical and topological information at different levels [71]. The most used standard for the exchange of polygonal meshes is the STL format. In STL format, the topological information is not available explicitly, and for many applications it is necessary to reconstruct a continuous representation [22, 23], or to extract features information from it [77]. The Object File Format (OFF) is also commonly used in 3D graphics and printing. The OFF format has also both binary and plain text versions, its plain text version has a structure that is intuitive and easy to understand. The main difference with the STL format is that in the OFF format polygons can have any number of vertices [OFF].

a Skin Model

The nominal product model of any workpiece has been the main way of describing and representing its geometrical information, this information is used by Computer-Aided Design (CAD), Computer-Aided Engineering (CAE), Computer-Aided Tolerancing and Computer-Aided Manufacturing (CAM) systems to perform activities like: design, simulation of manufacturing process, analysis of tolerance and mechanical simulations. The nominal product model is the departing point for many activities in design, it represents the design intent and it is of perfect shape. However, the high performance machines, the outbreak of smart sensors that have facilitated the data collection, and the widespread use of Artificial Intelligence (AI) in industries demand a more realistic product model.

The concept of Skin Model has been formalized and incorporated only since 2010 as a central part of the GeoSpelling language. It is the product of a research of at least 15 years of Ballu and Mathieu [7] and other precursors that worked in the field of geometric tolerance like Requicha [102] and Srinivasan [131] whose research on the concept of real or non-ideal part shape have set the foundation for the Skin Model concept for ISO standardization. It is defined in the ISO standard as a " model of the physical interface of the workpiece with its enviroment" [66]. It refers to the interface, or skin, of a part that separates its material from the surrounding environment. It conveys the designer's idea about all the possible defects on the nominal geometry. This surface model of non-ideal geometry is not unique and can take on an infinite number of forms and representations [118].

Skin Model perspectives

One can view the skin model from different perspectives. In Fig.1.3, four perspectives mentioned in the literature are shown. The conceptual perspective links the physical boundary of a part to its abstract representation. This duality is at the core of the definition adopted by the ISO. From the engineering perspective, the concept of Skin Model is used for both specification and verification with the aid of the specification and verification operators [20]. Because of these, for instance, the evaluation of a geometric characteristic in relation to the result of a measurement is possible.

From the science perspective, there exists efforts to come up with definitions from physics and maths. In [12], the authors provided a mathematical definition of the Skin Model concept from a topological perspective, saying that the skin model is a closed, orientable surface

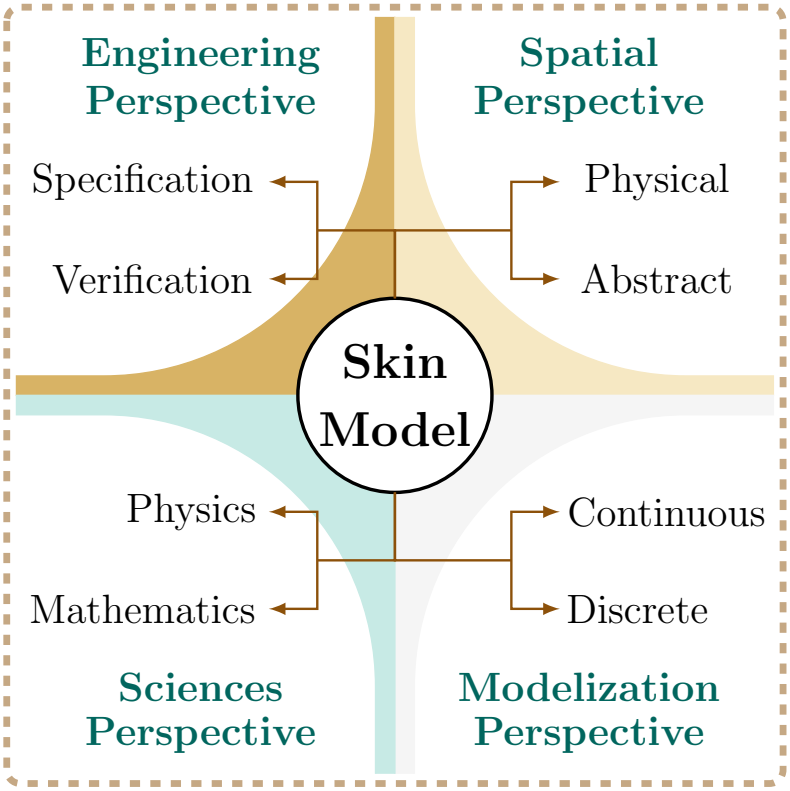

Fig. 1.3 Skin model perspectives

that has no boundaries, and that it is homeomorphic to a sphere or a finite connected sum of tori. The main idea behind this definition was the fuzziness in the region near the edges. The need for a mathematical definition a skin model comes primarily from the ISO standards as this concept is a foundation stone of their view on Geometrical Product Specifications and Verification (GPS). In [14], the authors used the notion of solid as a state of matter composed of atoms and molecules, as used in physics, and the definition of solid from set theory in mathematical sciences to give, at first, an abstract definition of a skin model as a "part/workpiece made up of matter in stable solid state" that can be modelled as a regular set of points. This definition of solid implies that the solid is considered rigid, continuous, and its boundary is a surface. The authors in [14] presented new ideas based on the morphological operation of *closing* to define a solid S_r as part of a family of solids $\{S_r\}$ whose limits are the S_0 and S_H obtained as the index r approaches 0 and $+\infty$ respectively. These limits are named as *molecular solid* for S_0 and *solid hull* for S_H. Any solid of this family in between these limits can be obtained using the *closing* operation of a set of points A and a structuring element B for any positive real value of r. This is a first effort for obtaining a mathematical

definition of a skin model; further operations with these solids are to be investigated.

From a modelization perspective, the skin model is presented as a continuous, non-ideal representation of a part as opposed to the nominal model (ideal representation) [118]. Both of these concepts consider the designer's vision of a model: on the one hand, the idealization of the shapes that conveys the design intent (nominal model); on the other hand, the possibility of imagining the actual variations of a part after being manufactured that are encompassed in the concept of skin model.

Although a broad, abstract conceptualization of the skin model is necessary to imagine the infinite possibilities of variations of a workpiece, an operationalization of the concept is necessary for engineering applications. Most of the research efforts on this field have been devoted to the implementation of instances of skin model called Skin Model Shapes (SMS). In Subsection b, the operationalization of skin model through discrete representation is explained.

b Skin Model Shapes

The Skin Model Shapes (SMS) is proposed as a model that enriches the nominal product geometry with geometric deviations that are expected, predicted or observed in manufacturing, measurement and assembly processes [12], thus overcoming the limitation of nominal geometry in consideration of real-world situations. In Fig.1.4a shows the number of publications per year on Skin Model Shapes from 2013 until June 2024. The last decade has witnessed the rapid growth of research devoted to the SMS regarding its simulation, representation and application. In Fig. Fig.1.4b, the countries with the most publications on the subject are listed, being China and France the two countries with the most publication on this subject.

Representation scheme

The Skin Model is imagined as a continuous surface capable of comprising the defects at any scale. From its definition, an infinite, continuous surface is necessary to represent all the defects coming from manufacturing processes [120]. A continuous model representation is desirable when expressing geometrical specifications, or when defining a verification operator in metrology; but when a quantitative analysis is needed, a discrete model is easier to manipulate [12]. Although conceptually the Skin Model is continuous, most of the research on the creation of digital instances of the same is done through discrete representation. Some

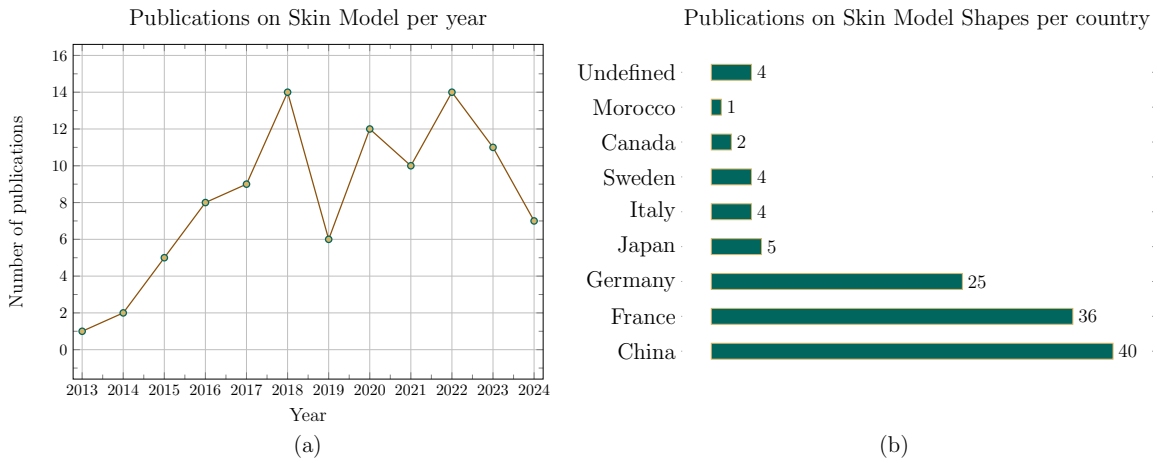

Fig. 1.4 a) Publications on Skin Model per year from 2013 until June 2024 in Scopus. The query was "Skin Model Shapes" searched only title, abstract and keywords. b) Publications on Skin Model Shapes per country from 2013 until June 2024 with the same query.

of the advantages cited by different authors [144, 118] for choosing the discrete over the smooth representations are:

- Flexibility on the approximation of product's surface
- Easiness on the representation of instances in computer systems
- Points clouds are already used by 3D-scanners in inspection and in manufacturing data
- There are little conversion problems across different platforms
- Polygonal meshes can be easily created from point clouds

The discrete representation through point clouds are approximations to the product's surface. Some of the topological information of the part is sometimes unavailable, making it difficult to fully exploit them in integrated systems. No representation scheme is prescribed by the standards in geometric design, so as far as the model is sufficiently precise and it is compliant with the standards, smooth or discrete representations can be used.

Deviation modelling

The discrete representation frameworks proposed in the literature guide the process for obtaining representative instances of surfaces with form defects [13, 144, 118, 79]. Fig.1.5 shows the general steps of the frameworks followed in the literature. They all adopt the nominal model as the starting point in the process, then the solids are partitioned into features

of interest following the operations described in the ISO [66]. Once the features are partitioned, a discrete representation of them is made through tessellation or meshing techniques. Once discretized, the deviation modeling can take place depending on the available data (i.e. measurements, simulations). The deviation modeling is divided in the framework in observation stage if some information about the geometric defects is already known through measurements or manufacturing process simulations, or prediction stage if the information about the geometric deviations is not available.

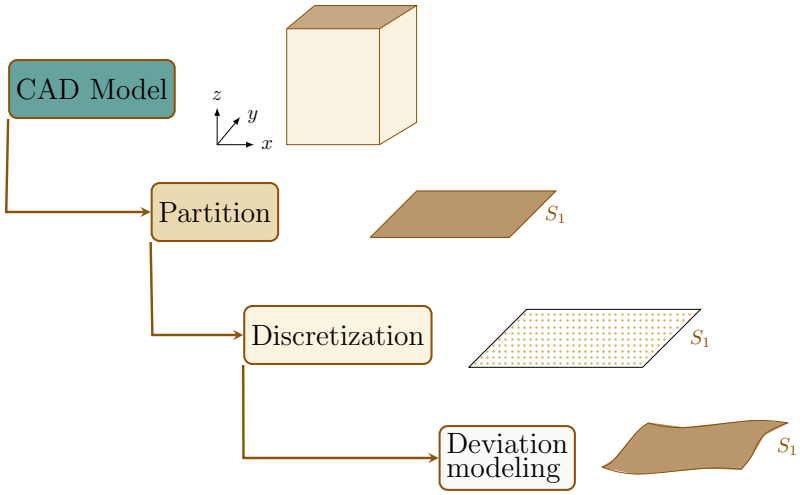

Fig. 1.5 General steps in the discrete frameworks presented in the literature.

In the prediction stage, the process is divided in systematic and random deviation modeling as it can be seen in Fig.1.6. The methods used for modeling the systematic deviations attempt at reproducing the errors induced during the manufacturing process that are present in most of the parts of a batch, and that are reproducible and predictable. These methods are generally classified in morphing or decomposition methods.The morphing methods represent the deviations of a feature by deforming the surfaces of a workpiece. The second order shapes have been proposed by [143] to model systematic deviations in planar features. The idea behind it is to deform a planar feature to a shape described by a second order function, being the most common the paraboloids, cones and spheres. Other authors deform the surfaces based on differential representations like gradient-based or Laplacian-based representations, or through local transformations like geodesic or harmonic propagation [28]. Authors in [47] deformed sheet metals parts using a small number of control points (that could be related to measurements) to perform variation analysis of assemblies using Monte Carlo simulation.

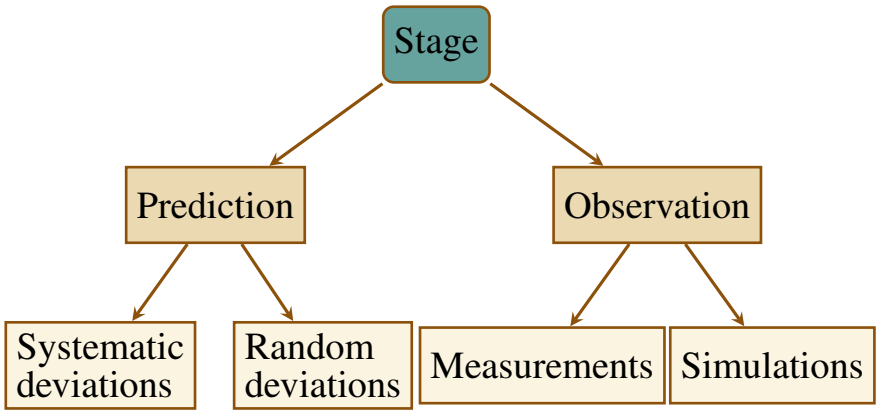

Type of method	Systematic deviations	Random deviations	Measurements	Simulations
Morphing	[108, 143]	[28, 47]	[142]	[49]
Deformation	[65, 146]	[116, 59]	[95, 105]	[95, 105]
Statistical		[117]	[141]	[50]
Machine Learning			[119]	[25, 50]

Fig. 1.6 Deviation modelling process and methods

In the observation stage, the information comes in the form of measurement or manufacturing process simulations is treated and added into the modeling process. In [142], the authors used statistical shapes analysis to find the variation modes from the measurements, then they used a semi-automatic thin plane spline (TPS) to deform the meshes into the variation shapes obtained from the measurements.

The discrete cosine transform (DCT) is a spectral method that is very frequently used in deviation modeling. The DCT decomposes a surface deviation into a series of independent error modes whose basis functions are orthogonal. Authors in [65] used this method to model the deviations of a planar surface in a stamping process. Another spectral method, called Zernike polynomials, has been used to model form defects in annular and spherical surfaces [146]. The idea behind this method is the same, decomposing the errors through orthogonal basis functions in spherical coordinates, then compose the errors though a linear combination of the basis functions. The modal decomposition by natural vibration modes is widely used in mechanics to simulate the geometric deviations for any type of features. The principle is to use finite element analysis to solve the equations of conservative system in linear dynamics

under the hypothesis of small displacements [116].

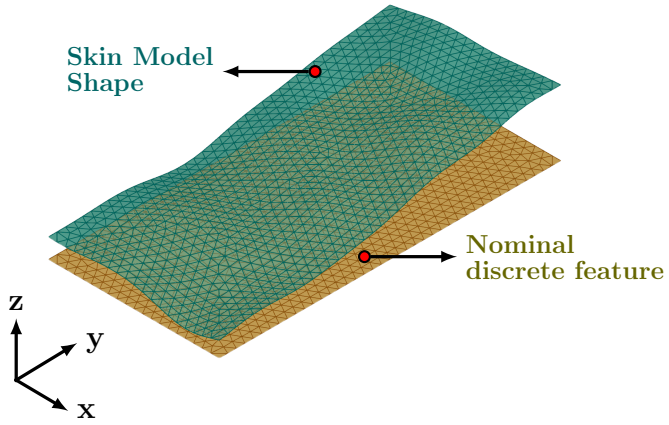

Fig. 1.7 Geometric deviation on planar feature using the modal decomposition the first vibration modes of a thin plate. the defects are magnify x20 for representation purposes.

Normally, the first three modes correspond to the rigid displacements of the feature, and the rest are different vibration modes. By composing the modes with a function, it is possible to simulate defects on features as it shown in Fig.1.7. The nominal feature can be deformed to obtained the Skin Model Shape (SMS) shown in blue. This is one of methods that will be used in the rest of this work.

In the observation stage, the Laplace-Beltrami Operator (LBO), a generalization of the Laplacian operator, has been used for geometric deviation modeling [95]. The advantage of this method is that it does not define *a priori* shapes to decompose, it is in that sense, shape-agnostic. It has been used to reproduce the deviations coming from measurements of physical parts [105].

The machine learning techniques take advantages of the SMS synthetically generated through other methods or through real measurements to feed the initial training set. The great advantage is that they are shape agnostic and they can generate both systematic and random deviations without further parametrization. In Appendix A, can be found a table with the advantages and disadvantages of the methods referenced before

In this section, a shape was defined at the abstract mathematical level and at the digital level. When it comes to their representation, some of the most used representation models in engineering were presented highlighting the need for representing not only the ideal shapes,

but also non-ideal ones. The concept of SMS was introduced, and the definition of feature and the obtainment of non-ideal features was presented for the skin model.

III Contact modeling in tolerancing

In mechanical engineering, contact modeling is vast field of research. Depending on the expertise it can take many different forms. The first consideration is generally the contact model to be used that can be roughly categorized in rigid, compliant (or deformable) and hybrid models. The contact modeling is a part of many different engineer applications, therefore the way to approach this activity depends on the phenomena to be described, and on the objective of the modeling.

Contact modeling is used in robotics for studying the grasping and manipulation of objects by a robot, and in motion planning [31]. For roboticists, the general goal with contact modeling is to obtain the contact configuration between the robot and the object that is being manipulated given certain conditions. The contact configuration provides the information about whether or not the contact is possible, and about whether that contact will be maintained or not [127]. In their models, the assumption of rigid bodies is typically employed, and the incorporation of friction models is a standard practice [80].

In the field of strength of materials, the motivation behind contact modeling is to assure that deformation happening at the interface between two surfaces does not exceed a certain threshold. In this field, the external forces, geometry and material properties serve at determining if the static or dynamic system respects a certain mechanical condition [62].

In tolerancing, the idea with contact modeling is to assess on the one hand the feasibility of a contact between two features, like in the case of a cylindrical pair, and on the other, to evaluate the respect of a functional condition given the deformation of the parts involved in the contact chain. The first case can be modeled through a purely geometrical approach by incorporating the external loading acting on the contact. Chapter 2 will develop this idea using prismatic polyhedra. The second case involves a deformation model to account for the local deformation between the parts in contact. Chapter 3 will develop this idea using the polyhedral-based model.

Considering the contact between non-ideal features using the prismatic polyhedra model implies mastering the description and representation of the duality between the forces (wrench) and the displacement restrictions (deviation space). Also, it becomes important to incorporate such representation in a digital tool. The next sections present the representation models and the Computerized-Tolerancing tools that are frequently used in mechanics.

IV Representation models for tolerance data

In the previous subsection, some of the mathematical models for tolerancing were presented. In this subsection, some of the most used models for the representation of tolerance data will be reviewed. Tolerance representation models are used to represent the semantics of the interpreted tolerance model (mathematical model), and they are generally built from them. A mathematical tolerance model can be represented in different ways, the available information depends on the data model and the representation model used. A data model defines data objects of any kind, it also defines the relationships among those objects. Data models are generally constructed to aid in the modelization process of an information system and they tend to be domain specific.

a Data modeling languages

Different data modeling languages have been used to model tolerance information [147]. A data modeling language can be viewed as a collection of different modeling techniques (i.e. UML Class diagrams, USE case diagrams) that can range from purely textual to purely formal [5].

EXPRESS model

The express modeling language is part of the STEP (Standard for Exchange of Product Model Data) created by the ISO [2]. The tolerance information that can be exchanged using the STEP format is implemented in EXPRESS. The logic used for the data description in EXPRESS is very similar to the one used in the object-oriented programming languages. In EXPRESS exists the notion of *parent* called *supertype*, and of *child* called *subtype*. The definition of an objects is an *entity* which has some *attributes*. A complete set of entities is called a *schema*.

EXPRESS has a graphical language called EXPRESS-G. In EXPRESS-G entities are represented in solid boxes, simple data types (i.e. Strings) are represented in solid boxes with a double line at the right end, and data types defines by the user are in boxes with dashed borders. The different relationships among *entities* are designed by thick, normal width and dashed lines between them [138].

This language has been used in the definition of vectorial tolerancing in product modeling [83]. In [138], Michaloski, et al. used EXPRESS to include feature-based tolerancing in a CAM/CNC manufacturing process. The STEP is a standard that tends to be invoked once the product development process is advanced rather than for the information produced through the process [43].

XML model

The Extensible Markup Language (XML) is an application profile of the Standard Generalized Markup Language (SDML) created by ISO [69]. The XML was first created with the goal of being easily usable over the internet and to support a wide variety of applications. The physical structure of a XML document is composed of *entities* that can refer to other ones to include them in the document. The document is composed of declarations that are indicated by markups. Generally, these markups start by the character $<$, and end by $>$. The characters not in markups are considered the content of the document. A XML document is composed of a string of characters with some start, end and empty-element tags [6].

In [147, 84], the authors used XML Schema to represent tolerance information. The article shows how an user could construct and XML instance data file to meet some functional requirements. The advantage of this representation is that provides unambiguous communication of tolerance information via the internet to achieve integrated measurement processes.

UML

The Unified Language Model (UML) is born from the software industry to deal with the rapid evolution of informatics during the 90s. Therefore, UML is a language particularly adapted to the creation of representation models of software. It is based on the object-oriented programming paradigm and the best industry practices for diagramming information. It serves a modeling, visualizing and constructing models and meta-models for any domain, but

more importantly, it serves at capturing and leveraging the knowledge of a specific domain.

The UML can be seen as a composition of different modeling techniques, some of them graphical some other textual. It is composed of nine types of diagrams: class, object, use case, sequence, collaboration, state-chart, activity, component, and deployment. The diagrams are grouped according to five architectural views: user, structural, implementation, behavioral and deployment [5].

The are some product models that uses UML language in their definitions. One example is the Core Product Model (CPM) and the Core Product Model 2 (CPM2) [44] which are abstract, generic models of product or artifacts that define its function, form and its behavior. The components of the CMP2 are two classes called *object* and *relationship*, which have some correspondence to the UML *classes* and *association classes*. In this model, function, form and behavior aggregate into an artifact; and form is conceived as an aggregation of the geometry and the material.

UML has also been used in the feature models for the specification of assemblies [107], for the representation of electro-mechanical assemblies [98] and for the Open Assembly Model (OAM) from the National Institute of Standards and Technology (NIST).

OWL

Ontology in information systems and in systems engineering is a borrowed concept from philosophy. The ontological studies in philosophy are concerned with the being and with things that exists and the relationships between them. In information systems, one of the accepted definitions of an ontology is "an ontology is an explicit specification of a conceptualization" [26]. Then, in information systems the ontologies concern is about the explicit representation of information. Ontologies are becoming more important for many applications in systems engineering, semantic web, and are helping to create consensual terminologies and taxonomies for many fields [106, 140].

The Web Ontology Language (OWL) is used to make the UML model computer-interpretable. It represents complex knowledge about things and their relationships to one another [89]. The concept ontology refers in computer science to a certain computational artefact, such as an XML schema, that is presented as a document. It is a set of precise descriptive statements about a domain of interest, it is not a programming language. A terminology of a domain, and the interrelation information is what constitutes a OWL document.

The basic notions in the OWL language are *axioms* (basic statements), *entities* (elements that refer to real-world objects) and *expressions* (complex description formed by the combination of entities) [89].

The people from NIST also created a model capable of interpreting the semantics of the products that are assemble based OWL [45]. The model is based in the OAM model, and the ontologies created for it can be translated from UML to the Ontological language. The main advantages of this model are that it can define on the same properties different constraints for different classes, which is not possible in UML; the structure of the semantic can be understood and interpreted by a reasoning software that can check the consistency of the model, meaning that it can be automatically tested if not only the syntax, but also the semantics make sense.

GeoSpelling

GeoSpelling is an unequivocal language that unifies the specification and verification for both micro- and macro-geometry [7]. It came from the idea of conceiving the parts with form defects that metrologists found during the verification process. The core of this language is the concept of Skin Model explained before. It is a language thought for the geometric dimensioning and tolerancing; the authors define a geometric specification as a "condition on a dimension defined by a characteristic expressed on geometric features". These geometric features are identified from the Skin Model by a series of operations defined in the language.

The language defines the base concepts like ideal and non-ideal features, and some characteristics that can be *intrinsic*, belonging to a feature and characterizing its geometry, or *situation characteristics* that are functions defined between two features. The operations defined in the language are six: partition, extraction, filtration, association, collection and construction. These operation are the basis for the description of the specification and verification operators [20].

In summary, the data models serve at capturing the information of a domain and are generally specific to an application system. The ontologies represent explicitly the specification of a shared conceptualization within a domain. The data models for the representation of tolerance information can or not be system dependent. Some of them, like all the models presented above, are independent of an application system. The system and the underlying models for tolerance representation are presented.

Computer-aided tolerance (CAT) software became necessary to properly conduct tolerance analysis, synthesis and optimization. The geometric requirements of complex systems cannot longer be calculated manually. The costs of design and production, and the quality of products depend today largely on how efficient our systems are. CAT systems contribute to the automation and standardization of many activities in tolerance management which results in significant cost saving and ensures consistent production quality

This section provides a more in-depth information about the representation models that are used for incorporating geometric information into digital tools that aid the tolerance analysis process.

V Computer-Aided Tolerancing

The frequent approach in CAT begins with the nominal geometric information obtained from CAD systems. The procedure starts with the definition of the individual parts in a CAD environment that are part of an assembly, then the specification of the tolerance types can be done on the features of interest in each part. Once all of the tolerances have been specified, the relationships between different parts can be defined. At this stage, it is possible to accommodate the dimensional and geometric variations on the assembly, then the Key Product Characteristics (KPCs) can be specified and must be satisfied in order to fulfill the functional requirements of the system [85]. KPCs are specific features of a part or assembly whose variation has a significant impact on the functional requirements.

The compendium of activities in Geometrical Dimensioning and Tolerancing GD&T is of such an extent to cannot be all fully encompassed in a single CAD workbench nowadays. CATIA V5 Functional Tolerancing and Annotation (FT&A) is based on Topologically and Technologically Related Surfaces (TTRS) model in which 28 different configurations are defined with seven different surface classes considering the degrees of freedom that let surfaces globally unchanged [40]. The FT&A tool in CATIA helps the user in the correct use of standards by providing automatic annotation support and dimensioning and tolerancing rules verification [52]. New CAT systems are created based on existing ones, like the Quick GPS system [11] that is implemented using FT&A, Visual Basic for Application (VBA) and Component Application Architecture (CAA). The Quick GPS system allows automatic generation of tolerance data for single parts through a VBA procedure, then tolerance data are retrieved from Excel using CATIA V5 CAA. Quick GPS was created to assist the designer in

the specification process.

ANATOLE 3D is a software developed by Digital Product Simulation (DPS society) and AIRBUS that is also integrated into CATIA V5. It uses a robust solver based on a open source initiative for the management of uncertainties and risks [21] that allows for worst case, and statistical and sensitivity analysis. ANATOLE 3D considers only iso-constrained assemblies, so it is necessary to release some components when working with an over-constrained system [48]. ANATOLE 3D is based on rigid body and small displacement torsor (SDT). A dedicated module for modeling flexible assembly has been developed under the name of ANATOLEFLEX [42]. It also provides a deviation modeler where the description of geometrical variations can be performed

3DCS from Dimensional Control Systems is fully integrated to work with SolidWorks, it uses variational analysis to conduct tolerance analysis. It work with three type of analysis: Monte Carlo, high-and-low mean and Geofactor relationship [134]. Another software solution integrated to SolidWorks is Sigmund from Varatech. In Sigmund, five type of analysis are available: Worst case, Root Sum Square (RRS), Modified RRS, PCRRS and Monte Carlo [128].

MECAmaster is another robust solution that allows to manage 3D variations from early design stages. It can compute 3D tolerances stacks-up and assist the designer on the identification of causes of variation. MECAmaster proposes two modeling modes, one using simple kinematic connections and another that takes into account surface-oriented contacts. MECAmaster also uses an automatic detection of over-constraint assemblies [35]. Other CAT softwares like eM-ToolMate and VSA from Tecnomatix make use of a variational approach for tolerance analysis. These CATs focus mainly on tolerance analysis and on the automatic generation of tolerance schemes, generally based on Monte Carlo simulations [123]. Form deviation modeling as part of CAT is starting to gain importance as it allows a more realistic representation at the feature level.

Another interesting software is RD&T [100] which is specialized in robust design and tolerancing. The tool has a module for sensitivity analysis, statistical variation using Monte Carlo simulation, and a FEA-based module that allows to simulate the elastic and compliant behavior of parts and assemblies. This tool has been used to incorporate the manual assembly complexity in the tolerance analysis process, and also to incorporate the influence of stress

during the assembly process [86, 129].

PolitoCAT is an open source software that allows to conduct tolerance analysis with the polyedral-based approach [37]. PolitoCAT allows to perform worst-case analysis of iso- and over-constraint assemblies. It has a polyhedral solver called politopix that is also available in open source. It does not include a statistical solver for performing Monte Carlo simulation, but the base operands have been used to conduct both statistical and worst case analysis, as well as tolerance synthesis [56].

All of the above are proprietary software that are created sometimes within companies, some other times with the aid of research labs. The existence of several commercial solutions for tolerance management has the advantages of promoting the competition among different industrial which can lead to constant improvements, and it helps to maintain the proper support of these platforms. However, property software has proven to have the following disadvantages:

- The slow on the implementation of new paradigms like the Skin Model
- The access to the underlying models and information is difficult.
- Most of the above software do not allow to explicitly evaluate the respect of a functional condition considering the deformation of the parts.

In the frame of this work, PolitoCAT will be used and improved to account not only for the modeling of non-ideal features, but also fore the inclusion of the local deformation between parts potentially in contact.

VI General framework for local deformation

The exposed literature shows that when it comes to effectively dealing with the challenges of geometric tolerancing, it is necessary to consistently describe and represent the geometric deviations and form defects. Depending on the application case, the level of detail in the description and representation should be adaptable.

In this section, a general framework for the inclusion of form defects, contact simulation and deformation is shown for discrete features using the polyhedral-based method.

As it was clear, the representation of tolerances is not carried out in the same manner in the different approaches, but even if the specific models for representing the tolerances and computing the deformations are very different, most of the revised literature agree with the general way to approach the tolerancing problem. In the general framework presented in Fig.1.8, there is a model preparation or pre-processing phase. There are two stages in this phase: identification and deviation modeling stage. In the identification stage, the key mating features are determined from the nominal model. This process can be carried out by the experience of the designers or by a sensitivity analysis in which the contact and geometric are taken into account; these features are then partitioned. In the deviation modeling stage, the partitioned features are meshed, and the geometric and form defects added on. The generation of SMS can is carried out with discrete shapes, by predicting methods or with measurement data as explain in this chapter. Once the non-ideal features are available, the difference surface method is applied to the mating features.

The second phase is the contact simulation. The rigid contact configuration must be found before considering the deformation. In Chapter 2, it is explained how to found the rigid contact configuration from the deviation space by taking into account the external mechanical loads.

Once the rigid contact configuration is established, the local deformation process can begin. For that, it is necessary to choose a mechanical model to describe the behavior of the contacts, and integrate the results into the tolerance model. In Chapter 3, the local deformation process is controlled from the deviation space by rigidly transforming the half-spaces involved in the contact between the mating features.

The last phase consists on an assessment of the functional requirements. In this case, it is done through the inclusion of the simulation results in the operand representing the functional condition.

This work contributes in that sense to the integration of new paradigms into open source solutions that are fully integrated in a CAD environment.

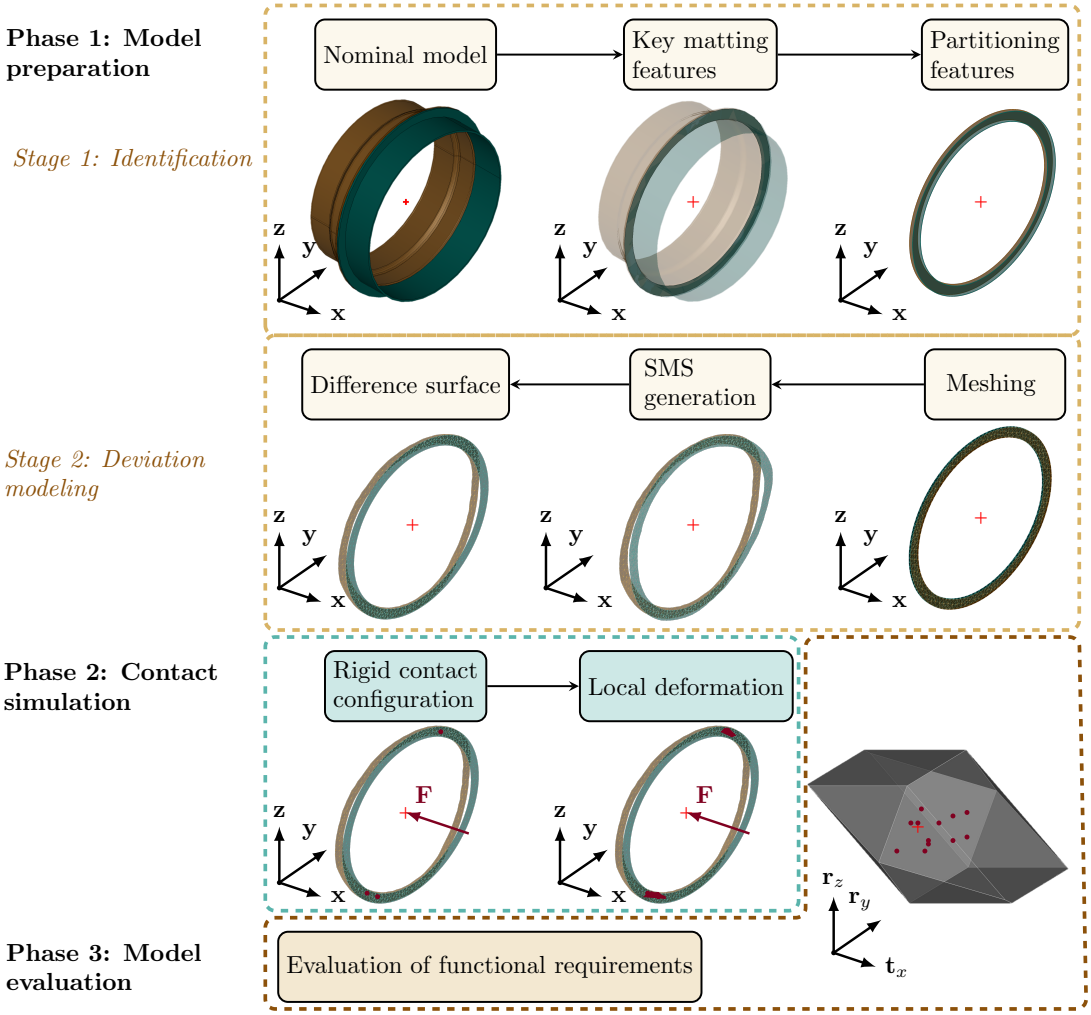

Fig. 1.8 General framework for the inclusion of geometric and form deviations, and local deformation using discrete features in the polyhedral-based approach

VII Summary and conclusions

In this chapter, a review of the tolerancing models for tolerances analysis was presented. The main advantages and drawbacks of the parametric methods and those based on set of constraints were presented. It was shown that as the manufacturing and the inspection capacities, the digital models need to be more accurate and realistic. Most of the models based on set constraints start at the feature level and move up to the whole assembly. The Skin Model paradigm was introduced and the framework for its implementation discussed. Even though the discrete representation has been taken implicitly as the standard for the representation, the continuous or smooth representations are valid instances of this model. The Skin Model paradigm is still being studied, specially to find a mathematical description

of it.

The main CAT systems were presented as part of the digital representation of shapes. One of the practical objectives of this thesis is to contribute to the implementation of a integrated environment that allows the CAD modeling, manage the geometric deviations, and simulate the contacts with or without deformation.

A general framework to deal with geometric and form deviations, and to include contact simulation with or without deformation was presented in Section II. It allows to adapt the level of detail which the system is model with, as many application might not need to deal with form defects or local deformation.

In summary, this work is about manage deviations by using a more realistic representation of features. This is done in the context of tolerance analysis. For the incorporation of all sorts of deviations, the skin model shapes are used. Both, geometric and contact features have to be defined using the prismatic polyhedra model. Especial emphasis is made on the contact modeling using this model as it will require the consideration of external forces.

A purely plastic deformation model will be incorporated into the polyhedral-based approach. The pure plastic model, although it is not fully generalizable to all contacts, allows us to represent the deformation from the deviation space which constitute a novelty in itself.

The models and algorithms presented here are incorporated in the CAT tool PolitoCAT to be able to execute real case studies.

Chapter 2

An enriched polyhedral-based approach for the contact simulation with form defects

I Introduction

The main objective of this chapter is to formulate the inclusion of external loads in the polyhedral-based approach. The inclusion of external loads is an enrichment of the current mathematical formulation, and it allows to calculate explicitly the contact points of two features potentially in contact, with or without form defects. Features potentially contact refers to those features that when assembled might come into contact. The precise nature of the contact depends on the geometric and/or functional requirements of the system. In effect, often case the geometric requirements on ideal features imply some assumptions that cannot be explicitly stated. If we take for instance the case of a planar contact, the geometric requirement of clearance leads to a specific contact configuration. When the clearance is zero, it implies that the features have to remain in contact, but generally no explicit formulation of this action is provided in tolerance analysis. This is partially due to the fact that when the features are considered as ideal, the geometric requirements are enough to resolve the contact problem. However, when form defects are considered, the implicit assumptions have to be explicitly formulated to be able to resolve the contact problem.

The explicit formulation of the forces acting on the features potentially in contact allows to model different contact configurations (floating, sliding and fixed) for any contact type. In this chapter, the sliding behavior of two mating surfaces is simulated to illustrate the potential

of the enriched polyhedral-based approach.

II The polyhedral-based approach for tolerance modeling

The polyhedral-based approach can be seen as a comprehensive polytope approach. A polyhedron is generally defined in this context as a 6d object that can be or not. In the polytope approach, the restrictions coming from the non-interpenetration constraints of two parts potentially in contact can be described with a set of constraints that define the boundaries of their relative displacements. Generally, the intersection of a finite set of constraints results in an unbounded set, defining an operand polyhedron instead of a polytope. In [64], the authors added artificial half-spaces to “cap” the unbounded sets (polyhedra) to turn them into bounded sets (polytopes). In [17], the authors proposed a truncation algorithm to obtain the list of vertices of a polytope (V-description) in $\mathbb{R}^n$ from its H-description (list of half-spaces). Both of these works were done to be able to perform operations, especially the Minkowski sum, with these operands. By “capping" a polyhedron, the topology of the operand changes and becomes more complex making each subsequent operation in the tolerance chain more time consuming, with the additional problem of having to trace back the artificial half-spaces propagated at each operation to differentiate them from the half-spaces coming from the actual geometric restrictions.

The authors in [18, 38] found that the “capping" process bounded the displacements related to the DoFs of the tolerance joints, or degrees of invariance of the toleranced features. To solve this issue, they proposed an approach based on polyhedra which consists of decomposing each set of geometric restrictions in the sum of a bounded set, representing the bounded displacements, and an unbounded set representing the DoFs. With this approach, the complexity of the operands and therefore the calculation time were significantly reduced.

The polytope approach has been used to model hyperstatic mechanisms considering form defects as in [57], and in approaches that consider surface deformation in tolerance analysis [145, 79]. The inclusion of form defects in the simulation of assemblies adds complexity to the model in the sense that the possible assembly configurations in the case of a sliding or fixed contact depend on the nature and amplitude of the form defects, and on the loading conditions to which the assembly is subjected. For the relative positioning of the parts with form defects, part of the reported research focus has been on the optimization methods that seek to minimize the distance between surfaces with form defects

along specific directions [121, 15], while another part focuses on finding experimentally the relative positioning in mechanical joints by exploiting the bijective relationship between the gap hull and the convex difference surface method [75, 4]. In [76], the authors used the convex difference surface method applied in spherical joints with form defects. In [139], the authors used the Small Displacement Torsor (SDT) and Linear Complementary Conditions (LCC) to simulate the assembly boundary conditions in assemblies that consider form defects.

a Geometric restrictions

According to [148], a polyhedron can be decomposed as the sum of a polytope (P) and a polyhedral cone (C) as shown in Eq.2.1. In Fig.2.1.a, a 3D representation of a cylinder is shown, if we are dealing with a geometric specification by zone of a planar feature as shown in Fig.2.1.b, then the restrictions from points P_1 and P_2 expressed at point M can be written as the double inequality shown in Eq.2.2, where c is the tolerance value; $\mathbf{t}_M$ is the translation vector of point M; $\mathbf{P}_1\mathbf{M}$ and $\mathbf{P}_2\mathbf{M}$ the position vectors from the points P_1 and P_2 to M; and $\mathbf{r}$ the rotation vector of the feature.

$$\Gamma = P \oplus C \tag{2.1}$$

For the geometric restrictions, the double inequalities describe two half-spaces at each point: $\bar{H}^+_{1inf}$ and $\bar{H}^+_{1sup}$ for point P_1; and $\bar{H}^+_{2inf}$ and $\bar{H}^+_{2sup}$ for point P_2.

$$\begin{aligned} -\frac{c}{2} \leq (\mathbf{t}_M + \mathbf{P}_1\mathbf{M} \times r) \leq \frac{c}{2} \\ -\frac{c}{2} \leq (\mathbf{t}_M + \mathbf{P}_2\mathbf{M} \times r) \leq \frac{c}{2} \end{aligned} \tag{2.2}$$

The intersection of these half-spaces, as shown in Eq.2.3, gives as a result the polytope P depicted in Fig.2.1

$$P = \cap_i \bar{H}^+_i \tag{2.3}$$

b Degrees of freedom in the polyhedral-based approach

In Eq.2.1, the decomposition of the polyhedron into a polytope plus some straight lines can be obtained in different ways. In this work, the decomposition of a polyhedron operand is performed in a prismatic way. The restrictions expressed by the polytope are perpendicular

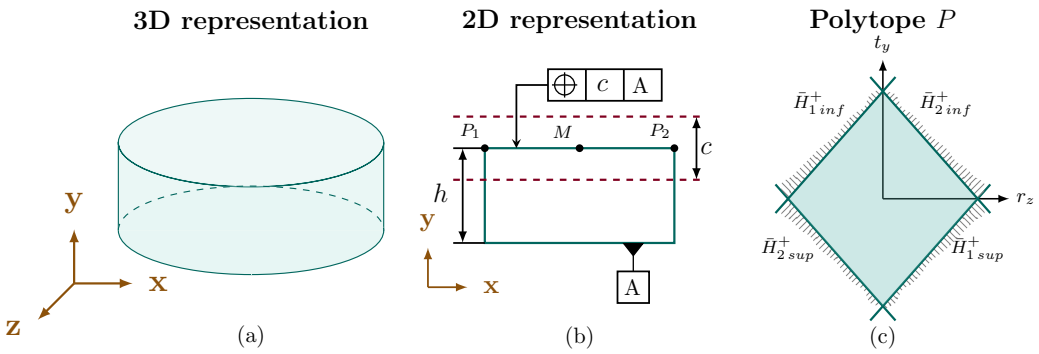

Fig. 2.1 a) 3D representation of a cylindrical part. b) 2D representation of the part shown in a) and a geometric specification of a planar feature. c) Polytope coming from the intersection of the four half-spaces from points P_1 and P_2 written at point M.

to the straight lines of C. When we are dealing with a geometric specification by zone, the straight lines Δ_i characterize one of the seven invariance classes as defined in the ISO 17450-1:2011 [66]. In Fig.2.2, the prismatic decomposition is illustrated. The polytope from the previous example is highlighted (Fig.2.2a). It represents the restrictions of the displacements in rotation along $\hat{z}$ (r_z) and translation along $\hat{y}$ (t_y). The straight line, in this case translation along $\hat{x}$ (t_x), obtained from the degree of invariance of a 2D planar feature (Fig.2.2b). The polyhedron composed of the sum of the polytope and the straight line can be seen as the polytope extruded in the direction of the straight line as depicted in the figure (Fig.2.2c).

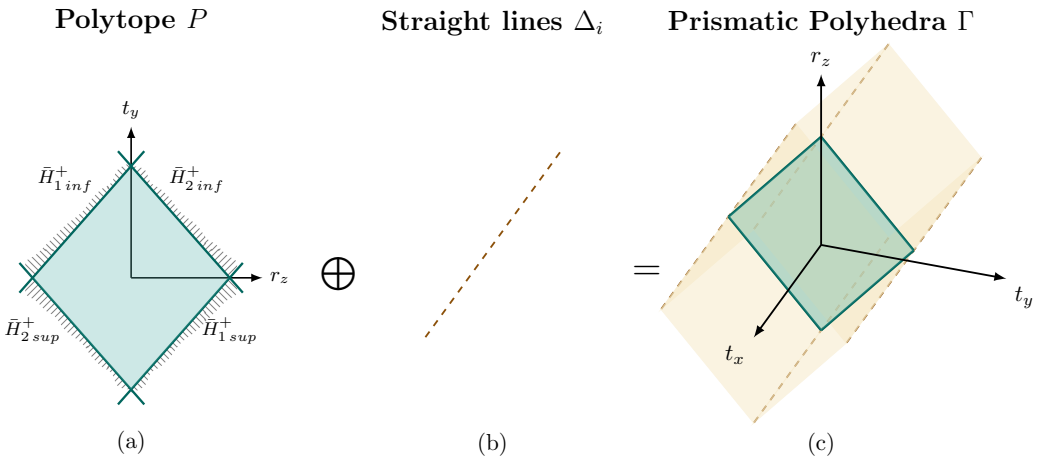

Fig. 2.2 a) Polytope obtained from the intersection of the four half-spaces from points P_1 and P_2 written at point M. b) the straight line from the degree of invariance of a 2D planar feature c) Polyhedron composed of the sum of the polytope and the straight line.

When dealing with contacts, the straight lines that characterize the degree of invariance in the geometric operand become the degrees of freedom (DoF) of the contact between two mating features [17]. The rest of the procedure remains globally the same.

The main motivation of this chapter is to simulate precisely the contact behavior of a rigid mechanism, with and without form defects, through a polyhedral-based approach, and to quantify the impact of form defects on a functional tolerance. With this work, we are contributing to: 1) the development of a framework for the simulation of rigid contacts with or without form defects; 2) an objective quantification of the impact of disregarding form defects for a given mechanism under some specific conditions; 3) the conceptual enrichment of the polyhedral-based method applied to contact modeling; 4) the notion of adaptability in design by providing objective output on the respect of a condition when changing load boundary conditions or disregarding form defects.

c Limitations

The main limitations when conducting tolerance analysis are:

- **Ideal features:** geometrical features are considered as ideal, the geometrical deviations modeled are generally limited to rigid transformations. It is often the case when using the polyhedral-based method.
- **Unbounded sets:** unilateral contact configurations lead to unbounded sets in the polyhedral-based method. As it was shown at the beginning of this chapter, the research on this subject leads to some form of artificial closure that can make the operands become more complex.
- **External loads:** the inclusion of the external loads in the polyhedral-based model has never been explicitly taken into account.

In the next sections, these issues will be addressed.

It is important to establish an explicit description of the load boundary conditions in relation to the relative position of rigid assemblies with form defects. This work further enriches the concept of contact polyhedra in the context of tolerance design by formalizing the representation of load boundary conditions in rigid assemblies as additional displacement restrictions. In this way, the contact restrictions are derived in three parts using a polyhedron:

a) the purely geometrical restrictions imposed by the physical limits of the contact; b) the restrictions coming from the load boundary conditions; c) and the mobilities of the contact. By decoupling the operand in the aforementioned way, it is possible, for instance, to simulate the sliding and fixed behavior of rigid contacts with or without form defects.

III Contact simulation

In the polyhedral-based method, the contact restrictions are written in a similar way to the geometric ones. The derivations that follow in the rest of this chapter aim at enriching the definition of a polyhedron coming from features potentially in contact and not the polyhedron operands obtained by the geometric specification by zone. When we are dealing with a contact of bilateral nature, in which a mating feature has lower and upper limits, a double inequality expressing the translations and rotations of each discretization point is obtained in the same way as shown before in Eq.2.2. In that case, c is not a tolerance value but a clearance value between the matting surfaces. The double inequality can be written as a negative closed half-space as described in Eq.2.4, where the coefficients $a_{k1}, \dots a_{k6}$ depend on the translation and rotation of a particular point P_i. The term b_k is what we called the *second member* or *constant* and it depends on the clearance that were set for the specific contact.

$$\bar{H}_i^+ = \{\mathbf{x} \in \mathbb{R}^6 : b_k + a_{k1}x_1 + \dots + a_{k6}x_6 \geq 0\} \tag{2.4}$$

For the bilateral case, each point of discretization defines two half-spaces (inferior and superior limits) whose intersection, as defined in Eq.2.3, results in a polytope P.

a Unilateral contact constraints

The modeling of the unilateral nature of a contact in mechanics takes into account, on the one hand, the constraints that arise from the actual physical restrictions, and on the other hand, the mechanical forces that make the contact possible and that maintain it or not. The restrictions coming from the physical constraints depend on the contact model used and the system architecture as it will be explained in the next subsection. In terms of the nature of the contact, there are a few possible configurations for the static case of two planar surfaces in contact as depicted in Fig.2.3.

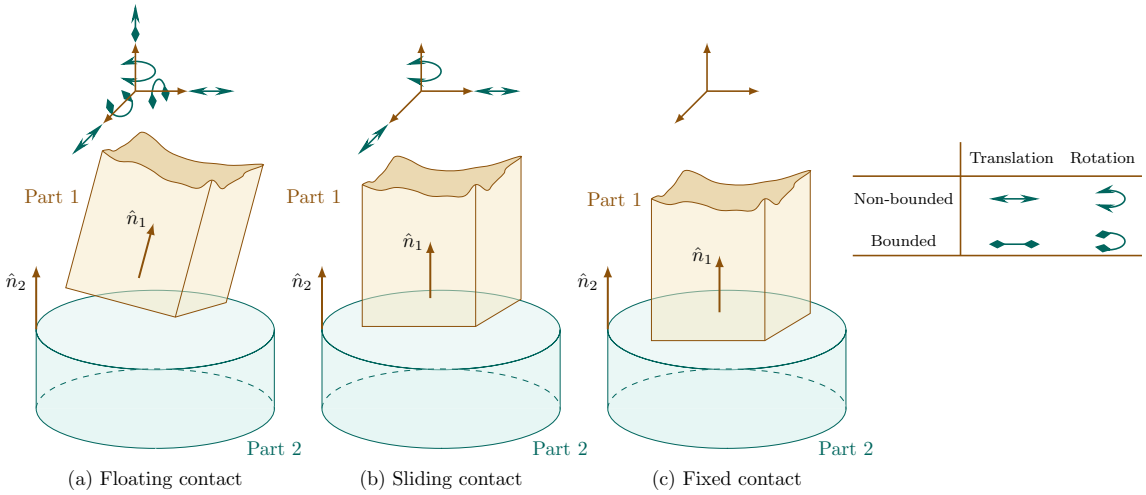

(a) Floating contact (b) Sliding contact (c) Fixed contact

Fig. 2.3 Cases of unilateral contact between two plane features

The relative displacements of the two parts change depending on the studied configuration. Fig.2.3a shows the floating configuration of the unilateral contact. In this case, all of the displacements, tangential and normal, are allowed. Since it is a planar contact, two translations and one rotation are nominally unconstrained (non-bounded) and the complementary two rotations and one translation are bounded by the physical limits of the contact. In [33, 99], the authors used regularized closure G functions and the virtual work principle to model the contact configuration.

Fig.2.3b represents a unilateral sliding contact in which the tangential displacements, non-bounded in the shown directions, are allowed between the parts. The normal displacements are null due to the action of a force that binds the two surfaces together in the direction of the contact surface normal. When modeling the relative displacements in unilateral cases, general approaches in the literature use a rigid or compliant models incorporating Linear Complementary Conditions (LCC) and frictional forces to establish the contact between two features [122, 139, 9]. This type of configuration is applied in this study.

Fig.2.3c shows a fixed contact, where all the relative displacements between the mating surfaces are null (zero DoF).

b Rigid contact model

The constraints that arise from a contact between two mating parts depend on the contact architecture, the materials at the interface and the forces to which the parts are subjected.

The parts in contact restrict the movements of one another, and they play a role in the general kinematic compatibility of the system. Efforts are transmitted from one workpiece to another giving place to interactions to happen through their interfaces. Due to the imperfections of the materials and the manufacturing processes used for building the workpieces, the interfaces are deviated from the perfect nominal description and are subjected to further distortion due to the deformation of the parts in contact and to their eventual deterioration. The contact model is chosen depending on the level of required accuracy or the type of phenomena to be considered. They are generally classified according to the rigidity of the pieces in contact in rigid [124], compliant or hybrid models [81].

Contact modeling is widely studied in the field of robotics [111, 72] and the modeling of the contact constraints in rigid body models is similar to the representation of contact restrictions in polyhedra approaches for tolerances analysis. Let us consider the two parts in Fig.2.4 to be in contact. The two points in contact, P_1 on part 1 and P_2 on part 2, are considered separately for the sake of the mathematical derivation of the following equations, but they are considered physically as a unique point.

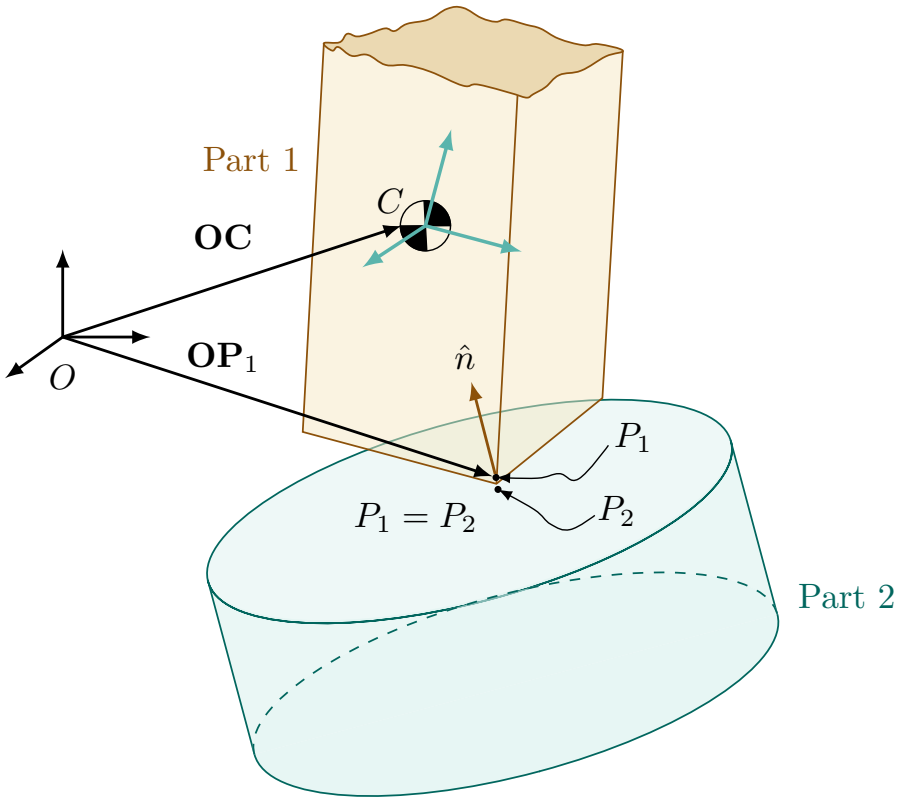

Fig. 2.4 Rigid-body contact model

From the screw theory perspective, the spatial velocity of a part can be expressed in terms of a *twist* [127]. We can define the twist of *Part 1* and *Part 2* relative to an inertial frame O as:

$$\mathbf{t}_1 = \begin{bmatrix} \omega_1 \\ v_1 \end{bmatrix}, \ \mathbf{t}_2 = \begin{bmatrix} \omega_2 \\ v_2 \end{bmatrix} \tag{2.5}$$

Where the angular velocity is $\boldsymbol{\omega} = (\omega_x, \omega_y, \omega_z)$ and the linear velocity of the centre of gravity relative to frame O is $\mathbf{v} = (v_x, v_y, v_z)$ for each part. The velocities on the contacts points P_1 and P_2 resulting from the twists of the two parts can be written as:

$$\dot{\mathbf{P}}_1 = \mathbf{v}_1 + \boldsymbol{\omega}_1 \times \mathbf{OP}_1, \ \dot{\mathbf{P}}_2 = \mathbf{v}_2 + \boldsymbol{\omega}_2 \times \mathbf{OP}_2 \tag{2.6}$$

Where $\dot{\mathbf{P}}$ is the velocity of the contact point and $\mathbf{OP}_1$ and $\mathbf{OP}_2$ are the position vectors of the contact points respect to the frame O. *Twists* are commonly expressed in the common world frame O, meaning that the linear velocity of a point rigidly attached to the part is considered as if it were currently at the origin world frame. If we consider only a first order analysis of the model, meaning that only the contact normal (disregarding the relative curvature of the parts in contact) is taken into account, the impenetrability of condition of a rigid-body can be written as:

$$\hat{\mathbf{n}} \cdot (\dot{\mathbf{P}}_1 - \dot{\mathbf{P}}_2) \geq 0 \tag{2.7}$$

In Eq.2.7, if $\hat{\mathbf{n}} \cdot (\dot{\mathbf{P}}_1 - \dot{\mathbf{P}}_2) = 0$ then the two parts in contact can slide relative to each other. The rest of the chapter will focus on this type of contact behaviour.

The unilateral nature of the contact implies that two parts remain in contact by the action of a force that binds them together. If an unit force is acting in the contact point in the direction of the normal $\hat{\mathbf{n}}$, we could define a generalized force as a wrench written at the world frame O as:

$$\mathbf{w} = \begin{bmatrix} \mathbf{OP}_1 \times \hat{\mathbf{n}} \\ \hat{\mathbf{n}} \end{bmatrix} \tag{2.8}$$

The first row in Eq.2.8 corresponds to the moment of an unit force relative to the world frame, the second is the unit force along the normal. Generally, when considering the contact between two parts, one is considered to be fixed and the other in movement. Let us consider *part 2* as being fixed, Eq.2.7 would be simply $\hat{\mathbf{n}} \cdot \dot{\mathbf{P}}_1 \geq 0$. This equation can be rewritten in terms of the *twist* and the *wrench* of a unique contact point as:

$$\mathbf{t}^T \mathbf{w} \geq 0 \tag{2.9}$$

In Eq.2.9 the inequality must be greater or equal to zero because the constraint is considered as stationary. This formulation is valid for frictionless contact only. If several forces are acting on the contact, each one of them would define a half-space that restricts the six-dimensional velocity space and their intersection defines a polyhedral convex cone that represents the feasible twists.

The first-order contact model for rigid bodies used in robotics is analogous to the polyhedral approach used in tolerance analysis as they both take advantage of the dual properties of twist and wrench spaces. In tolerance analysis by polyhedra, parts in contact are considered in a stationary state and the twists are used to define the kinematic compliance of the contact architecture of the system, special emphasis is made on the subspace of bounded displacements, that is the same subspace where the force restrictions lie, and in which the contact restrictions define a polytope that represents all the attainable positions of the two features in contact. In the next section, the polyhedral method and the incorporation of force half-spaces to simulate unilateral contact restrictions are explained.

IV Enriched polyhedra approach for mating surfaces

a Load boundary conditions

The half-spaces described in Eq.2.4 can represent a unilateral contact between two mating features. In this case, only one half-space per discretization point is obtained as the feature is only bounded either on the upper or lower limit. The intersection of such sets of constraints gives as a result an unbounded polyhedral operand instead of a polytope. When there are no form defects, the geometric specification of clearance equal to zero ($J = 0$) is enough to solve the contact as all of the restrictions intersect at the origin. When we include form defects, the specification of clearance is no longer enough. We propose here a method that enriches the definition of prismatic contact polyhedra by including load boundary conditions of parts in contact for, including but not limited to, bounding an open operand as the one obtained in the unidirectional case. The proposed method is explained for a rigid-body model disregarding frictional forces.

The work presented here is aligned with the method presented in Sec.III and since we are dealing with rigid body displacements, the Small Displacement Torsor (SDT) theory is subjacent when describing the displacements of a surface as described in [7]. To illustrate the method proposed in this work, it is necessary to review the basic assumptions underlying the definition of a unilateral contact using polyhedra.

b Ideal features

To better understand the contact between two ideal mating features, a procedure for defining a contact polyhedron, the inclusion of a force half-space, and the traceability of the vertices from the subspace of bounded displacements to the actual contact points in the geometry is illustrated in Fig.2.5. On the left of Fig.2.5, the two mating surfaces are shown: the rectangular planar surface S_1 and the circular planar surface S_2. At the top of Fig.2.5.a, the two mating features are represented, the contact element is defined from the intersection of both features and it is discretized in four points (P_1 to P_4). The point M is a calculation point with respect to which the contact restrictions are written.

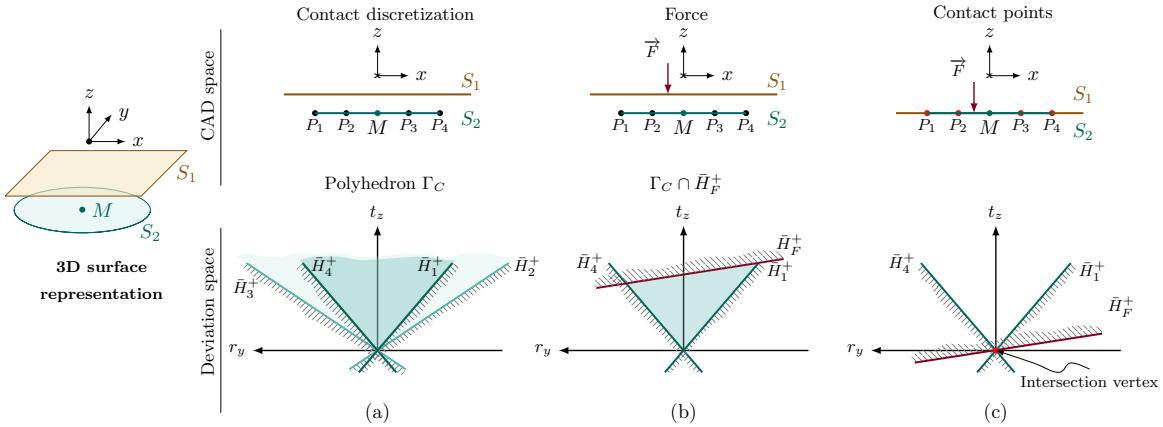

Fig. 2.5 On the left: 3D representation of two planar surfaces. (a) Top: 2D representation of two planar features without form defects; bottom: all of the half-spaces written at the points in the geometry. (b) Top: inclusion of force in the geometry; bottom: polyhedra coming from the intersection of the half-spaces and additional restriction coming from the force. (c) Top: the two surfaces are in contact by the action of the force; bottom: minimization of the volume.

By setting a contact clearance equal to 0 the contact restrictions can be derived from Eq.2.4, each of those restrictions represents a half-space in the subspace of bounded displacements, translation along z (t_z) and rotation along y (r_y), as it shown at the bottom part of

Fig.2.5.a. A discretization point in the *geometric space* will generate one half-space in the *Deviation space* as we are dealing with unilateral contact restrictions, so point P_1 generates half-space $\bar{H}_1^+$, point P_2 generates half-space $\bar{H}_2^+$, and so on. The bar at the top of $\bar{H}$ just means that the half-space frontier is included and the sign $+$ means that we remain on its positive. The intersection of the four half-spaces results in the convex polyhedron depicted in the darker blue region in between $\bar{H}_1^+$ and $\bar{H}_4^+$, the other two half-space are less restrictive.

The polyhedron is unbounded due to the unilateral contact. In order to perform the subsequent operations between polyhedra, specially for the Minkowski sum, bounded operands are introduced. Authors have tried to bound these operands with artificial half-spaces [64] leading to more complex topology of the operand which increases the computation time. Instead of adding artificial half-spaces to bound the operand, we propose to integrate into the polyhedra model the effect of external mechanical forces. At the top part of Fig2.5.b a force F is depicted between P_2 and M. Let us name its point of application as N and its local normal as $\hat{\mathbf{n}}$. This force will push feature S_1 towards S_2 and eventually it will prevent partially or fully the relative displacements between two mating features. We can write a generalized force as a *wrench* using Eq.2.8 as:

$$\begin{cases} \sum F \cdot \hat{\mathbf{n}} \\ \sum \mathbf{MN} \times (F \cdot \hat{\mathbf{n}}) \end{cases} \tag{2.10}$$

In Eq.2.10, F can be taken as the unit force in the direction of $\hat{\mathbf{n}}$ and its moment expressed in M as the position vector $\mathbf{MN}$ times the unit force. This generalized force describes an additional restriction that can be expressed in the same way as the half-spaces coming from the actual contact restrictions as in Eq.2.11. The additional restriction is of a different nature than the restrictions coming from the contact, the difference resides in the second member b_f which is 0 for all of the half-spaces coming from the contact with no form defects but it is initially undefined for the force half-space, this means that this half-space is actually floating in the subspace of bounded displacements.

$$\bar{H}_f^+ = \{\mathbf{x} \in \mathbb{R}^6 : b_f + a_{k1}x_1 + ... + a_{k6}x_6 \geq 0\} \tag{2.11}$$

For a force to bound an unbounded contact polyhedron, it is important to verify certain requirements. Fig.2.6 shows the verification process for bounding an unbounded polyhedron operand through a generalized force. After writing the generalized force, the kinematic compliance of the contact needs to be checked, this means that there cannot exist components of the force in the directions of the unbounded displacements of the contact. Each one of the

unbounded displacements of the contact is characterized by a straight line Δ_j in $\mathbb{R}^6$ passing through the origin as shown in Eq.2.12.

$$C = \sum_{j=1}^{d} \Delta_j, \text{ with } d \leq 6 \tag{2.12}$$

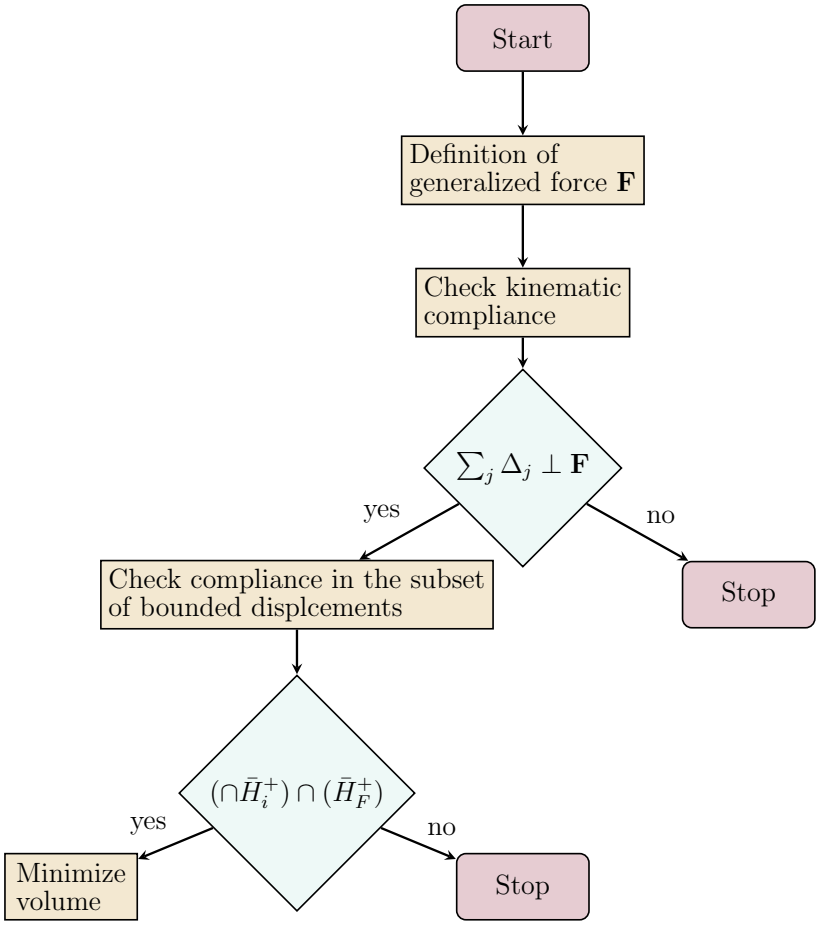

Fig. 2.6 Verification process for bounding an unbounded polyhedron

The verification of the kinematic compliance can be done by checking the perpendicularity of the straight lines with respect to the direction of the generalized force. If this is not achieved, it simply means that the system is not in a stationary state and further analysis cannot be done. If there is kinematic compliance, then the compliance in the subset of bounded displacements can be checked. This verification can be done by considering the direction and the point of application of the force. A half-space coming from a force bounds an operand if $(\cap \bar{H}_i^+) \cap (\bar{H}_F^+)$ is bounded. In the case shown at the top of Fig.2.5.b, the direction of the force is perpendicular to the straight lines that describes the unbounded displacements of the contact (t_x), the point of application of the force (in between M and

P_2) dictates the orientation of the half-space. Its direction, from S_1 to S_2, determines the side, positive or negative, of the half-space to be kept. The force has to be applied within the physical limits of the contact element, and the unstable limits are the two points at the extremities of the feature S_2, beyond those, the described half-space cannot longer bound the polyhedron.

At the bottom of Fig.2.5.c, a vertex coming from the intersection of all of the half-spaces is found by searching for the vertex that minimizes the volume of the bounded operand. This search will retrieve, in stable cases, a vertex in the subspace of bounded displacements, as this vertex comes from the intersection of some (or all) half-spaces, the actual points in contact (P_1 to P_4) can be retrieved from the polyhedron to the CAD space as seen at the top of Fig.2.5.c. The solution here is trivial as we are dealing with planar surfaces with no form defects. When there are no form defects, a singleton centred at the origin of the subspace of bounded displacements will be always found. This solution is implicitly in the geometric specification of clearance equal to zero ($J = 0$).

A polyhedron operand can be decomposed as shown in Eq. 2.13. A polytope plus a set of the straight lines that describe the degree of freedoms of the contact. The polytope can be further decomposed into the actual contact restrictions that define a bounded or unbounded set; and a generalized force, or set of forces, that serves at bounding an open set and at finding the contact points between two mating features by minimizing the volume of the operand. This definition enriches the concept of contact polyhedra used in tolerance analysis.

$$
\begin{aligned}
&\Gamma = P \oplus C \\
&\text{where:} \\
&P = min[(\cap \bar{H}_i^+) \cap (\bar{H}_F^+)]_{vol} \\
&C = \sum_{j=1}^{d} \Delta_j, \text{ with } d \leq 6 \\
&\text{with} \begin{cases} \bar{H}_i^+ & = \{\mathbf{x} \in \mathbb{R}^6 : b_k + a_{k1}x_1 + ... + a_{k6}x_6 \geq 0\} \\ \bar{H}_F^+ & = \{\mathbf{x} \in \mathbb{R}^6 : b_f + a_{k1}x_1 + ... + a_{k6}x_6 \geq 0\} \end{cases}
\end{aligned}
\tag{2.13}
$$

c Non-ideal features

Taking into account the form defects of mating surfaces does not change the approach mentioned in the previous subsection. The topology of the polyhedral operand becomes more

complex, making the restrictions, when the clearance is equal to 0, not pass all through the origin of the deviation space. At the left part of Fig.2.7, the two mating surfaces S_1 and S_2 are not ideal features. Their representation can be seen at the top of Fig.2.7.a. The procedure is the same as before: the two features are discretized and the contact element is the intersection of the two features. The lines represent the form defects for both S_1 and S_2. Dealing with the contact between an ideal and a non-ideal feature is easier than between two non-ideal features, that is why in the middle part of Fig.2.7.a, a difference surface [115] is computed by taking the deviation at each point of S_2 and subtracting the deviation of the corresponding point of feature S_1. The result is a difference surface that embodies the form defects from both of the surfaces (S_{diff}), and an ideal surface S'_1. At the bottom of Fig.2.7.a, we can see that the restrictions do not intersect at the origin and that only one half-space ($\bar{H}_3^+$) does not restrict the resulting operand. The polyhedron is depicted as the darker blue region product of the intersection of the restriction imposed by P_1, P_2 and P_4.

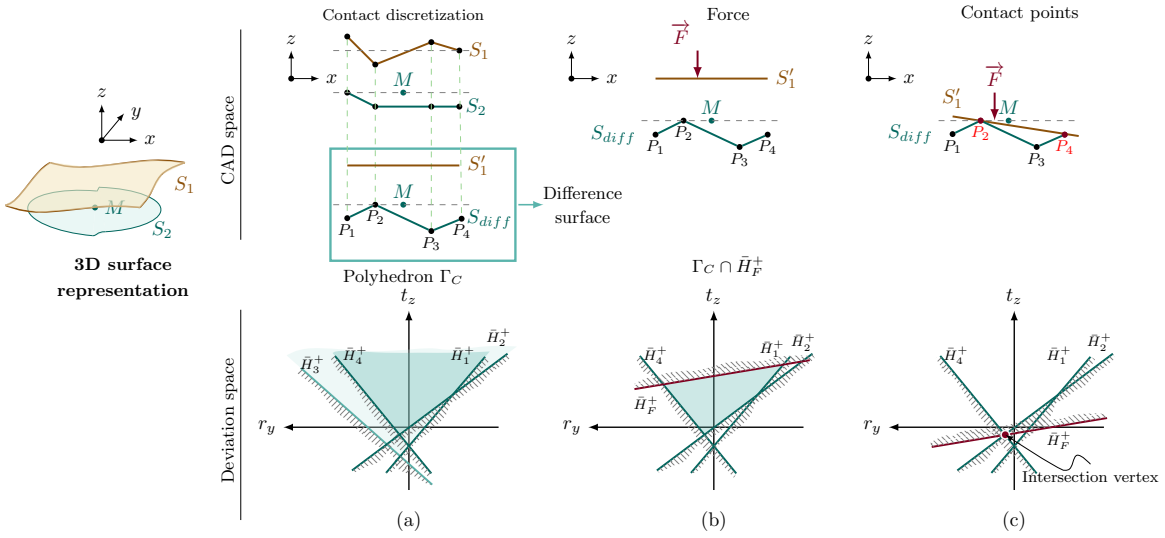

Fig. 2.7 On the left: 3D representation of two planar surfaces with form defects. (a) Top: 2D representation of two planar features with form defects; middle: difference surface; bottom: all of the half-spaces expressed at point M in the geometry. (b) Top: inclusion of a force in the geometry; bottom: polyhedra coming from the intersection of the half-spaces and additional restriction coming from the force. (c) Top: the two surfaces are in contact by the action of the force; bottom: minimization of the volume.

In Fig.2.7.b, the depicted force pushes S'_1 against S_{diff} to establish the contact. Once the verifications shown in Fig.2.6 are done, the force can be represented as the additional half-space in red shown at the bottom of Fig.2.7.b. The search for vertex (edge or facet) that minimizes the volume in the deviation space will retrieve the contact points in geometric

space as shown in Fig.2.7.c. In this case, the vertex that minimizes the volume is the one coming from the restriction written at P_1 and P_4 meaning that these are the points in contact in the geometry.

V Case Study

The described method has been applied to the case of a spectrometer whose CAD model is shown in Fig.2.8a. This example was previously used in [38] for modeling the contact between three parts, disregarding the form defects and not including the load-boundary conditions. The spectrometer is conceived for measuring the spectral properties of an ion beam in a portion of the electromagnetic field. The two coils, fixed on the massive part, generate an electromagnetic field for spacing the electrons in the ion beam so they can be counted. For the current case, only two parts from the system are considered: the massive part $(2,0)$ and the magnetic pole $(3,0)$.

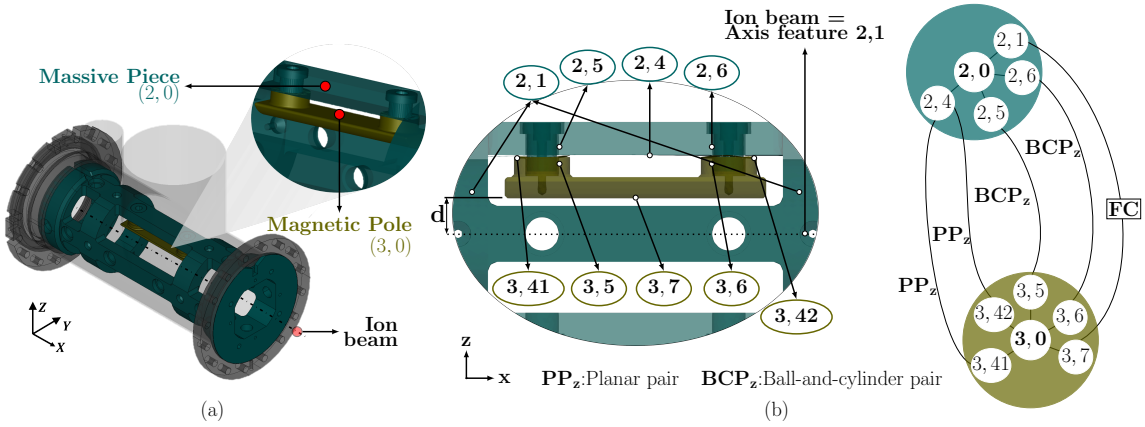

Fig. 2.8 (a) CAD model of the system. (b) On the left: parts in contact with influential features; on the right: contact graph

The small displacements between the two cylindrical coils fixed to $2,0$ with respect to the two cylindrical holes in the magnetic pole $(3,0)$ impose the limits in translation in x and y (t_x, t_y) directions and in rotation along the z direction (r_z). The amplitude of such small displacements depends on the clearance of the contact and the form defects of both parts. The parts are linked by two screws that pass through two cylindrical coils. They restrict the relative movements between the two planar features in translation along z (t_z), and rotation along x and y (r_x, r_y). This means that the *Degrees of Freedom* (DoF) of the planar contact are limited by the relative displacements of the two cylinders in the two holes. In other words,

the sliding behaviour of the planar contact is limited by the ball-and-cylinder contacts.

Fig.2.8b is composed of a zoomed 2D view at the contact with its influential features on the left; and a contact graph on the right. Regarding the topology of the graph on the right, all the nodes belonging to one part are connected to at least one node in another part, and an edge linking two matting surfaces from distinct parts describes a contact polyhedron. A secondary node represents one of the features (i.e. a surface) that takes part in the studied contact. A primary node ($2,0$ and $3,0$) represents a part involved in the contact. An internal edge links the part to a feature and it is represented by a geometrical polyhedron that describes the geometrical variations and form defects of that feature in the part. Features $3,41$ and $3,42$ are the two planar features from the magnetic pole in contact with feature $2,4$ from the massive part and they are considered separately as seen in the contact graph. Features $3,5$ and $3,6$ correspond to the cylindrical surfaces of holes in the magnetic pole and $2,5$ and $2,6$ to the cylindrical surfaces of the two coils fixed to the massive part.

The *functional condition* (FC) to study is the positioning of the ion beam respect to feature $3,7$ (distance d) that is half of a cylinder at the bottom of the magnetic pole. The ion beam is assumed to be the axis of a unified featured made up of two coaxial cylindrical features from the massive part as indicated in Fig.2.8b. The two features that participate in the FC ($2,1$ and $3,7$) are referred to here as *handle features*. The FC is represented as a polyhedron with a functional tolerance.

$$\Gamma_R = \Gamma_{3,7/3,0} \oplus \Gamma_{3,0/2,0} \oplus \Gamma_{2,0/2,1} \tag{2.14}$$

The contact graph is reduced through a composition of operations (Minkowski sums and intersections) as shown in Eq.2.14 in which each of the terms is a prismatic polyhedra and $\oplus$ is the Minkowski sum. The operands $\Gamma_{3,7/3,0}$ and $\Gamma_{2,0/2,1}$ are the two handles features. To obtain $\Gamma_{3,0/2,0}$, the operations described in Eq.2.15 need to be performed.

$$\begin{cases} \Gamma_{3,0/2,0} = \Gamma_{3,0/2,0-a} \cap \Gamma_{3,0/2,0-b} \cap \Gamma_{3,0/2,0-c} \cap \Gamma_{3,0/2,0-d} \\ \Gamma_{3,0/2,0-a} : \text{Contact polyhedron between } 3,41 \text{ and } 2,4 \\ \Gamma_{3,0/2,0-b} : \text{Contact polyhedron between } 3,42 \text{ and } 2,4 \\ \Gamma_{3,0/2,0-c} : \text{Contact polyhedron between } 3,5 \text{ and } 2,5 \\ \Gamma_{3,0/2,0-d} : \text{Contact polyhedron between } 3,6 \text{ and } 2,6 \end{cases} \tag{2.15}$$

Breaking down operand $\Gamma_{3,0/2,0-a}$, the term $\Gamma_{3,41/2,4}$ is the contact polyhedron between the two matting features with form defects ($3,41$ and $2,4$) and it embodies its DoF and the contact restrictions. It is the same for the rest of the operands ($\Gamma_{3,0/2,0-b}$, $\Gamma_{3,0/2,0-c}$ and $\Gamma_{3,0/2,0-d}$). The reduction of the graph gives as a result in this case a singleton in $\mathbb{R}^6$ as it will be shown later in Fig 2.11.

$$\begin{aligned}\Gamma_F &= \Gamma'_{3,7/3,0} \oplus \Gamma'_{2,0/2,1} \\ &= \tfrac{1}{2} t_{f_1} \Gamma'_{3,7/3,0} \oplus \tfrac{1}{2} t_{f_2} \Gamma'_{2,0/2,1}\end{aligned} \tag{2.16}$$

Once the Γ_R is obtained, it is necessary to verify its inclusion in the functional polyhedron, but more importantly, to find the optimal tolerance of circumscription as specified in [38]. The functional polyhedron (Γ_F) can be calculated as shown in Eq.2.16. $\Gamma'_{3,7/3,0}$ and $\Gamma'_{2,0/2,1}$ are operands created from the handle surfaces, and t_{f_1} and t_{f_2} are functional tolerances (inititally set to 1) that serve to obtain the optimal tolerance of circumscription of the operand. The tolerance of circumscription that defines the circumscription polyhedron ($\Gamma_{F_{circ}}$) is calculated using the method explained in [38].

a Deviation modeling and operand creation

The framework mentioned in Section 1 was used for obtaining the Skin Model Shapes (SMS). From the CAD model, the features are partitioned and then meshed as shown in Fig. 2.9.a. The features coming from the magnetic pole ($F3,41$ and $F3,42$) share the same mesh; feature $F2,4$ was meshed differently.

The features were partitioned and meshed in Salome platform and then imported to PolitoCAT, an open source Computer-Aided Tolerancing tool based on OpenCascade kernel, in which the deviation modeling [104] and operand creation took place. At the top of Fig.2.9.b, the two matting planar features are shown with form defects that were induced during the deviation modeling phase. A modal-based method using vibration modes [116] was used to model systematic deviations for the three features. The modal signature decreases following the function $\frac{1}{n}$ [115], where n is the number of modes, one-hundred in this case. The maximum amplitudes for features $F3,41$ and $F3,42$ were set to $0.1\,mm$, and it was $0.2\,mm$ for feature $F2,4$. Random Gaussian Fields method was used to simulate the random deviations for the three features as well. Once the SMS have been generated, the difference surface is computed, leading to a feature of perfect form ($F2,4'$) and two equivalent features ($F3,41$

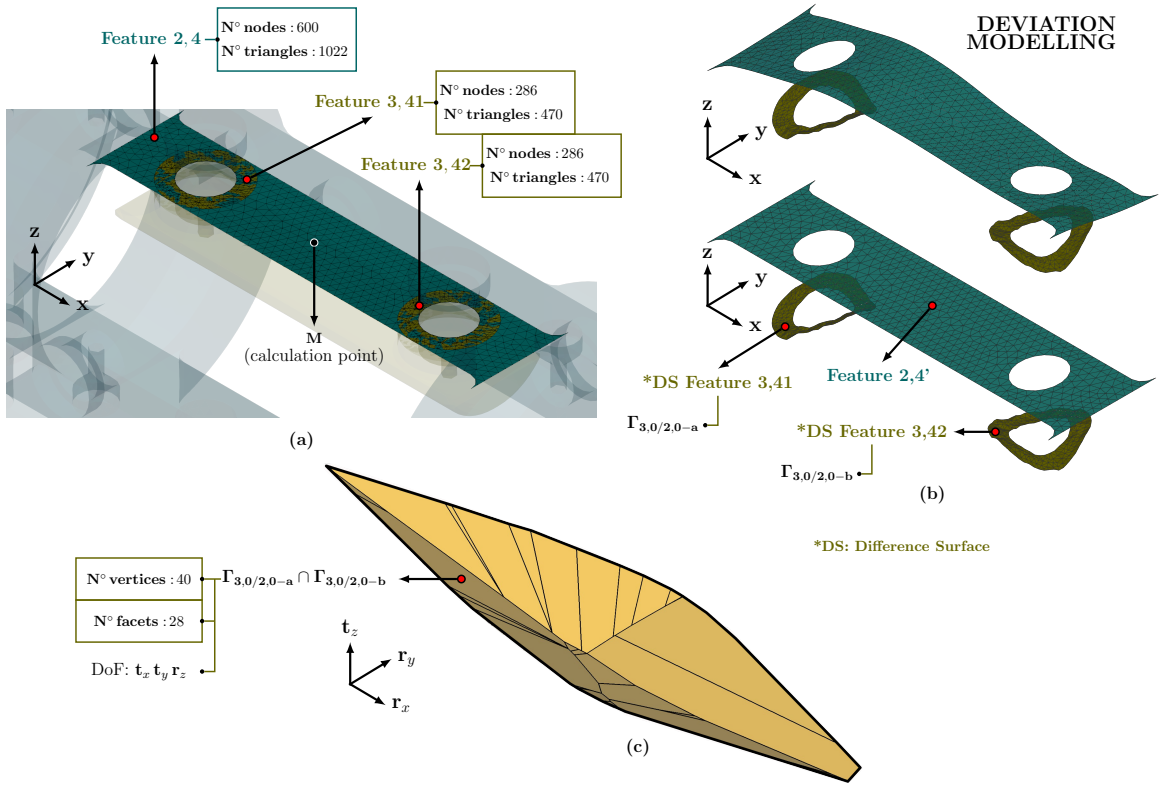

Fig. 2.9 a) Partitioned and meshed planar features. b) On the top: planar features with form defects (defects x10 times bigger for visualization); at the bottom: difference surfaces and ideal surface. c) Prismatic polyhedra coming from the intersection of the two features with form defects.

and $F3,42$) that embody the deviations from $F2,4$ and themselves as shown at the bottom of Fig.2.9.b. Each of those equivalent features results in a polyhedron operand described by the operand shown in the image which is a part of Eq.2.15.

The intersection of the restrictions coming from the previous features gives as a result an unbounded polyhedron shown in Fig.2.9.c. This polyhedron exists in the subspace of bounded displacements characterized by the rotation along x and y and the translation along z. The operand is unbounded due to the unilateral nature of the contact. The straight lines of the polyhedron operand (Eq.2.12) describe its degrees of freedom, here the translations along x and y and rotation along z.

For the features involved in the ball-and-cylinder pairs ($F3.6$, $F2,6$, $F3,5$ and $F2,5$) form defects were not considered. The features were partitioned and meshed directly in PolitoCAT using only six discretization nodes as it can be seen in Fig.2.10.a. The length

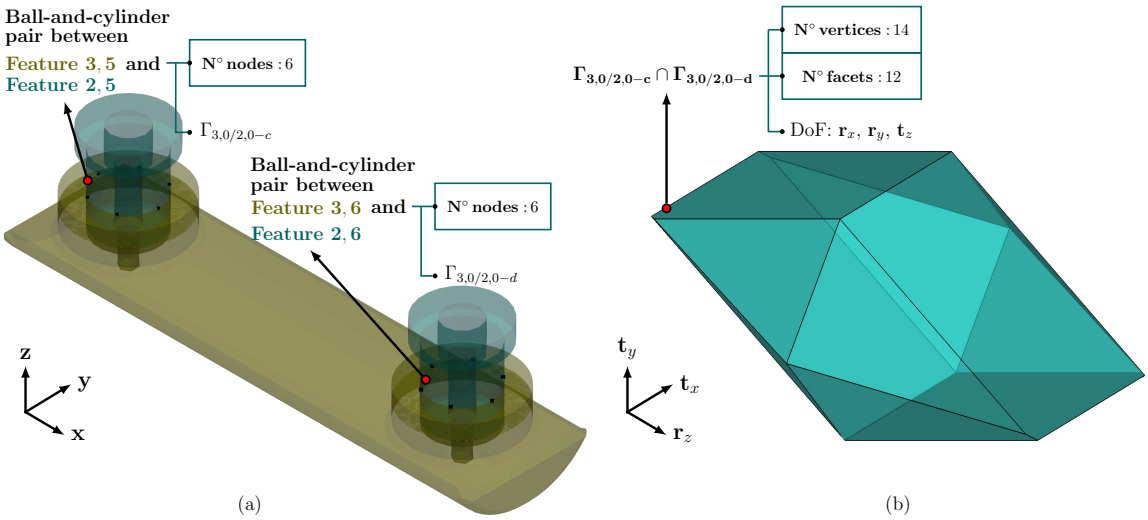

Fig. 2.10 a) Partitioned and meshed ball-and-cylinder pairs. b) Prismatic polyhedra coming from the intersection of the two features without form defects.

of the coils entering the two holes is considered to be short, so the contact is reduced to a line. The features are restricted in translation along x and y and in rotation along z. These restrictions define, for each of the features, a polyhedron operand as described in Eq.2.15. The clearance value for both ball-and-cylinder pairs was initially 0.034. In Fig.2.10.b, the bounded operand results from the intersection of $\Gamma_{3,0/2,0-c}$ and $\Gamma_{3,0/2,0-d}$. The operand is bounded in this case because the contact is of bilateral nature. Its topology is invariant for different clearance values if the number of discretization points is kept the same. The 14 vertices of the polyhedron operand represent the extremal positions of the two ball-and-cylinder pairs, therefore the limits of the relative displacements between the planar features.

b Load boundary conditions

The magnetic pole and the massive part are kept in place by the action of two screws that pass through the coils making the two planar surfaces to be in contact. The two screws exert each a force along $-z$ and it was considered that they were tightened simultaneously. The action of both forces can be written as a generalized force at point M using Eq.2.8 as:

$$\mathbf{w_1} = \begin{bmatrix} \mathbf{MF_1} \times -\hat{\mathbf{z}} \\ -\hat{\mathbf{z}} \end{bmatrix} \qquad \mathbf{w_2} = \begin{bmatrix} \mathbf{MF_2} \times -\hat{\mathbf{z}} \\ -\hat{\mathbf{z}} \end{bmatrix} \tag{2.17}$$

The calculation point M is in the middle between the two coils. In Eq.2.17, $\mathbf{MF_1}$ is the position vector from the calculation point to the force passing through the left screw whose value is $-50\,mm$ in the x direction. The intensity of the force is not important in our case because the parts are considered rigid, so the forces acting through both screws can be taken as an unit force along the $-z$ direction. In Fig.2.11.a, the resultant force is depicted at calculation point M. This force generates an additional restriction in the deviation space as seen in Fig.2.11.b. The only component of the force is perpendicular to the straight lines representing the DoF of the contact ($\mathbf{t}_x$, $\mathbf{t}_y$, $\mathbf{r}_z$) meaning that there is kinematic compliance (first requirement in Fig.2.6). Since the forces lie within the physical limits of the contact, and that their directions activate the contact between the two mating surfaces, then the half-space can turn the unbounded operand into a bounded one.

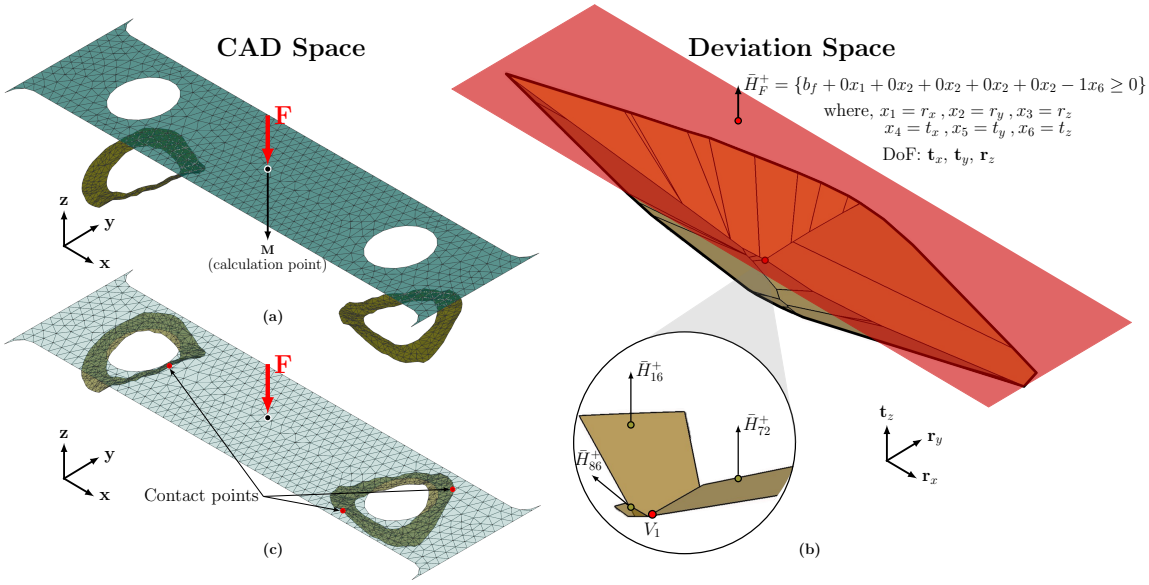

Fig. 2.11 a) Equivalent force from the two screws expressed at calculation point M. b) Unbounded prismatic polyhedra with the additional half-space coming from the load boundary conditions. Below: zoom at the vertex that minimizes the volume coming from the intersection of three half-spaces. c) Contact points in the geometry traced back from the deviation space.

At first, the additional restriction does not have a specific value for its constant (b_f in the equation shown in Fig.2.11.b), meaning that the half-space is floating in the subspace of bounded displacements. The value of its constant will be only determined once the minimization of volume has taken place. In Fig.2.11.b, V_1 is the vertex of the polyhedron that minimizes the volume of the operand. Since the resulting polyhedra operands are always convex and prismatic, the minimization simply consists of searching for the farthest vertex in the polyhedron. The vertex V_1 comes from the intersection of three half-spaces ($\bar{H}_{16}^+$, $\bar{H}_{72}^+$

and $\bar{H}_{86}^{+}$), which come from the contact restrictions written at the contact points depicted in Fig.2.11.c, which shows the perfect traceability that exists from the deviation space to the CAD space, and vice versa.

c Sliding contact simulation

For simulating the sliding behavior of the planar contact, we assumed that the two surfaces are not in contact and that the two coils are perfectly centered in the two holes. The previous simulation was carried out with a clearance value of $0.034\,mm$ for both ball-and-cylinder pairs. The amplitude of the clearance for the ball-and-cylinder pairs constrains the maximum relative displacements allowed between the two planar features. The simulations were carried out for only one instance of form defects as explained in section a, but since they are discrete, a small change in their relative positioning makes that the difference surface has to be recalculated. The polytope depicted in Fig.2.10.b represents the 14 extremal positions of the two ball-and-cylinder pairs, which means that for a given clearance value, there are 15 different configurations for the two planar surfaces: the initial configuration, that corresponds to the case where the two coils on the massive part are perfectly centred in the two holes on the magnetic pole; and the 14 extremal positions represented by the polytope in Fig.2.10.b. Each one of these 15 positions generates an unbounded polyhedron coming from the planar features. The additional restriction coming from load boundary conditions bounds the operand and the minimization of its volume results in a unique singleton in $\mathbb{R}^6$, meaning that for a given clearance value we have 15 singletons in $\mathbb{R}^6$ coming from the minimization of the volume of 15 polyhedra operands.

We ran simulations for six different clearance values ($0.034\,mm$, $0.063\,mm$, $0.094\,mm$, $0.125\,mm$, $0.25\,mm$ and $0.5\,mm$). Each one of those clearance values results in 14 singletons, meaning that we have 84 singletons for all the clearance values. An extra simulation without form defects was also ran. In Fig 2.12, the shown polytope is the operand that circumscribes the 84 singletons shown in black the zoomed view. The red cross inside the circle is the singleton coming from the simulation without form defects. As it can be seen, adding form defects results in a cloud of points that is more restrictive to the circumscription than when disregarding the form defects.

d Topological evaluation of the resultant polyhedron

We have 14 polyhedra for each one of the six clearance values of the ball-and-cylinder pairs. These polyhedra result from the intersection of the two annular planar features with the planar

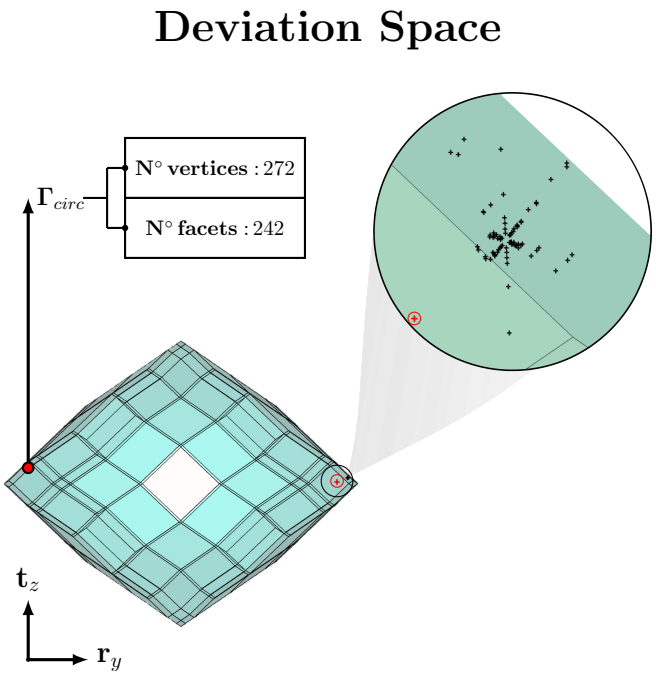

Fig. 2.12 Circumscription polyhedron with topological information. The black crosses are the 84 points coming from the simulation with form defects for different clearance values. The red cross inside the circle is the singleton coming from the simulation without form defects

feature from the massive piece as explain in Fig.2.9. This intersection is performed each time that the relative displacement between the matting surfaces is updated. The resultant polyhedron from this intersection is never the same to any of the other 14 polyhedra regarding the position of each vertex and its extensive properties. However, the local topology of the vertex that minimizes the volume of the operand can be invariant for all the polyhedra.

In table 2.1, the half-spaces that generate the vertex that minimizes the volume for each one of the 14 polyhedra per clearance are shown. We can see that for the clearance values from 0.034 *mm* to 0.125 *mm* there exist local topology invariance as the vertex is generated with the same half-spaces. For the clearance of 0.25 *mm*, out of the 14 polyhedra, 10 of the vertices that minimizes the volume are generated by the same half-spaces than before, and 4 are generated by other half-spaces meaning that in this case, the topology of the operand changes locally in relation to the other operands. For the last clearance, there are three topological different polyhedral operands.

Table 2.1 Table Caption

Clearance	Case	Frecuency	Half-spaces	Percentage
0.034	case 1	14	$\{\bar{H}_{16}^{+}, \bar{H}_{72}^{+}, \bar{H}_{86}^{+}\}$	100%
0.063	case 1	14	$\{\bar{H}_{16}^{+}, \bar{H}_{72}^{+}, \bar{H}_{86}^{+}\}$	100%
0.094	case 1	14	$\{\bar{H}_{16}^{+}, \bar{H}_{72}^{+}, \bar{H}_{86}^{+}\}$	100%
0.125	case 1	14	$\{\bar{H}_{16}^{+}, \bar{H}_{72}^{+}, \bar{H}_{86}^{+}\}$	100%
0.25	case 1	10	$\{\bar{H}_{16}^{+}, \bar{H}_{72}^{+}, \bar{H}_{86}^{+}\}$	71.4%
	case 2	4	$\{\bar{H}_{16}^{+}, \bar{H}_{73}^{+}, \bar{H}_{87}^{+}\}$	28.6%
0.5	case 1	7	$\{\bar{H}_{16}^{+}, \bar{H}_{72}^{+}, \bar{H}_{86}^{+}$	50%
	case 2	4	$\{\bar{H}_{16}^{+}, \bar{H}_{73}^{+} \bar{H}_{87}^{+}\}$	28.6%
	case 3	3	$\{\bar{H}_{16}^{+}, \bar{H}_{86}^{+},, \bar{H}_{97}^{+}\}$	21.4%

The change on this topology depends on a manifold of variables including: the mesh density and distribution, the type of defects on the features and the clearance value for the ball-and-cylinder pairs.

e Quantification of the impact of form defects

In Fig.2.13, the graph shows the impact of form defects in the tolerance of circumscription for different values of clearance of BCP_x. These simulations were conducted for only one instance of form defects, from the smallest to the largest clearance value, and the vertices from the polytope generated at each stage were kept for the subsequent simulations; so the simulation with a clearance value of $0.063\,mm$ includes the vertices from the polytope with a clearance of both $0.063\,mm$ and $0.034\,mm$. As it is clear, the impact of the form defects becomes larger as the amplitude of the small displacements between the two planar features increases.

$$r_{form} = \frac{(Tol_{opt})_{Form} - (Tol_{opt})_{NoForm}}{(Tol_{opt})_{NoForm}} \times 100 \tag{2.18}$$

The value of tolerance of circumscription is an indicator that only has meaning relatively, so in order to know the contribution of the form defects to the functional tolerance we performed the same simulation but considering only the rigid displacements of the features, meaning that we filtered out the form defects from the two planar surfaces. In this case, only one simulation is necessary as the difference surface is invariant in this case. The rate r_{form} shown in Eq.2.18 gives the percentage of the impact of the form defects on the tolerance

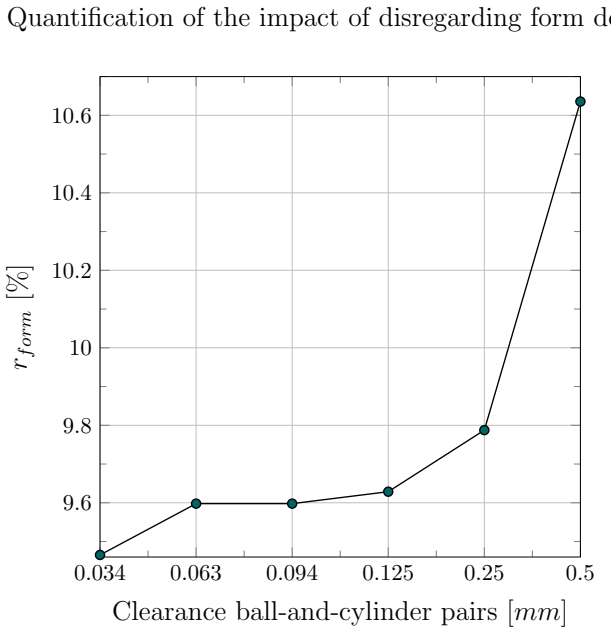

Fig. 2.13 Impact of the form defects on the functional tolerance for different values of clearance of the ball-and-cylinder pairs

circumscription. Including the form defects for the case of a clearance value of 0.034*mm* results in a 9.46% bigger tolerance of circumscription than without form defects, and in 10.64% for the case of 0.5*mm* clearance. These values shows the impact of the form defects on the translation along *z* and the rotation along *y* for the functional condition.

VI Computational complexity

To illustrate the complexity, let us take a simple example of the stacked cubes shown in Fig.2.14.a: the action of a external force maintains the contact between the two blocks.

In this example, both features were identically meshed and the density was varied from 25 nodes to 625 nodes as it is shown in Table 2.2. The different activities for obtaining the vertex that minimizes the volume of the operand cannot currently be run automatically one after the other, a process of preparation time is needed before and after the difference surface calculation. Table 2.2 shows the runtime for the generation of instances of skin model. All of the simulation were performed with a Intel(R) Core(TM) i5-8265U CPU of 1.60GHz. The time here does not vary significantly as the same modal base method was used for all of the instances. The modal signatures were different for top and bottom features. The time taken

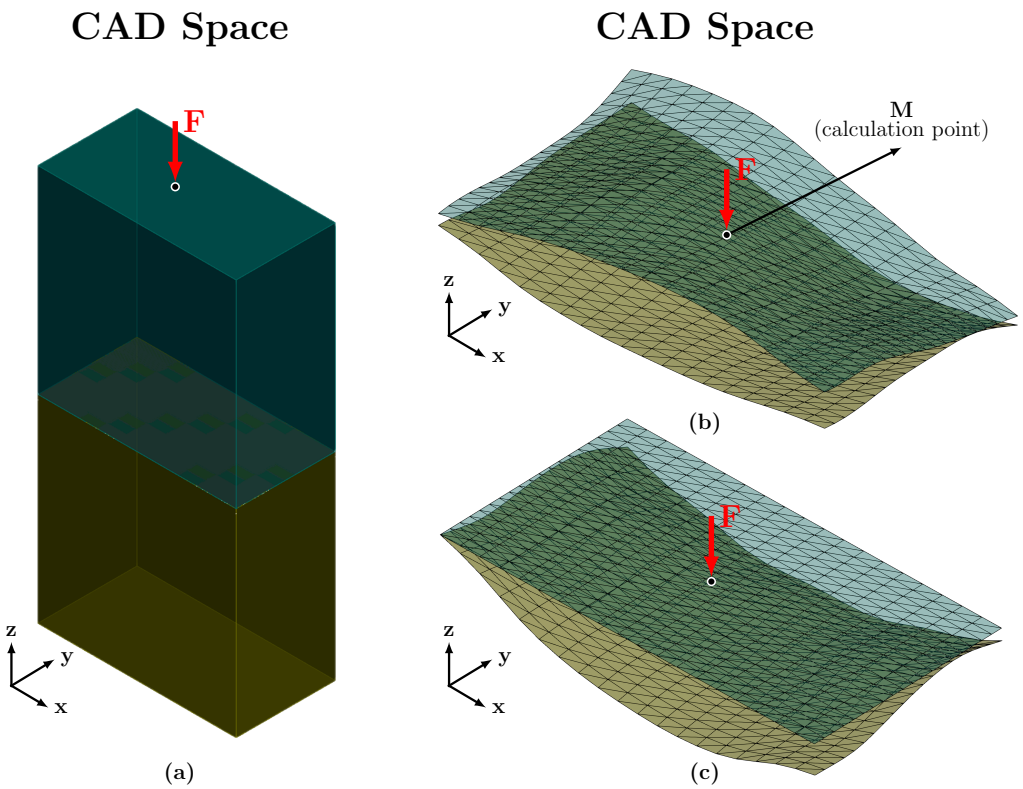

Fig. 2.14 a) 3D model of two stacked cubes under the action of a force. b) Skin Model Shapes of the two features in contact. c) Difference and equivalent surfaces of features in contact

in this stage was mainly due to the loading of the modal base of one hundred modes. When we used a base already loaded in PolitoCAT the deviation computation took only about 200 *ms* per instance.

In this case, the difference surface can be obtained by subtracting the deviation values of top feature from the deviation values in the bottom one. This is because the meshes are the same for both features. As it is seen, the time taken to compute the difference slowly increases as the number of nodes does. The last operation (Runtime Minimization in the table) consists of two operations: first, computing the double description of the polytope resulting from the difference surface. This operation allows us to exploit not only the half-spaces but also the vertices in the polytope. As the number of half-spaces increases, the computation of the double description grows exponentially. The second part consists on finding the vertex that minimizes the volume of the operand. This took about 200 *ms* for each one of the instances of the difference surface.

Mesh	**Number of nodes**	**Runtime SMS generation (ms)**	**Runtime difference surface (ms)**	**Runtime Minimization (ms)**	
				HV-Description	**Total**
Bottom 1	25	2195	16.2160	66	267
Top 1	25	2322			
Bottom 2	100	2263	25.636	266	479
Top 2	100	2357			
Bottom 3	225	2265	30.644	1199	1385
Top 3	225	2376			
Bottom 4	400	2367	32.51	4066	4292
Top 4	400	2492			
Bottom 5	625	2468	33.516	12539	12794
Top 5	625	2482			

Table 2.2 Runtime by activities (units in milisenconds). Computation time for: computing the Skin Model Shapes, the difference surface, and to find the vertex that minimizes the volume of the bounded operand.

The minimization time is virtually the same for all of instances because the topological complexity of operands does not change that much as the number of nodes increases. This can been in Fig.2.15 in which the operand showed in Fig.2.15.a corresponds to the contact features with a mesh density of 25 nodes and only 6 half-spaces generate the operand, and the last operand Fig.2.15.e corresponds to the contact features with 625 nodes each and for which only 18 facets generate the resulting operand. The 6 nodes from the first case and the 18 from the last one mean that only six nodes from the first contact and 18 nodes from the last contact are part of the convex hull of the difference surface in the euclidean space.

We can note that there is no difference between the operands with 225 and 400 nodes in the number of vertices and facets. The amount of nodes that constraint a polyhedral operand depends on the nature of its defects: difference surfaces that are very convex will generate more complex topologies in the deviation space, while less convex geometric defects will result in less amount of restrictive half-spaces.

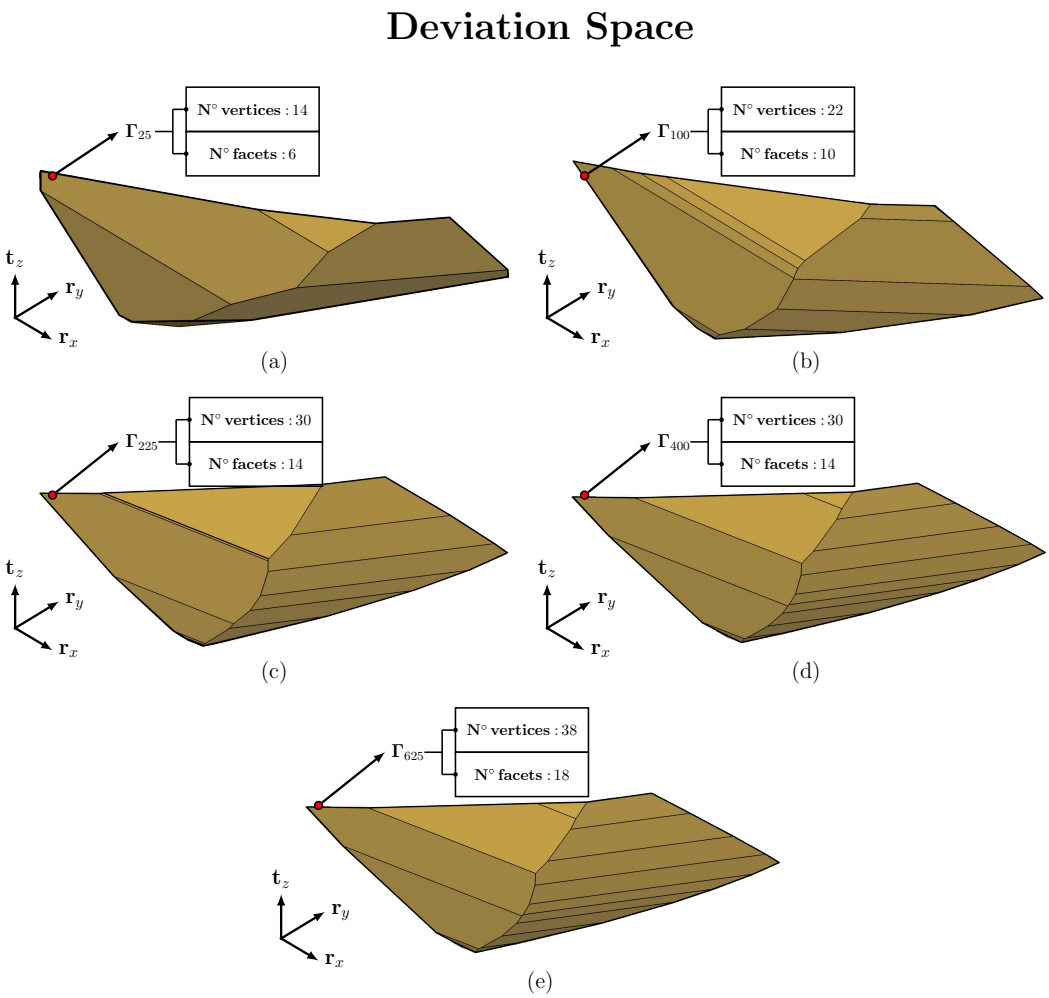

Fig. 2.15 a) Polytope from geometry discretization of 25 nodes. b) Polytope from geometry discretization of 100 nodes. c) Polytope from geometry discretization of 225 nodes. d) Polytope from geometry discretization of 400 nodes. e) Polytope from geometry discretization of 625 nodes

VII Conclusions and perspectives

In this work, a method for the inclusion of load boundary conditions in a polyhedral-based method was presented. A richer definition of a polyhedron operand in the context of tolerance modeling was proposed. With this new definition it is possible to describe the geometric or contact restrictions, the load boundary conditions and the degrees of freedom of a contact with the same operand. In the context of this work the method served at bounding unbounded operands coming from unilateral contact restrictions. The method is perfectly reproducible for finding the contact points in bilateral contacts, for which the conditions expressed in Fig.2.6 need to be respected: the global and local kinematic compliance, and the direction

and the point of application of the loads.

As it was shown, the method is also suitable for simulating the sliding behavior of assemblies when parallel architecture consumes the degrees of freedom. The way to approach this problem accounts for the interaction between separate chains of contacts: the contact restrictions of one pair of features limits one or more mobilities of the other pair of features. In the example presented, only the form defects of the planar contact were considered, but form defects for the ball-and-cylinder pairs could have also been taken into account using the same approach. The accuracy of the results depends on the discretization of the contacts, in this case specially on the discretization of the circle for both ball-and-cylinder pairs. It would be interesting in the future to quantify the accuracy of the results by varying the mesh density and distribution.

The proposed method has the advantage that it can be applicable to any type of features with or without form defects given that there is a perfect traceability of the vertices in the polyhedron to the contact nodes in the geometry. In this work, the process signature is simulated with different methods through Skin Model Shapes. In the future, measurements coming from real parts will be used to reconstruct non-ideal parts with the manufacturing signature. The instability can also be studied from the deviation space. In the case study presented before, the solution of the minimization of the volume converged always to a single vertex in the subspace of bounded displacements, however, there are cases in which the minimization might be achieved with an edge or even a facet of the polyhedron. In those cases some stabilization criteria must be developed.

The next step for improving the fidelity of the proposed model is the inclusion of local deformations. Chapter 3 presents the inclusion of an erosion-based method to add the local deformation in the contact zones between two mating surfaces. Applying a local deformation method in a polyhedral-based approach implies that the resulting polyhedron Γ_R needs to be updated at each increment of the local deformation, new contact zones will appear and the relative positioning of the matting features might change. The work presented here takes advantage of the dual properties of the wrench and twist spaces and it has a intimate relation to the dynamic interaction models used in robotics [127].

Chapter 3

Polyhedral approach for local deformation

For many years, the literature on geometric tolerancing has focused on a manifold of mathematical and representation models whose hypothesis rely on the one hand on the ideal features paradigm, and on the other on the rigid-body assumption. Under these two assumptions many mechanical systems of moderate and even high complexity can be modeled, but as the demands for better performing, lighter and more environmental friendly systems become the new standard, these assumptions are no longer enough for modeling mechanical systems with tight requirements.

In the previous chapters, it was shown the inclusion of non-ideal features and external loading in the polyhedral-based tolerance analysis process. In this chapter, the contact modeling is carried out taking into account the local deformation between mating features. A purely plastic model is presented and implemented in the proposed polyhedral approach. The duality between wrench and twist plays a fundamental role on defining the new contact positions and portions of surfaces on the contact feature. The novelty of this method resides in the use of the deviation space to update the relative position of the mating surfaces through the successive deformation steps. The deformation process is modeled as a dynamic or quasi-static problem, it takes into account the relative displacements between the mating surfaces at each deformation step.

I Local deformation models in tolerancing

The rigid-body assumption is ubiquitous in the tolerancing field. The models that deal with deformable bodies have as departing point the rigid contact configuration between two features. The way to incorporate the local deformation due to assembly and other forms of interaction in tolerance design is dependant on the type of mathematical model used for tolerance representation. In [133], the authors proposed the integration of local deformation in a tolerance analysis approach using the vectorial tolerancing model. They applied their method in a crank mechanism by calculating analytically the deformation of the crankshaft using the bending method, they also considered the hydrodynamics of the lubrication of the bearings as well as their motion path. Their method allowed only for dimensional tolerancing in 2D, and they considered only ideal features under elastic deformation.

The local deformation process has been widely studied on thin-wall parts, specially on the deformation of sheet metal parts. These studies often used the Method of Influence Coefficient (MIC) to better predict the contact variation [32, 78]. The Finite Element Method is used to compute the rigid and compliant deformation of the parts. One of main drawback of these studies is that they do not couple the bulk with the local deformation.

A more recent research carried out by authors in [79] included form defects and local deformations into a tolerance analysis framework. Two major steps were part of this framework. First, the key mating surfaces are obtained from experience and/or FEM and CAT calculations from the nominal model, then a Monte Carlo simulation is included for the generation of instances of skin model shapes (SMS), the difference surface computation, the calculation of local surface deformation, and the evaluation of the functional requirements. These authors used Discrete Cosine Transform (DCT) [132] to model the SMS, SDT to represent the errors in a deviation domain, and the Conjugate Gradient Fast-Fourier Transform (CG-FFT) as algorithm in the boundary element method (BEM) for calculating the local deformations. They considered only the elastic deformation on rectangular surfaces. Following this research, the authors in [125] applied the same framework to a cam mechanism using the same modeling technique and algorithm for BEM.

The authors in [124] applied the same framework to conduct tolerance analysis in spur gears. In addition to the steps described before, the authors evaluated the transmission performance by including the transmission error, the tooth contact pattern and the contact pressure distribution. They considered only the elastic deformation of one tooth contact. For all the aforementioned research, the authors worked with discrete models for the computation

of SMS.

In a recent research, authors in [113] proposed a method based on stable contact with form defects using NURBS. The framework they proposed is similar to the one proposed by previous authors with the difference that they added a step for the evaluation of the contact stability. The stability is assessed using the density-based spatial clustering of applications with noise (DBSCAN) algorithm. The verification of the geometric requirements of a SMS was done through Principal Component Analysis (PCA).

In another research [92], authors used the functional tolerancing based on positioning features (CLIC) [10] to describe the geometric specifications on a hyperstatic mechanism. They simplified the model to 2D and applied the Castigliano theorem to calculate the displacements on the nodes of beam-like elements to then verify the geometric condition of straightness.

In general, the local deformation problem can be solved in an analytical way or through numerical methods for ideal and non-ideal features that are considered as discrete or continuous. The mechanical model chosen to simulate the local deformation can consider elastic and/or plastic behavior, and deal or not with stability. In the next sections, a discrete model dealing with non-ideal features is used to develop the local deformation process for contacts considering the plastic deformation.

In this chapter, a purely plastic model will be used. The erosion model assumes the parts as semi-infinite bodies just as in the Boundary Element Method. As it will become clear later, the reaction forces at the contact points in the plastic regime are considered as constant. This is cause the discrete forces are linked directly to the rigidity of the softest of the two materials in contact. Although the consideration of only local and plastic deformation simplifies the real complex behavior of the deformation problem, the erosion model used here allows a direct implementation of the mechanic behavior into the geometric prismatic polyhedral model.

The novelty of this chapter does not reside on the sophistication of the mechanical model, but primarily on the direct representation of the deformation phenomenon from the polyhedral-based approach. In that sense, this chapter investigate what happens on the deviation space, that describes the contact restrictions between parts, when one part penetrates the

other.

II General framework for local deformation

Even if the models for representing the tolerances and computing the deformations are very different, most of the revised literature agree with the general way to approach the local deformation problem in tolerance design. In the general framework presented in Chapter 1 there were three main phases: model preparation, contact simulation and model evaluation. This chapter is concerned with the second stage of the contact simulation stage shown in Fig.3.1. The model preparation phase is a pre-requirement of the second and third phases.

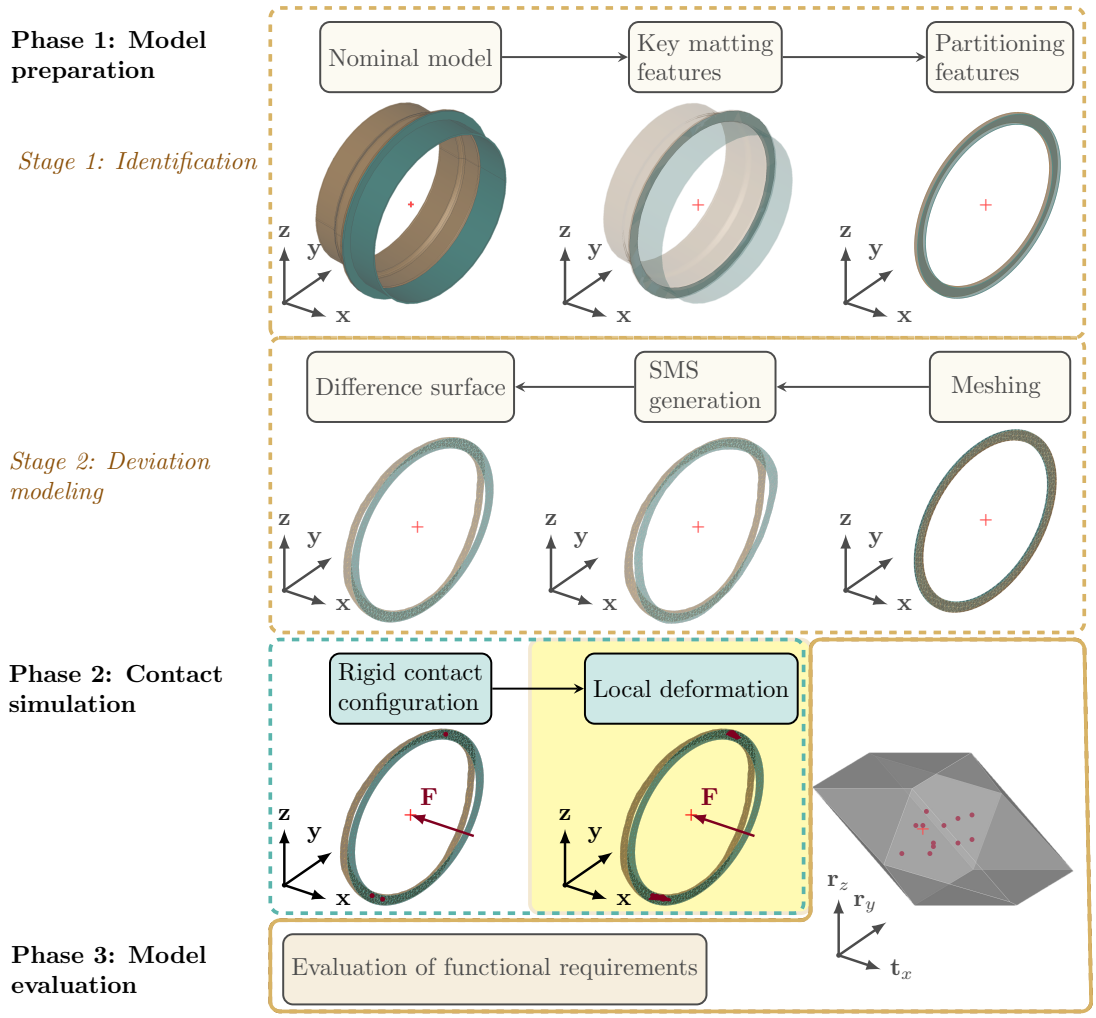

Fig. 3.1 Simulation phases for local deformation in tolerance design

The rigid contact configuration must be found before considering the deformation. In this chapter, the rigid contact configuration will be briefly explained in the 2D-case for the sake of comprehension of the following derivations.

The literature on local deformation in the context of tolerance design shows some limitations and challenges to still be addressed. One of them concerns the choice of the model to describe the mechanical behavior of the parts. It is common to solve the problem through numerical methods like the Boundary Element Method (BEM) that has gained popularity in the tolerancing field as it can provide fairly precise results, and it is faster than the traditional Finite Element Method (FEM) methods. The more restrictive assumption of BEM is that the thickness of the underlying material is infinite. In the cases of thin plates with non-uniform loads this method would retrieve less accurate results. Other remarks regarding the inclusion of the plastic behavior of the contacts, the shape-dependent analysis, and the lack of integration of mechanical solver in a CAD/CAT environment.

In the next sections, an erosion-based deformation model is explained and integrated directly in the polyhedra approach. The deformation of a contact feature is directly integrated in the deviation space coming from the contact points as a displacement of the boundaries of the restrictions. Since the deformation is directly expressed in the deviation space, the method is independent of the type of contact being modeled. This work contributes to the simulation of local deformations in the context of tolerancing. The method is highlighted in a 2D case for better understanding.

III Local deformation on the polyhedral-based model

a Local deformation process

In this chapter we present the process to simulate the local deformation in the polyehdral-based model (Fig.3.2). The starting point is the rigid configuration, discussed in subsection b, from which we can determine the intensities of the reaction forces at the contact points using the wrench definition. Once the force reactions are determined for the rigid case, the next step consists on recalculating the value of the reactions under the hypothesis of the plastic model as explained in subsection c. If the condition for the plastic regime to start operating holds (subsection d), then the initial contact points C_i are eroded bya small quantity; otherwise, the process is stopped.

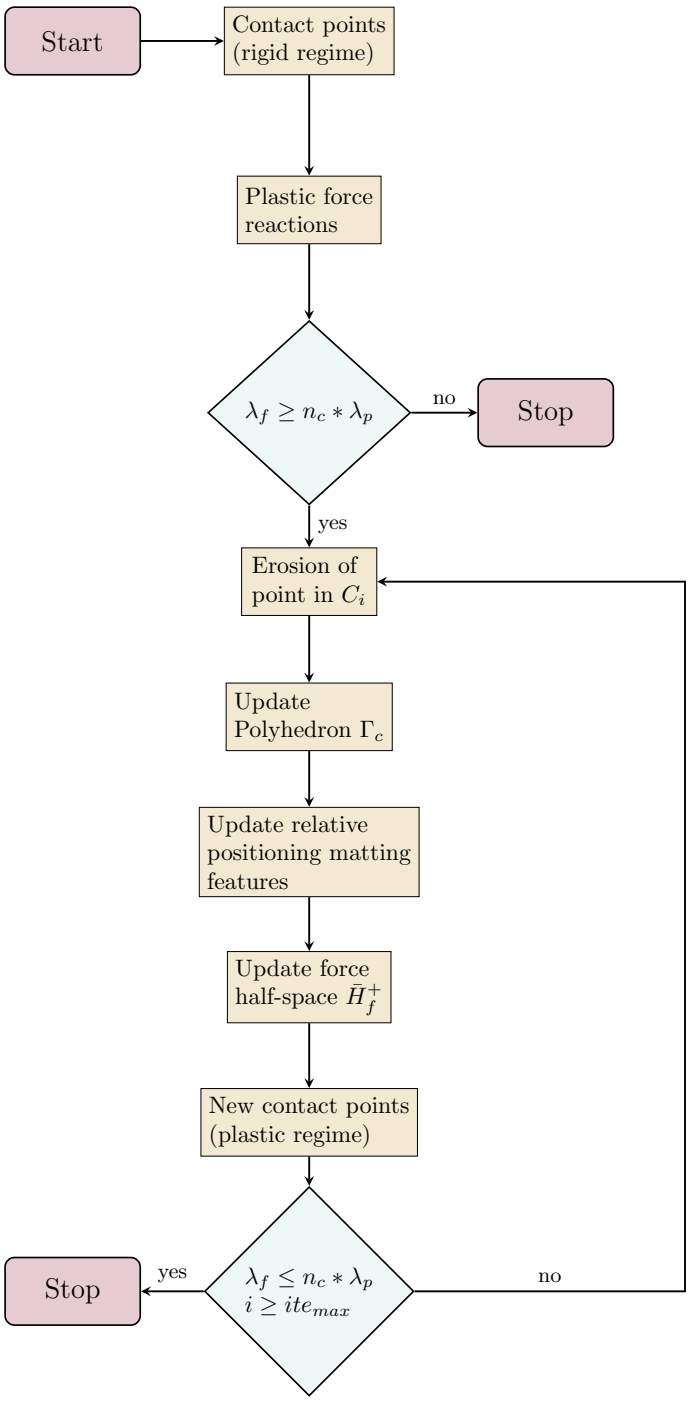

Fig. 3.2 Local deformation process

The next step in the process shown in Fig.3.2 is to update the contact polyhedron Γ_c taking into account the erosion of the active contact points. In this step, the problem is written as a dynamic one to include the effects of both translation and rotation of the mating features.

The procedure is explained in subsection g. In the next step, the relative position between the mating features is updated by applying a rigid transformation to the mating features using the coefficients of the small displacement torsor obtained from the deviation space as presented in subsection f.

The erosion process continues until the stop conditions (subsection h) are met; otherwise, the process described above (erosion step, update the contact polyhedron, update the force half-space and finding the new contact points) is repeated.

b Contact points from rigid configuration

As it was previously mentioned, the starting point for local deformation procedure is the contact position coming from the rigid configuration. The number of contact points for an infinitely rigid contact depends on the type of contact being modeled and the nature of the joint. The physical contact between two matting features subjected to external mechanical loading actually happens between portions of surfaces and not between localized points.

The local deformation process will be explained throughout the following subsections with the aid of the 2D example shown in Fig.3.3. The crisp line represents the difference surface discretized in 7 points (P_1 to P_7), and the top surface is the equivalent surface S_0 whose defects have been transferred to the difference surface. The top surface is pushed against the bottom one by the action of an external force $\mathbf{f}$ at point P_f that coincides vertically with the calculation point M.

In Fig.3.4, the contact polyhedron is presented only with the contributing half-spaces ($\bar{\mathbf{H}}_1^+$,$\bar{\mathbf{H}}_3^+$,$\bar{\mathbf{H}}_6^+$ and $\bar{\mathbf{H}}_7^+$). The polyhedron results from the intersection of these half-spaces. The hatched lines indicate the direction in which the half-spaces are constraining the deviation space. The result of the intersection of the force half-space and the contact polyhedron is, in stable cases, a singleton. The force half-space is not hatched here only for readability purposes, the hatch lines go in the positive direction of the translations along $\hat{y}$ (t_y) . The half-space $\bar{\mathbf{H}}_f^+$ represents the external loading, and its intersection with half-spaces $\bar{\mathbf{H}}_3^+$ and $\bar{\mathbf{H}}_6^+$ means that the contact is produced at points P_3 and P_6, whose reactions are forces $\mathbf{f}_3$ and $\mathbf{f}_6$, respectively.

We can write the fundamental principle of statics as a sum of wrenches as shown in Eq.3.1, where $\mathbf{W}_i$ are the wrenches from each point in contact i, and $\mathbf{W}_f$ is the wrench of the

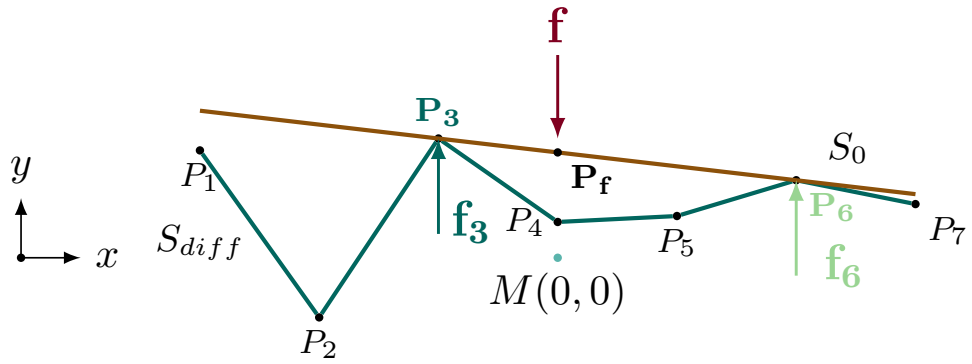

Fig. 3.3 2D representation of a planar contact between two surfaces. At the bottom, the difference surface is discretized in 7 points. At the top, the surface whose defects have been transferred to the difference surface. The contact is assumed to be frictionless

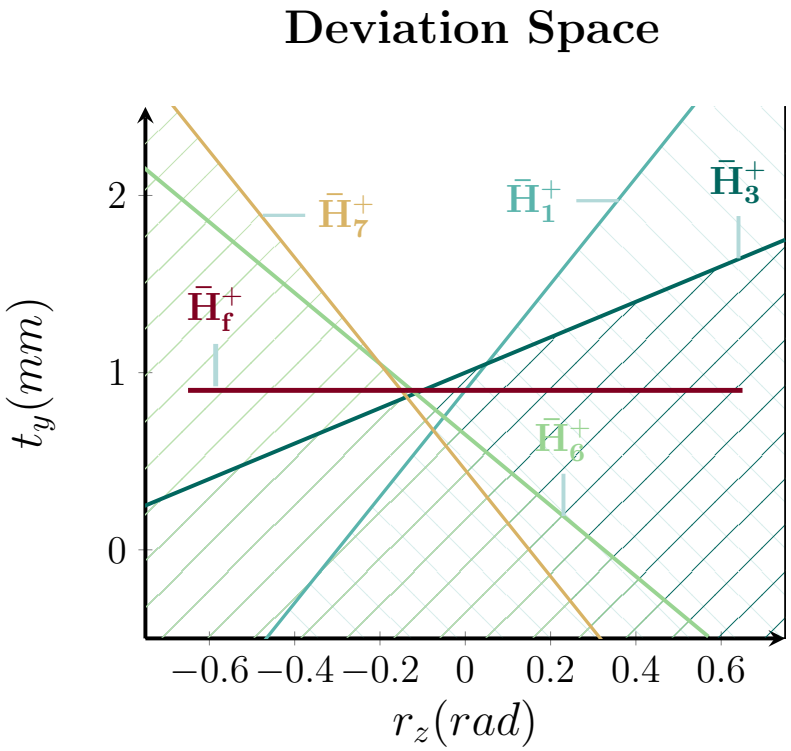

Fig. 3.4 Deviation space in the rigid configuration. Only the half-spaces that contribute in the intersection are presented. The half-space $\bar{\mathbf{H}}_f^+$ represents the external effort. Its intersection with half-spaces $\bar{\mathbf{H}}_3^+$ and $\bar{\mathbf{H}}_6^+$ allows us to trace back the contact points in the geometry. The vertical axis is scaled by a factor of 2 for visualization purposes.

equivalent external loads.

$$\sum_i \mathbf{W}_i + \mathbf{W}_f = \mathbf{0} \quad \text{for } i \in \{3,6\} \tag{3.1}$$

In the previous chapter, only the direction of the external load was necessary to find the contact position in the rigid configuration. In this case, it is necessary to calculate the magnitude of the reactions at the contact points in the rigid configuration to know if any deformation will occur. The wrenches $\mathbf{W}_i$ and $\mathbf{W}_f$ describe the force and its action on a given point as shown in Eq.3.2.

$$\mathbf{W}_i = \begin{bmatrix} \mathbf{MP}_i \times \lambda_i \cdot \hat{\mathbf{n}}_i \\ \lambda_i \cdot \hat{\mathbf{n}}_i \end{bmatrix}, \mathbf{W}_f = \begin{bmatrix} \mathbf{MP}_f \times \lambda_f \cdot \hat{\mathbf{n}}_f \\ \lambda_f \cdot \hat{\mathbf{n}}_f \end{bmatrix} \tag{3.2}$$

Where $\mathbf{MP}_i$ and $\mathbf{MP}_f$ are the position vectors from the points P_i in contact and the point of application of the force P_f to a given calculation point M; $\hat{\mathbf{n}}_i$ and $\hat{\mathbf{n}}_f$ are the unit vectors that express the direction of the local reaction forces and the external load respectively; and λ_i and λ_f are the magnitude of the reaction forces and the external load respectively. This equation serves at calculating the reaction in the rigid configuration.

The coordinates of the points in Fig.3.3 are shown in Table.3.1. Their location is given in relation to the origin which is coincident with the calculation point M. The form defects are expressed here as the local gaps between the two features along y axis with values shown on the third column of the table.

Table 3.1 Nodes' coordinates from Fig.3.3

Point	$\mathbf{X}\,[mm]$	$\mathbf{Y}\,[mm]$
P_1	-40.0	0.9
P_2	-30.0	-0.5
P_3	-20.0	1.0
P_4	-10.0	0.3
P_5	0.0	0.35
P_6	10.0	0.65
P_7	20.0	0.45
P_f	0.0	0.8833

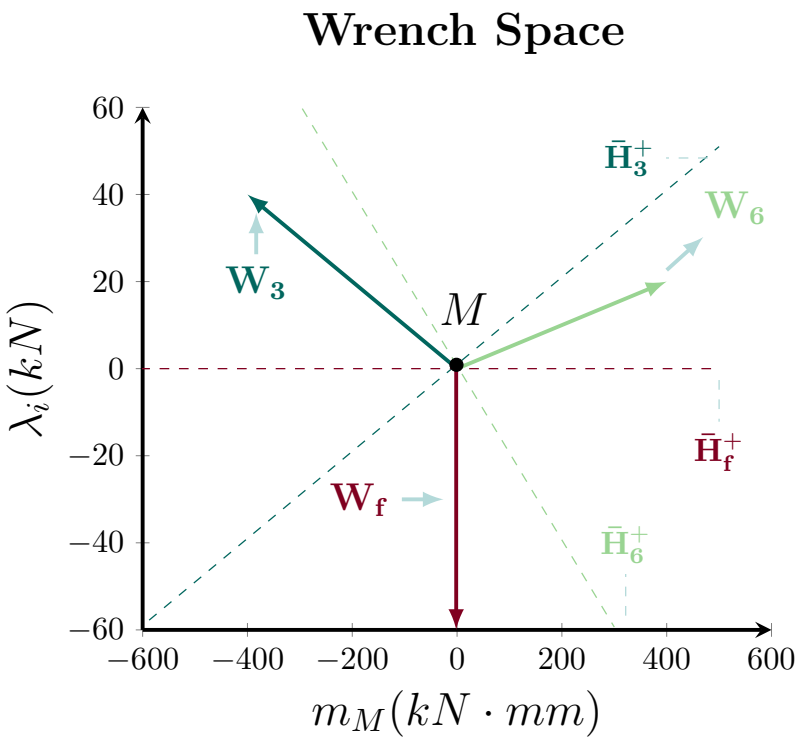

Fig. 3.5 The wrench space, orthogonal to the deviation space with force and moment components. The wrenches are all expressed at the calculation point M.

Knowing the value of the coordinates and having that the two matting surfaces are kept in contact by the action of a force **f** with a magnitude of $60\,kN$, we could represent the inital configuration with the wrenches shown in Fig.3.5. As it can be seen, the normal fan of the vertex generated by half-spaces $\bar{H}_3^+$ and $\bar{H}_6^+$ gives us the directions of the wrenches $\mathbf{W}_3$ and $\mathbf{W}_6$. The vertical axis corresponds to the force magnitude λ, and the horizontal axis to the moment around the **z** axis.

The magnitude of reaction at the contact points can be obtained from Eq.3.3 by replacing the nodes' coordinates and the external force magnitude. The magnitude of the reaction at points P_3 and P_6 are $\lambda_3 = 20\,kN$ and $\lambda_6 = 40\,kN$, respectively. The external force is applied at point P_f and does not generate a moment around M. From Fig.3.5, it is clear that the inital rigid state is in static equilibrium and it is isostatic. When the initial state is statically indeterminate, the traditional approaches like iterative based methods, or the force and displacement methods can be used to find the magnitude of reactions at the initial hyperstatic configuration.

$$\begin{aligned} \sum M_M &= 0 \\ \mathbf{MP}_3 \times \lambda_3 \cdot \hat{\mathbf{n}}_3 + \mathbf{MP}_6 \times \lambda_6 \cdot \hat{\mathbf{n}}_6 &= \mathbf{0} \\ \sum F &= 0 \\ \lambda_3 \cdot \hat{\mathbf{n}}_3 + \lambda_6 \cdot \hat{\mathbf{n}}_6 - \lambda_f \cdot \hat{\mathbf{n}}_f &= \mathbf{0} \end{aligned} \tag{3.3}$$

c The erosion model

In this work, a semi-analytic purely plastic deformation model is used to compute the deformations. The contact is assumed to happen, as in the case of BEM, between two semi-infinite bodies. This assumption allows us to consider only the surfaces in contact and disregard the volume of the parts.

From the rigid contact model only external forces in the subspace of bounded displacements of the contact are allowed, and no frictional forces are considered. The purely plastic regime adopted in this work bounds the local contact pressures with the hardness of the feature chosen as the difference surface, or with an equivalent rigidity of the two feautres in contact. The feature with no form defects is considered as being infinitely rigid.

Authors in [136] used a similar approach in an elasto-plastic model for rough surfaces of metal gaskets for evaluating their sealing performance. The model used here comes from a purely plastic model used in [58] for the analysis of local deformation of a flange to be used in a hip prosthesis. The novelty in the method presented here lays in the exploitation of the dual properties between the deviation and the wrench spaces, and in the determination of the contact zones from the deviation space.

Plastic force reactions

According to the erosion model, the reactions forces in the plastic regime are considered as constant and are bounded by the hardness of the softest material as shown in Eq.3.4, where λ_{pi} is the constant plastic reaction at the points of contact in the plastic regime; H is the hardness of the softest material; and s is the total area of the nominal contact feature.

$$\lambda_p \times n = H \times s \tag{3.4}$$

The contact pressure in this type of model is limited by hardness and it does not take into account the strain-hardening phenomenon. The hardness can be approximated for mild steel metals as being the elastic limit σ_y multiplied by a factor C_F ranging between 2.1 and 3.0 [97, 73].

d Necessary condition for plastic deformation

The contact zones in this model are identified through a set of discrete number of points. In order to start the deformation process, the external loading has to be larger than the sum of the reaction forces at the contact points in the plastic regime. This condition can be expressed as shown in Eq.3.5, where n_c is the number of contact points in the rigid configuration, which corresponds to the degrees of freedom of the joint for isostatic conditions. λ_p is the intensity of the force in the plastic regime, the same for all the nodes in the discrete feature. The term λ_f is the intensity of the external effort.

$$\lambda_f \geq n_c \times \lambda_p \tag{3.5}$$

This condition is necessary for the process to be launched. If we continue with our 2D example, and assume that the nominal contact feature was discretized in exactly the same way as the difference surface, 7 nodes with six segments of the same size ($10mm$) and unit width so each segment has an area $10mm^2$, meaning that $s = 60mm^2$; and the deformable material has a hardness of $H = 1800MPa$, then we could verify that $60kN \geq 2 * 15,4kN$. There are other two conditions that need to be verified to guarantee the existence of at least one solution to the problem. They can be expressed as shown in Eq.3.6. The first one can be analysed as the need of a minimum portion of surface that can withstand the external pressure, and the second one imposes a minimal discretization density, where n is the number of discretization points in the feature and n_r the degrees of freedom of the studied joint.

$$\begin{aligned} H \times s &\geq |\lambda_f| \\ n &\geq n_r \end{aligned} \tag{3.6}$$

Once the above conditions are satisfied, an initial erosion step is carried out in the direction of the external load. The erosion step can be dynamically defined by calculating the distance from the intersection vertex, in the deviation space that minimizes the volume,

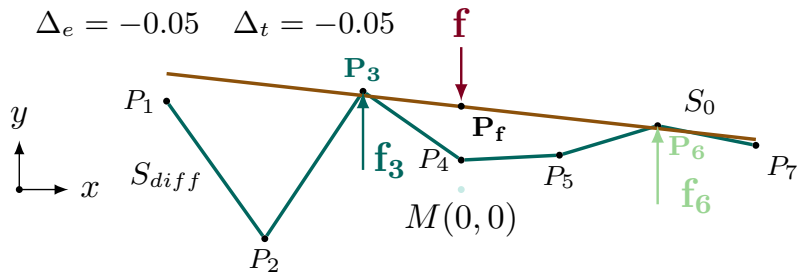

Fig. 3.6 First erosion step ($\Delta_e = -0.05$, $\Delta_t = -0.05$). The direction of the first erosion step was defined as the direction of the external load. Contact points remain the same.

to the second furthest vertex in the polyhedron. It can also be defined as a fixed step value, small enough to not miss the intermediate positions that could change the results. For the rest of the example, an arbitrary small step value has been set to $\Delta_e = 0.05mm$. This first erosion step demands an update of the polyhedron as the half-spaces at the contact points have been displaced.

e Computation of eroded polyhedron

The direction of the first erosion step was taken as the direction of the external loading. This initial erosion step takes into account only the translation along y axis, in fact, the feature S_0 in Fig.3.6 is parallel to feature S_0 from the rigid case (see Fig.3.3). The approach used in this chapter will consider both the relative rotation and translation between the features as it will be shown later on.

In table 3.2, the transformed coordinates values are presented. Δ_e is the erosion step which is fixed, and Δ_t is the accumulated erosion step. The contact points did not change for the first erosion step, however, their height changed. Contact points P_3 and P_6 were eroded of Δ_e in the direction of the external load, so they change from 1.0 to 0.95 for P_3, and from 0.65 to 0.6 for P_6. This change implies that the actual restrictions expressed at the calculation point M have changed.

The contact restrictions for each point are expressed as shown in Eq.2.4. The second member (b_k) is the quantity associated to the form defect for each point. At each erosion step, this constant is modified producing a transformation in the restriction's position in the deviation space. Only the active half-spaces (the ones generated by the contact points) are modified, the remaining half-spaces stay at the previous position. In Fig.3.7, the new polyhedron is presented. The vertex from the polyhedron that minimizes its volume is still the one resulting from the intersection of half-spaces $\bar{\mathbf{H}}_3^+$ and $\bar{\mathbf{H}}_6^+$. This vertex gives the SDT

Table 3.2 Nodes' coordinates from Fig.3.6

Point	$\mathbf{X}_0\,[mm]$	$\mathbf{Y}_0\,[mm]$	$\mathbf{Y}_i\,[mm]$
$\Delta_e = -0.05$		$\Delta_t = -0.05$	
P_1	-40.0	0.9	0.9
P_2	-30.0	-0.5	-0.5
$\mathbf{P_3}$	$\mathbf{-20.0}$	**1.0**	**0.95**
P_4	-10.0	0.3	0.3
P_5	0.0	0.35	0.35
$\mathbf{P_6}$	**10.0**	**0.65**	**0.6**
P_7	20.0	0.45	0.45
$\mathbf{P_f}$	**0.0**	**0.8833**	**0.8333**

parameters to update the relative positioning between the matting features.

It can happen that by taking into account the rotation between the features in contact, one of more of the initial contact points will be not maintained. In that case, the erosion value of that point must be reduced up until its value in the rigid configuration. The height of the erosion at each point is variable and different at each iteration because of the relative translation and rotation between the features.

f Relative positioning between mating surfaces

The coordinates of the vertex at the intersection of the half-spaces will retrieve the components of the small displacement torsor, which will then be applied to the mating surfaces to update their relative positioning. It can be expressed as shown in Eq.3.7, where $\mathbf{t}_{P_i}$ is the translation of the point P_i in the discrete feature; $\mathbf{t}_M$ is the translation at point M; $\mathbf{P}_i\mathbf{M}$ the position vector and $\mathbf{r}$ the rotation vector. This equation can be applied because the angular displacements are small.

$$\mathbf{t}_{P_i} = \mathbf{t}_M + \mathbf{P}_i\mathbf{M} \times \mathbf{r} \tag{3.7}$$

By applying this transformation to the feature S_0, the relative position between the mating features is updated. This reflects in the geometry and in the deviation space. Table 3.4 shows the new coordinates by applying the SDT $(-0.011667(r_z), 0.833(t_y))$ parameters to feature

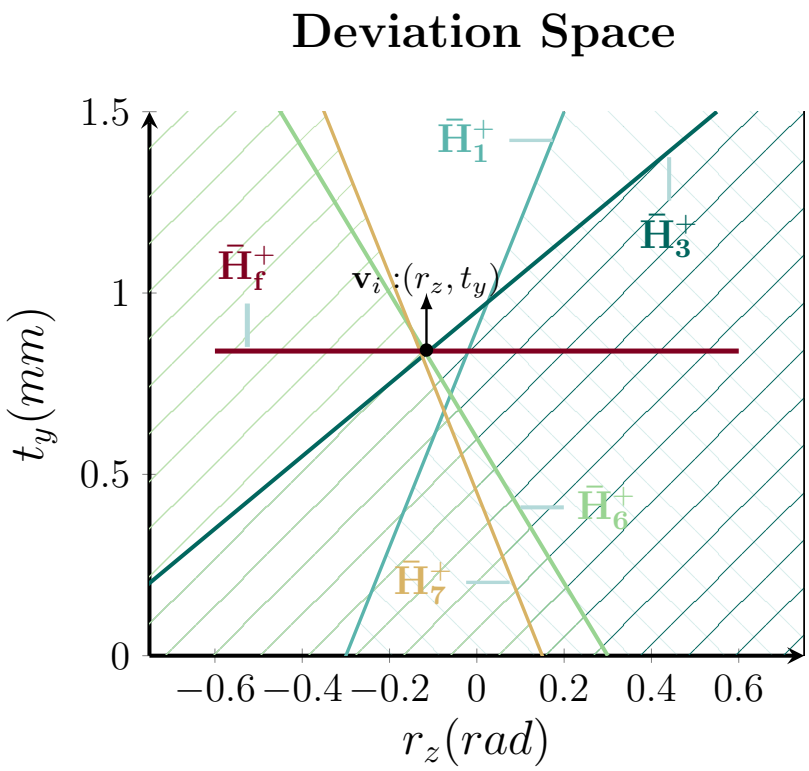

Fig. 3.7 First erosion step ($\Delta_e = -0.05$, $\Delta_t = -0.05$). The second member of the active half-spaces has been modified. The coordinates of the minimization vertex at the intersection between half-spaces $\bar{\mathbf{H}}_3^+$, $\bar{\mathbf{H}}_6^+$ and $\bar{\mathbf{H}}_f^+$ give us the SDT parameters for the relative positioning between the features in the geometric space.

S_0.

It can be seen that for the erosion step of $\Delta_e = -0.05$, the point P_3 has eroded the most (-0.0617) compared to point P_6 (-0.0267) which indicates that feature S_0 is actually turning in the counterclockwise direction. Point P_f, aligned with point M, is exactly -0.05, so it is actually our pivot point in this case.

g Dynamic equilibrium

After the first erosion step has been completed, feature S_0 will continue eroding difference surface, which is fixed in our case. Meaning that, up until the equilibrium is found, the system is statically unbalanced. Because of this unbalance, the forces acting on the contact will tend to cause the system to rotate, making it necessary to incorporate this dynamic

Table 3.3 Nodes' coordinates - updated relative position $\Delta_t = -0.05$

Point	$\mathbf{X}_0\,[mm]$	$\mathbf{Y}_0\,[mm]$	$\mathbf{Y}_i\,[mm]$
$\Delta_e = -0.05$		$\Delta_t = -0.05$	
P_1	-40.0	0.9	0.9
P_2	-30.0	-0.5	-0.5
$\mathbf{P_3}$	$\mathbf{-20.0}$	**1.0**	**0.9383**
P_4	-10.0	0.3	0.3
P_5	0.0	0.35	0.35
$\mathbf{P_6}$	**10.0**	**0.65**	**0.6233**
P_7	20.0	0.45	0.45
$\mathbf{P_f}$	**0.0**	**0.8833**	**0.8333**

process in the modeling.

Dynamic wrench calculation

Since the reaction forces at the contact points in the plastic regime are constant as shown in Eq.3.4, the system in the plastic regime will not longer be in static equilibrium, meaning that a new search of equilibrium must be performed taking into account the dynamics of the contact.

In Fig.3.8 the wrench of the plastic regime is shown. The reaction forces at point P_3 and P_6 are the same ($15.4\,kN$) as it is depicted in the vertical axis of Fig.3.8; on the other hand, since both of the reaction forces are the same, the moment they generate is different, making the system not balanced neither in the vertical axis (force), nor in the horizontal one (moments).

To derive the dynamic equations, let us consider a body b consisting of rigidly connected point masses m_i and for which the location of a mass i is $\mathbf{r}_i = (x_i, y_i, z_i)$. The sum of all the masses can be simply calculated as the sum of the individual point masses as show in Eq.3.8. If we assume that the body is moving with a given angular and linear velocity (twist), we can say that the force acting on a point mass is simply the mass of that point times the second derivative of the time-varying position of m_i ($\ddot{\mathbf{p}}_i$) as shown in Eq.3.9.

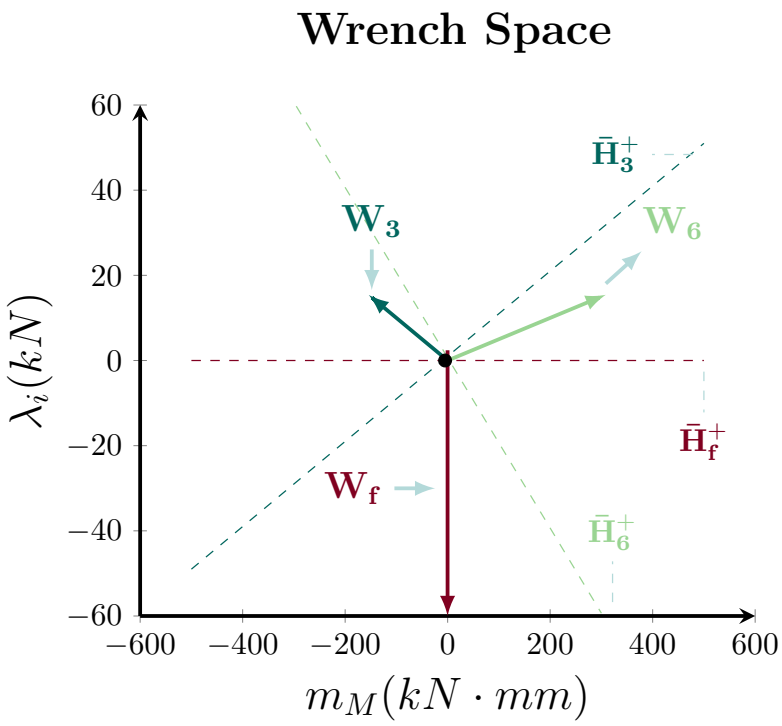

Fig. 3.8 Wrench space in the plastic regime. The wrenches are perpendicular to the restrictions in the deviation space showed here in dashed lines. It is clear that the system is not in static equilibrium along the moment axis.

$$\sum_i m_i \tag{3.8}$$

The moment of a mass point m_i can be calculated as shown in Eq.3.10, where $\mathbf{r}_i$ is the point location and $\mathbf{f}_i$ the point force.

$$\mathbf{f}_i = m_i \ddot{\mathbf{p}}_i \tag{3.9}$$

$$\mathbf{m}_i = r_i \mathbf{f}_i \tag{3.10}$$

We could write the wrench of the sum of the total force and moment in the body b as being:

$$\mathbf{W}_b = \begin{bmatrix} \mathbf{m}_b \\ \mathbf{f}_b \end{bmatrix} = \begin{bmatrix} \sum_i m_i \\ \sum_i f_i \end{bmatrix} \tag{3.11}$$

The sum of the forces in the body in linear dynamics is written as shown in Eq.3.12; where ω_b and $\mathbf{v}_b$ are the angular and linear velocity of the body.

$$\mathbf{f}_b = m(\dot{\mathbf{v}}_b + \omega_b \mathbf{v}_b) \tag{3.12}$$

Similarly, the sum of moments is shown in Eq.3.13, where $\mathbf{I}_b$ is the rotational inertia matrix.

$$\mathbf{m}_b = \mathbf{I}_b \dot{\omega}_b + \omega_b \mathbf{I}_b \omega_b \tag{3.13}$$

We can look at the local deformation problem as the manipulation of a fixed object and a series of manipulators (contact points) that impose forces and displacements in an object. The manipulation task can be formulated as a dynamic problem or as a quasi-static one. In the dynamic formulation, the body's twist, the spatial inertial matrix and the external wrench are necessary to find a consistent, inconsistent or ambiguous solution. In the general approach for rigid bodies, the idea is to find in $\sum_i k_i \mathbf{W}_i$ the set of $k_i \geq 0$ that satisfy a dynamic or quasi-static equation.

In this chapter, we consider the system as quasi-static, meaning that the velocities and acceleration of the bodies are small so that the inertial effects can be neglected. The quasi-static state can be written as shown in Eq.3.14, $\mathbf{W}_{ext}$ is the external wrench; $\mathbf{W}_i$ the wrenches at the contact points; and k_i the set of coefficients that satisfy the given condition.

$$\sum_i k_i \mathbf{W}_i + \mathbf{W}_{ext} = 0, \quad k_i \geq 0 \tag{3.14}$$

In our case, we will consider the contacts as being in dynamic grasp [80, 127], meaning that inertial forces are used to keep the two mating surfaces pressed against each other as the contact points are displaced. It does not exist an exact analytical solution to this problem in the plastic regime. Rather than finding only a set of parameters that meets the equilibrium conditions, we integrated the inertial forces of the contact by summing the reaction forces and the external loads.

Let's consider the wrenches in Fig.3.8. With the wrenches $\mathbf{W}_3 = (-10\lambda_p, 0, \lambda_p)$ and $\mathbf{W}_6 = (20\lambda_p, 0, \lambda_p)$ there exists a relative movement between the matting surface that we could write as a dynamic grasp as:

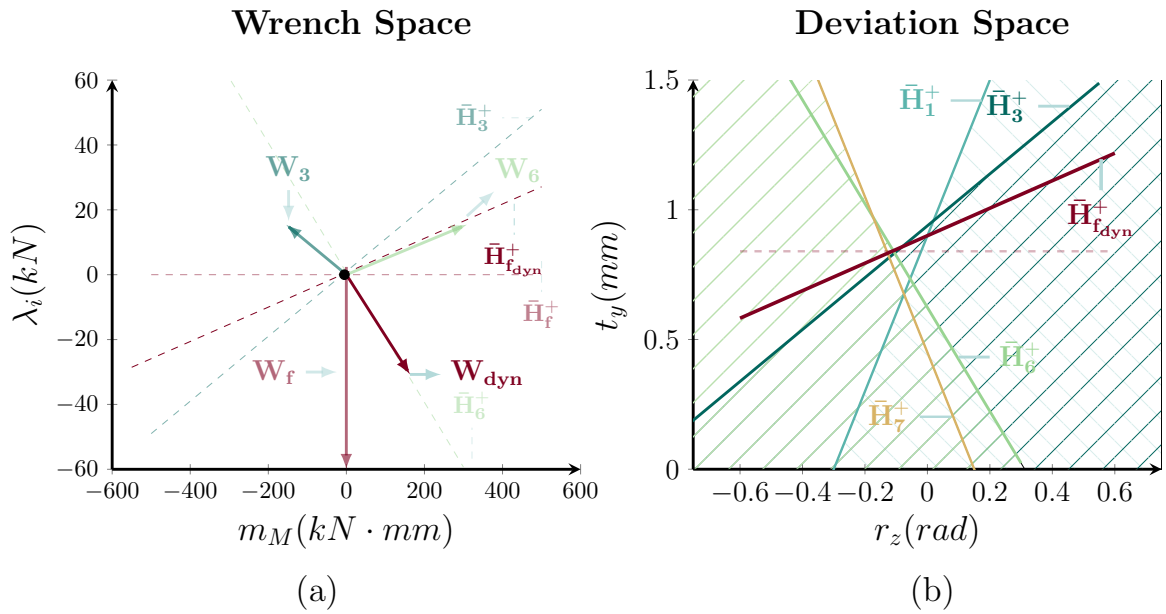

Fig. 3.9 a) Wrench space depicting at the back, in low opacity, the configuration shown in 3.8; at the front, the resulting wrench. b) The deviation with the new restriction coming from the wrench calculation ($\bar{\mathbf{H}}_{f_{dyn}}^+$).

$$\begin{aligned} \mathbf{W}_3 + \mathbf{W}_6 + \mathbf{W}_{ext} &= (m_z, 0, f_y) \\ (-10\lambda_p, 0, \lambda_p) + (20\lambda_p, 0, \lambda_p) + (0, 0, -60) &= (m_z, 0, f_y) \end{aligned} \tag{3.15}$$

The term $\mathbf{W}_{ext}$ is the wrench of the external force, applied at the point p_f. The term in the right corresponds to the wrench needed to cause a given angular and linear acceleration in the contact. The total wrench to apply to the feature S_0 is given by $(10\lambda_p, 0, 2\lambda_p - 60)$. In the back of Fig.3.9.a, in low opacity, the initial plastic state, at the front, the resultant wrench. The dual of this wrench will give us the new direction of the force restriction ($\bar{\mathbf{H}}_{f_{dyn}}^+$) in the deviation space as depicted in Fig.3.9.b.

With a new direction of the wrench, we can find the next points in contact by finding the vertex in the polytope that minimizes the volume (see chapter 2). In this case, the vertex is still the same as before, so we move forward in the erosion process. In the next erosion step, there are no new contact points so the feature S_0 continues eroding the difference surface in the direction given by the translation and rotational component obtained from the deviation space. In the fifth erosion step ($\Delta_t = -0.25$), a new contact point is found as it can be seen in Fig.3.10. It looks like half-space $\bar{\mathbf{H}}_7^+$ is also part of the intersection, but when applying

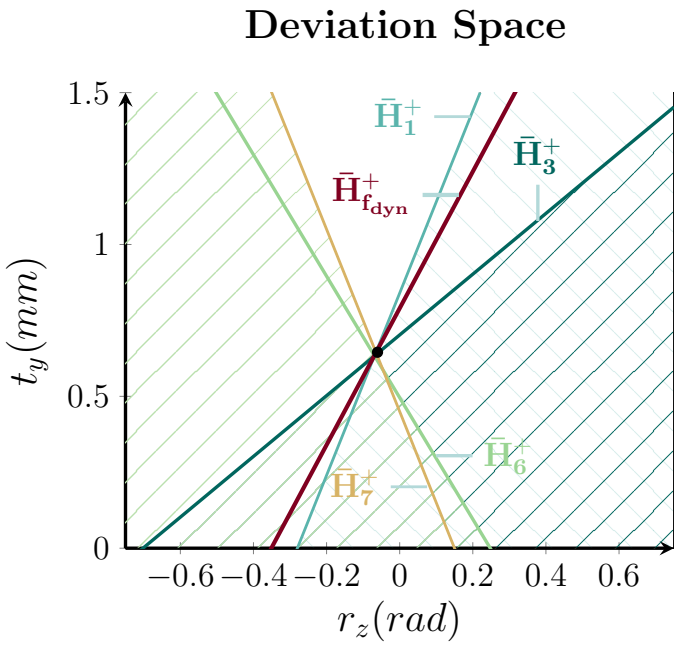

Fig. 3.10 Erosion step ($\Delta_e = -0.05$, $\Delta_t = -0.25$). The constant of the active half-spaces has been modified. The coordinates of the minimization vertex at the intersection between half-spaces $\bar{\mathbf{H}}_3^+$, $\bar{\mathbf{H}}_6^+$, $\bar{\mathbf{H}}_1^+$ and $\bar{\mathbf{H}}_f^+$ give us the new SDT parameters for the relative positioning between the features in the geometric space.

the SDT to the given deviation at every erosion step, we found that feature S_0 is actually $0.01\,mm$ apart from point P_7.

Table.3.3 shows erosion values for each one of the eroded points. As it it is clear, Point P_1 starts to get eroded at current iteration ($\Delta_t = -0.25$). The new contact point generates a new reaction force at point P_1 that has to be included in the wrench calculation, and it will change the direction of the $\bar{\mathbf{H}}_{dyn}^+$ obtained before. The total deformation for point P_1 is $-0.6\,mm$, for P_3 is $-0.2978\,mm$ and for P_6 is $-0.1544\,mm$, which shows that up until now the feature S_0 is rotating in counterclockwise direction.

It is necessary to check if with the new wrench and force half-space $\bar{\mathbf{H}}_{\mathbf{f_{dyn}}}^+$ direction the obtained intersection vertex is still the same as before. We can see in Fig.3.11.a, the new wrench resultant at the front in full opacity; at the back in low opacity, the three wrenches coming from the reactions at the three contact points.

In Fig.3.11.b, the deviation space with the new force half-space ($\bar{\mathbf{H}}_{f_{dyn}}^+$) direction which is comprised between $\bar{\mathbf{H}}_1^+$ and $\bar{\mathbf{H}}_3^+$. In fact, $\bar{\mathbf{H}}_1^+$ and $\bar{\mathbf{H}}_7^+$ constitute the physical limits of the

Table 3.4 Nodes' coordinates - updated relative position $\Delta_t = -0.25$

Point	$\mathbf{X}_0\,[mm]$	$\mathbf{Y}_0\,[mm]$	$\mathbf{Y}_i\,[mm]$
$\Delta_e = -0.05$		$\Delta_t = -0.25$	
$\mathbf{P_1}$	**−40.0**	**0.9**	**0.84**
P_2	−30.0	−0.5	−0.5
$\mathbf{P_3}$	**−20.0**	**1.0**	**0.7022**
P_4	−10.0	0.3	0.3
P_5	0.0	0.35	0.35
$\mathbf{P_6}$	**10.0**	**0.65**	**0.4956**
P_7	20.0	0.45	0.45
$\mathbf{P_f}$	**0.0**	**0.8833**	**0.6333**

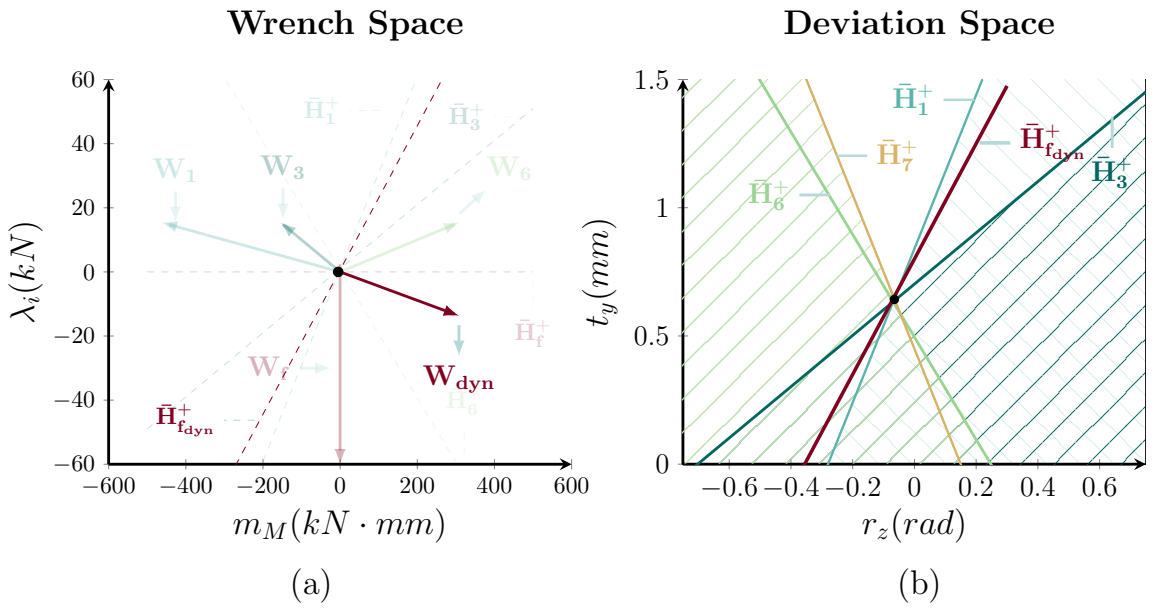

Fig. 3.11 a) Wrench space depicting at the back, in low opacity, the wrenches of the three contact points for a total erosion of $\Delta_t = -0.25$; at the front, the resulting wrench. b) The deviation with the new restriction coming from the wrench calculation ($\bar{\mathbf{H}}^+_{f_{dyn}}$).

part, any of the resultant force half-spaces will be limited by these boundaries even when its direction might surpasses any of them. This is because beyond these frontiers the equilibrium cannot be guaranteed.

h Stop conditions

The process continues until sufficient surface has been eroded. We can express this condition as in Eq.3.16 which states that if the external effort is less or equal than the sum of forces, then sufficient points in the discrete surface have been eroded. Another stop criterion is the maximal number of iterations.

$$\lambda_f \leq n_c \times \lambda_p \tag{3.16}$$

Given the discrete nature of the approach, an exact solution is not possible. The convergence of the simulation process is highly dependent on the discretization scheme and the quality of the mesh. During the simulation process, it is necessary to check when unstable cases show and choose the points that minimizes the angular displacements.

IV Advantages, limitations and perspectives

In the present chapter, a purely plastic deformation model was presented. The model abstracts the actual contact geometry and instead deals with points' coordinates and a contact polyhedron. During the deformation process, the new contact points are found from the deviation space by updating the convex polyhedron and by incorporating the dual of the sum of wrenches into the deviation space. The simulation iterates over a value of erosion that leads to the re-computation of the contact polyhedron and the sum of wrenches.

The primary advantages of this approach can be categorized as follows:

- **Generalization**: The behavior of the contact is dealt with from the deviation and wench spaces, so the specific contact type is abstracted and therefore treated in the same way.
- **Integration**: The model is easy to integrate into the polyhedral-based approach which will allows for a comprehensive tolerance analysis in the same CAT environment.
- **Calculation time**: As the model is dealing directly with the convex polyhedra the computation of the deformation should be as fast or even faster than the traditional FEM methods. This must be still proved by simulating a whole assembly.

The limitations of the present model can be grouped in the following categories:

- **Mechanical model**: The pure plastic mechanical model may not be the most adapted behavior model in all cases. For the case thin plates with very non-uniform loading conditions this method may provide less accurate results. The hypothesis of small displacements must be also respected since both the tolerance and mechanical model are based on this assumption. In future work, it would be interesting to include not only a layer describing the elastic behavior, but also include the strain-hardening phenomenon into account.

- **Instability**: The presented model did not include any stability criteria to deal with unstable contacts. When dealing with deformations between features with form defects, instability can occur quite often making the results to be less accurate.

- **Local deformation**: The presented model deals only with local deformation and not bulk deformation. Bulk deformation is specially important in systems subjected to large plastic deformations like metal forming process or machining simulations.

- **Discretization**: The obtained results in this chapter are highly influenced by the mesh density and regularity. Since local deformation is dealt with from the deviation and wrench spaces, the model is mesh dependent.

- **Industrial assembly simulation**: An industrial assembly simulation with several parts is on the perspectives of the present work. The integration of the local deformation algorithms into a CAD/CAT environment would facilitate the analysis of more complex geometry.

In order to integrate the contact simulation in the tolerancing context, that is, accounting for not only for the impact of the relative positioning between the mating features, but also the impact of the local deformation on a functional condition. For this to happen, the algorithms, methods, and objects need to be part of a integrated software solution. The next chapter presents the integration of the algorithms and methods for the simulation of skin model shapes and contact modeling of ideal and non-ideal features. They were integrated in PolitoCAT which makes it possible to simulate the deviation and carrying out the contact modeling directly in a CAD/CAT environment.

Chapter 4

Development of an integrated cross-platform framework for tolerance analysis

I Introduction

Computer-Aided Tolerancing (CAT) software have known a great improvement both in the models adapted to digital use and in the always-growing computational power. The integration of parametric models and some of the models based on set of constraints has been possible because of the common effort of industry and academia. Most of the tools in the market for performing tolerance analysis are commercial, developed by big groups like Dassault Systems, Dimensional Control Systems and Tecnomatix. Since the development of new software solutions is intrinsically linked to the needs of the market, it is often case that the implementation of new representation paradigms happens slowly which can represent an additional challenge to many industries.

The exchange of information among platforms is a crucial activity in the design process of any product. The current formats (STL, STEP, IGES, etc.) allow the exchange of geometric and tolerancing related information across platforms, which facilitates the use of different software solutions throughout the design process. Many companies have started to come up with solutions that cover most of the activities in design so less exchange is made across platforms. Their integrated solutions account for the activities in design, mechanical simulation and manufacturing allowing a more holistic way of approaching the conception

of new products.

This chapter presents the integration of the Skin Model paradigm in a open source CAT. The CAT software works with substitution surfaces, a type of ideal surface, from which geometric and contact constraints are expressed in the form of inequalities and represented through polyhedra. One of the objectives of this thesis is to contribute to more realistic description of parts based on the Skin Model Shapes paradigm. This chapter also presents the integration of the contact modeling module, divided in two parts. The first part presents the contact modeling of features with or without form defects by considering external loads, under the rigid body hypothesis. The second part presents the integration of the contact simulation in the open source CAT.

II Involved platforms and software

a PolitoCAT/Politopix

PolitoCAT is an open source software that uses Open Cascade Kernel for conducting tolerance analysis using polytopes and prismatic polyhedra [38]. PolitoCAT uses a mathematical solver called Politopix developed in C++ under GNU LGPL/GPL license. Politopix is a polyhedral modeling tool that allows the operations of Minkowski sums and intersections of operands in n-dimensions. PolitoCAT along Politopix have been used as a stand alone software for the tolerance analysis of iso-constrained and over-constrained assemblies. Generally, a STEP file generated in an external CAD modeler is imported into the software where the polyhedral operands for geometric and contact features can be generated.

PolitoCAT usually works with substitute surfaces, an ideal surface associated to the real manufactured surface from which the form defects have been filtered out [17]. These surfaces are suitable to conduct tolerance analysis for many systems.

b Salome platform

Salome is an Open Source platform that allows the integration of custom CAD applications [114], it can be seen as a cross-platform solution for pre and post-processing numerical simulation. Salome is based on OPEN CASCADE 3D kernel. It counts with different modules included on the installation, a *Geometry* module that is used for the creation, modification, importation/exportation, reparation and evaluation of CAD models. A *Mesh* module with a great variety of meshing algorithms, it also allows to import and export meshes, modify

mesh data and check quality of meshes as it can be seen in Fig.4.1.

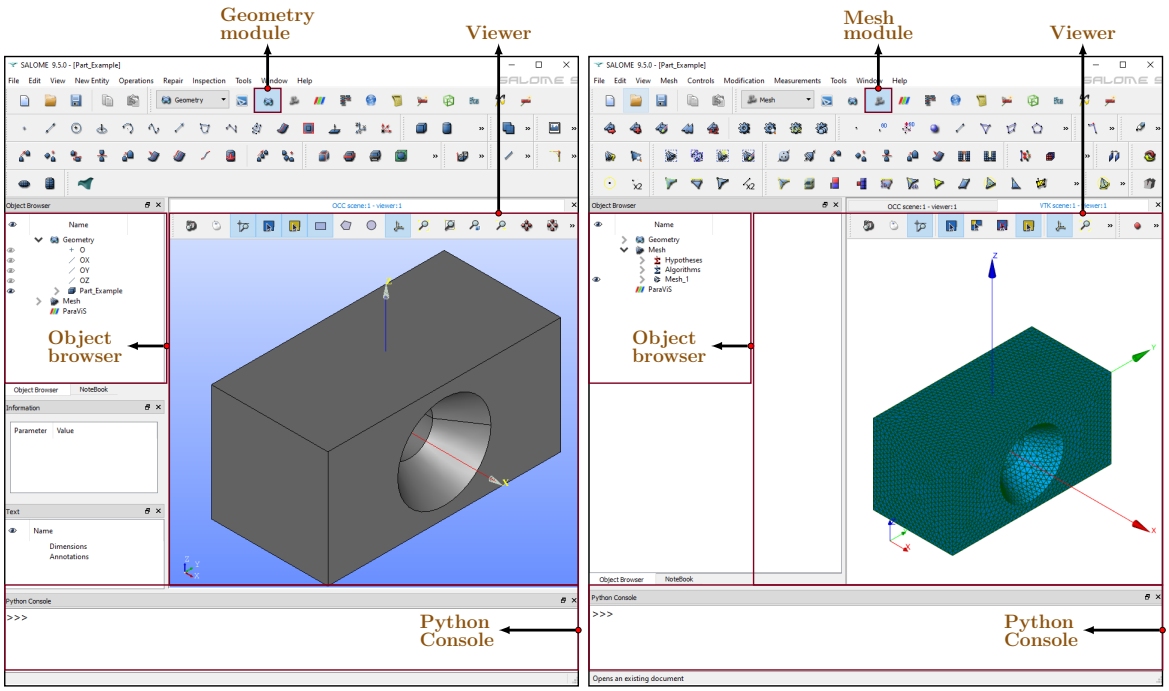

(a) (b)

Fig. 4.1 a) Geometry module from Salome. The main windows are shown in red. b) Salome module from Salome. The main windows are shown in red

There exist a Python API that maps all the Salome functionalities in Python. This allows the automation of complex use cases. Once a project has been created using the Salome GUI, a dumped file containing the code for regenerating the same case can be downloaded. It can also be further parameterized to add other operations that were not part of the downloaded dumped file.

III Integration of Skin Model Shapes

The integration of the Skin Model paradigm in PolitoCAT use the previous architecture of the software adding the option of the generation of SMS. The SMS generator was conceived as an independent module, meaning that a user should be able to use the system only with the purpose of generating instances of non-ideal features. In order to achieve this objective, a tolerance data modeling was carried out. The data modeling comprises the general architecture of the current and desired system, as well as the model and process view.

For the successful integration of the Skin Model paradigm different case scenarios were considered. The use cases help to define the requirements for the new classes. UML class diagrams were used to represent the existing and new classes.

The process of integration shown in this section concerns only the parts and not the assemblies. The Skin Model is consider as a surface model and it is feature-based. Not all of the features belonging to a part have to be represented through skin model shapes. Generally, only certain key features are modeled using SM. In Section f, an example of this implementation is shown for a single part.

a PolitoCAT: architecture

The simpler way to look at PolitoCAT is as a system that produces tolerance data once it's been fed with geometric and specification data have been fed to it. The geometric data comes in form of a CAD model, generally in STEP format, and the specification data are the necessary geometric and dimensional tolerancing information of the features.

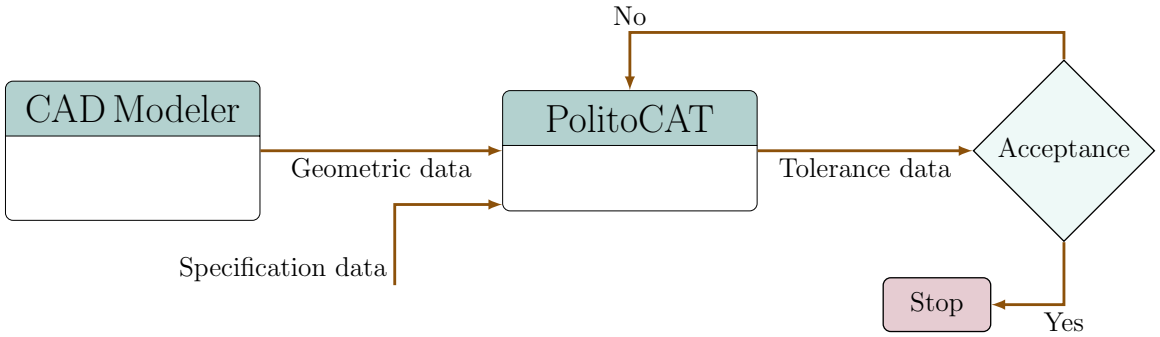

Fig. 4.2 PolitoCAT's previous version architecture adapted from [104]

In Fig.4.2, this architecture is shown. The output from PolitoCAT are the polyhedra and polytope data in the form of native extension files. The compliance with a functional specification can be accepted or not. In the case it is not accepted, a new set of tolerances has to be provided to the software until compliance is achieved. In the previous version, the discretization process was taking place only in PolitoCAT given that only ideal features were used. The mesher in PolitoCAT has been adapted to mesh what constitutes the physical limits of the toleranced features, so for a planar feature of rectangular contour only the four vertices at the extremities are taken into account. For planar features with circular or oval contour,

the number of points in the contour can be set. The number of discretization points changes the topology of the polyhedron and the precision in relation to the theoretical operand. For complex surfaces, the tessellator from OpenCascade is used. This tessellator is pretty limited on its parametrization allowing only the modification of the angular and linear deflection coefficient.

The generator of instances of skin model is incorporated in PolitoCAT. Therefore, it is necessary to adapt a module inside PolitoCAT's existing architecture so it can function independently. Besides the classes needed for the generation of the SMS, it is necessary to make PolitoCAT also work with external meshes. In Fig.4.3, the new architecture is shown. The geometrical data can come in PolitoCAT in the form of a STEP file or any other of the recognized formats for exchanging geometrical information.

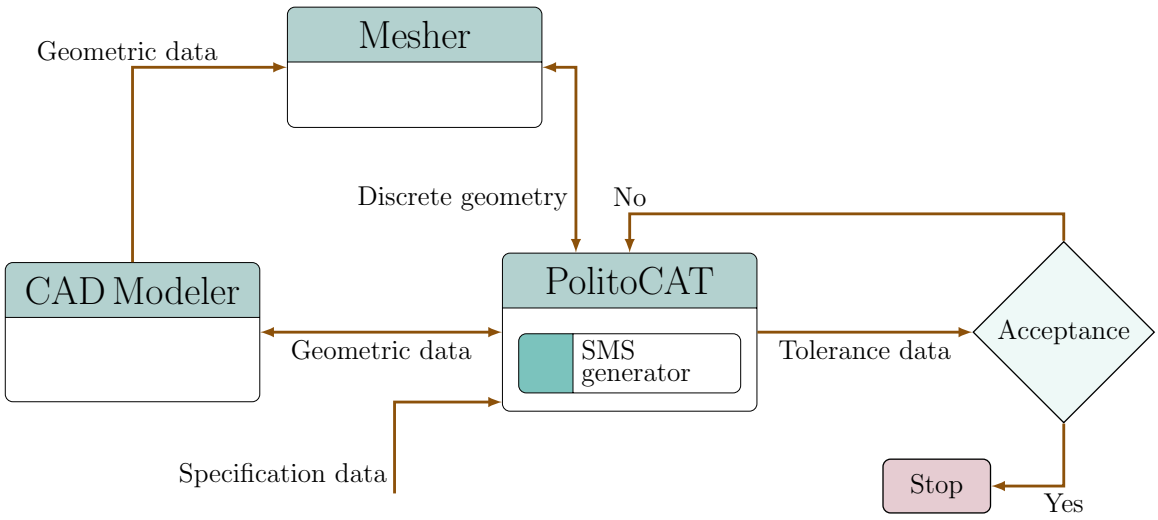

Fig. 4.3 General architecture of the new system allowing the use of external discrete information and the integration of a SMS generator inside PolitoCAT.

For the case of the discrete model, the discretization process can take place inside the software using OpenCascade native mesh classes, or by importing an external mesh. By allowing external meshes in the model, STL files obtained from measurements or manufacturing process simulations could be imported. The meshes can be generated in any external software capable of exporting STL files. The skin model shapes generator is included in PolitoCAT and it will be explained in detailed in the following sections. PolitoCAT is based on OpenCascade technology, the basic modeling features are available through the command window and it allows to export the transformed geometrical data to be used in any other

software as shown in Fig.4.3.

Additional geometric specification data must be entered by the user in order to be able to construct the polyhedral operands. The data are the tolerance or clearance value, the nature of the contact (bilateral, unilateral) and its restrictions (line, point, none) and the number of toleranced features.

b Model view

The implementation of the SMS paradigm and the algorithms for the contact simulation with form defects was carried out through a data and process modeling. A data model serves at visualizing the data of a project, the relations between data and structures, and at defining the behavior of a system. It represents the structure of the data elements for a specific domain, so in this sense, the semantics of the data model is not formal as it is for more specialized ontologies [130].

The development of the integrated platform was done following a bottom-up approach since an existing software structure was already in place. The starting point are data coming from Salome and PolitoCAT that will later allow the generation of skin model shapes. In the system different models coexist and interact, meaning different representation of the actual geometric objects. In the new architecture, five models can be identified: nominal, discrete, observed polyhedral and skin model. We began by taking the inputs and outputs of the different surface and geometric models as shown in Fig.4.4.

The starting point for the generation of SMS is the nominal model, whose input is the design intent of the designer, and the output is a CAD model in the form of a native or a STEP file as shown in Fig.4.4.a. Then, the discrete data coming from the a tessellator or a mesher whose inputs are features coming from the nominal model and its outputs the discrete features in the form of meshes as seen in Fig.4.4.b. Another source of data are the measurements of physical parts. These data are generally in the form of clouds of points or meshes coming from the measurements (Fig.4.4.c). The predicted model (Fig.4.4.d) is the result of the deviation modeling, the points of the nominal mesh are deviated with a priori information.

The skin model shapes can be generated from the observation or from the prediction models. Since we are working in a CAD environment, the geometric information coming from the nominal model is also necessary. The output of the skin model shapes in this

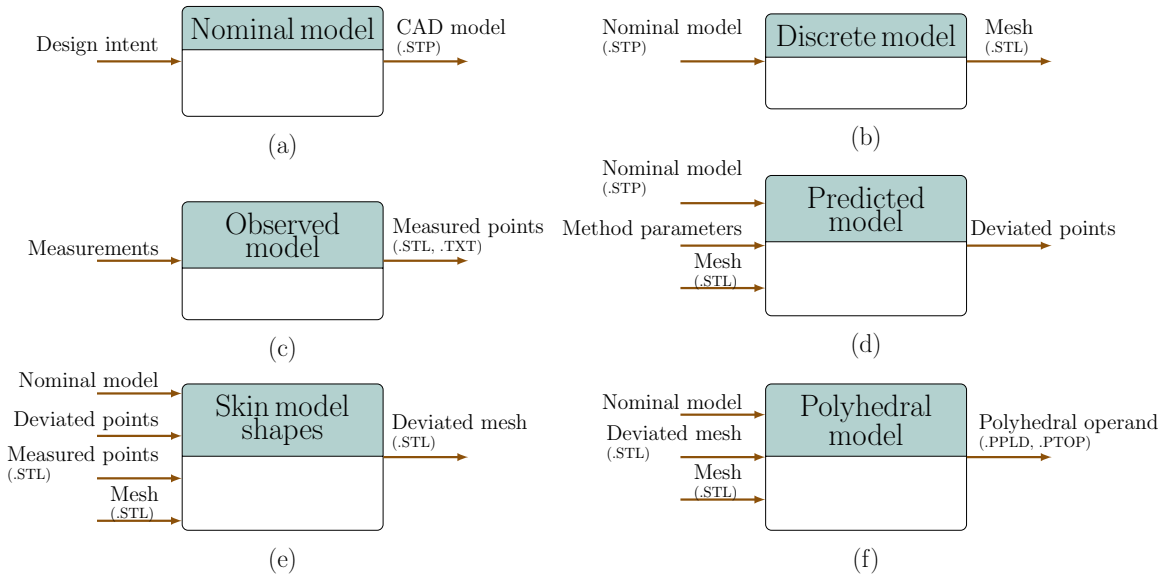

Fig. 4.4 Inputs and outputs of a) Nominal model. b) Discrete model. c) Observed model. d) Predicted model e) Skin Model Shapes f) Polyhedral model

system is a deviated mesh (Fig.4.4.e). Finally, to represent the tolerance information model we have the polyhedral model data which can be generated from features with or without form defects. The polyhedral model captures the geometric data from all the other models and some specification data entered by the user. The output of this model is constituted of polytopes and polyhedra objects in native extension files as shown in Fig.4.4.f.

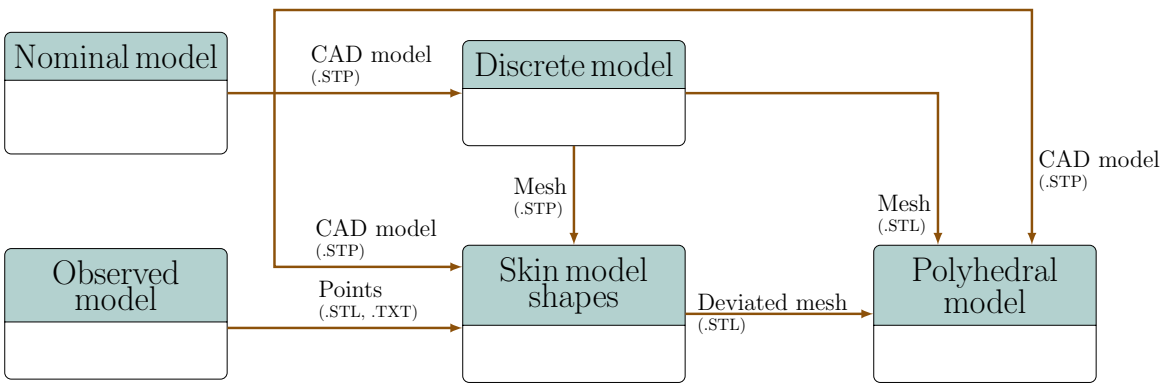

Fig. 4.5 Connections among the different models

It is important to preserve the geometric and topological information to be able to easily trace back the information at every stage of the process. The CAD model is the starting point in the design process and its information is necessary for generating instances of the skin model, and to represent the geometrical variations and the contact simulation through

polyhedra. In the Fig.4.5, the connections among the models are shown. This allows to consider the data dependencies and to think of ways to interface the different modules. There are two clear paths for representing the tolerance information through polyhedra. One is using the skin model shapes model, and the other is working with ideal feature models. It is worth mentioning that the system is conceived to be modular, meaning that the user could make use of it as a deviation modeler or tolerance analysis tool.

c Process view

The complete process view for conducting tolerance analysis with the integrated approach is shown in Fig.4.6. The first part consists on the idealization process from which we obtain the CAD model and its partitioned features.

Then, the discretization takes place through a tessellator or a mesher. The external mesh serves at the deviation modeling process, and it can be also used to generate operands with ideal features. The deviation modeling part is optional, in this step we can model the deviations and collect the individual features back together.

The polyhedra operand creation can take place from ideal or non-ideal features. It allows the creation of geometrical, contact and functional polyhedra for carrying tolerance analysis. The polyhedral operands are created for individual features. A feature can be an individual surface or a collection of two or more surfaces considered functionally. Finally, the compliance evaluation is done by verifying that the resultant operand for a given set of tolerance respects the functional requirement. If it is not the case, a new set of tolerances can be assigned, and/or new instances of skin model can be generated.

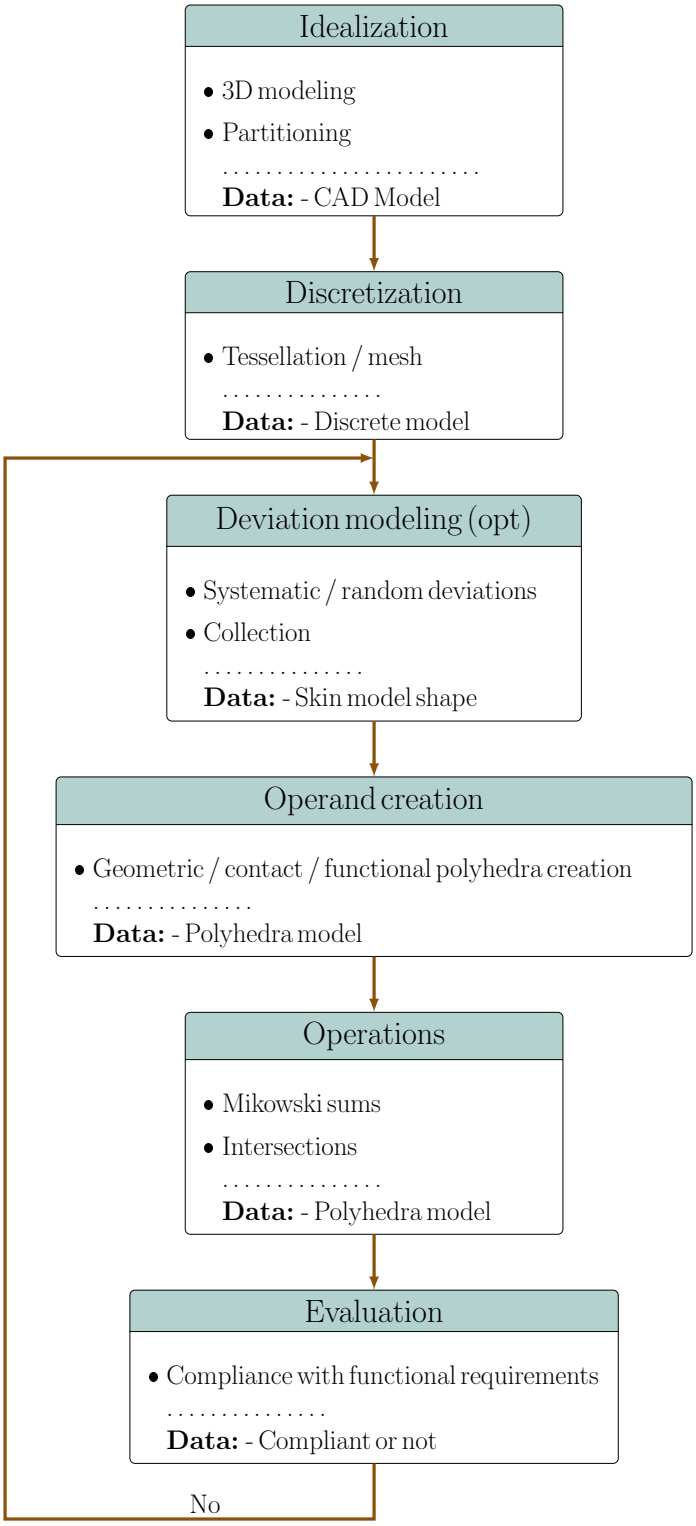

Fig. 4.6 Tolerance analysis process in the integrated platform. The deviation modeling step is optional, the polyhedra can be created from ideal or non-ideal features. The compliance is a binary response, if it is not compliant, new instances of skin model are created and/or new set of tolerances are tried.

d System functionality

In order to explain the functionality of the systems, the UML Use Case diagrams were used. Use cases are a way to foreseen the actual behavior of the system, and they help on the construction of classes and objects [5]. In Fig.4.7, the little human-like icon represents the actors of the system, which can be users of the system or other systems like in the case of the modeler and mesher.

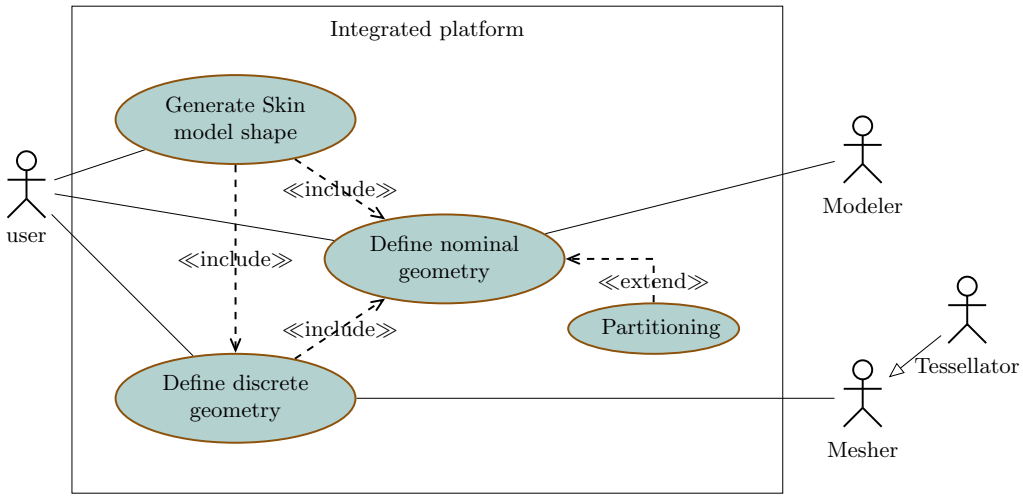

Fig. 4.7 Use case integrated system.

The use cases represents the functionalities or services provided by the system and they are in oval shapes (Generate Skin model shape, define discrete geometry...etc.). The line connecting an actor to an use case is called a communicates relationship and it means that the actor uses or participates in the specific functionality. The arrows from *Generate Skin model shape* and *Define discrete geometry* to *Define nominal geometry* labeled with an "include" stereotype indicate that *Generate Skin model shape* and *Define discrete geometry* uses *Define nominal geometry* use case. The same with the "include" relationship from *Generate Skin model shape* to *Define discrete geometry*.

The arrow from *Partitioning* to *Define discrete geometry* with the "extend" stereotype indicates that *partitioning* is an option from the *Define nominal geometry* use case. The big rectangle represents the boundaries of the system. The line from the actor *Tessellator* to *Mesher* is generalization relationship.

Fig.4.8 elaborates the *Generate Skin model shape* use case. In this use case, the user is depicted inside the boundaries of the use case. In order to generate a skin model shape, an association of the discrete features to the its continuous representation coming from the CAD model must be used, as well as the deviation computation process. The word association is used here to refer to the action of linking a polygonal mesh to the correspondent feature in the CAD model, it is not used in the sense of operation specified by the ISO GPS [66, 67].

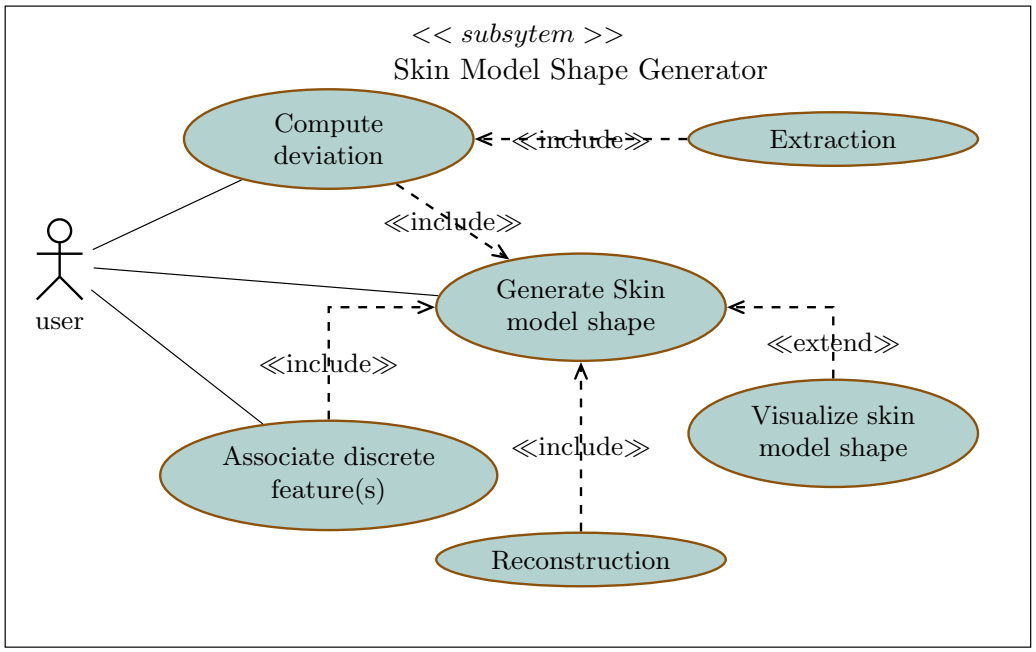

Fig. 4.8 Use case: skin model shape generator

Since the computation deviation process uses the discrete geometry of features as seen in Fig.4.8, the points from the discrete model are extracted and deviated, then a reconstruction of the deviated mesh takes place. The *Visualize Skin Model Shape* use case extends the *Generate Skin model shape* as it is an optional color map visualization of the deviated feature.

The use case *Compute deviation* is elaborated in Fig.4.9. The compute deviation use case is a generalization of the use cases *Compute systematic deviations* and *Compute random deviations*. These two include the extraction operation mentioned before. When the user is generating deviations for more than one feature, an identification of the shared vertices is necessary to be able to properly deviate those vertices in the right directions.

The use case *Visualize skin model shape* is elaborated in Fig.4.10. In order to create this visualization, the system has to use the functionality *find the discrete model* with no deviation

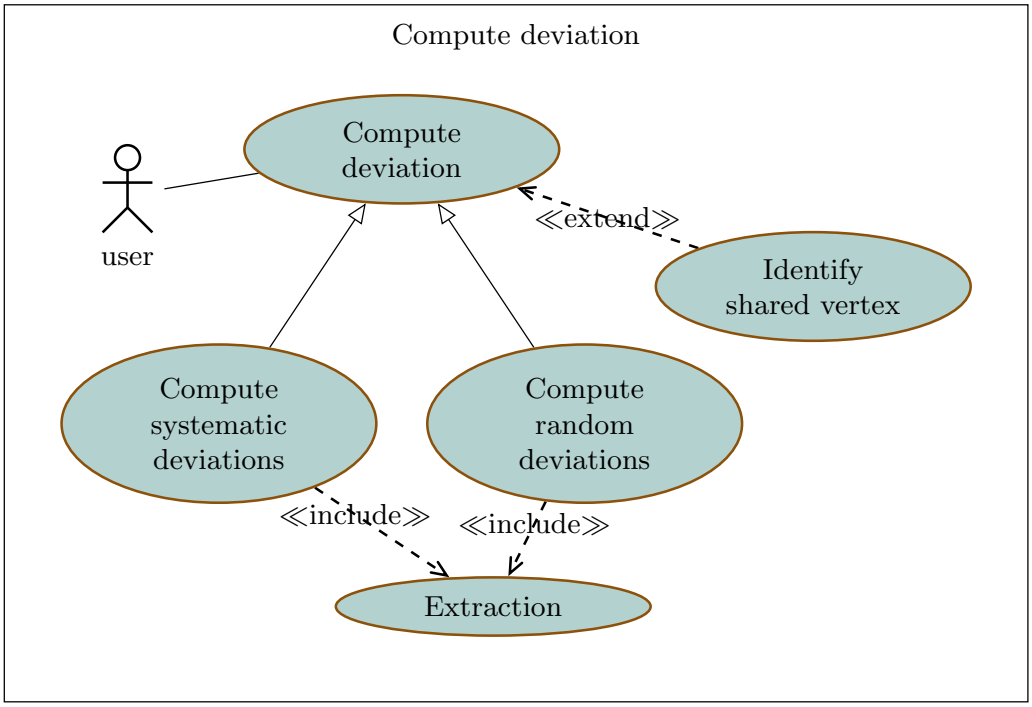

Fig. 4.9 Use case: compute deviation

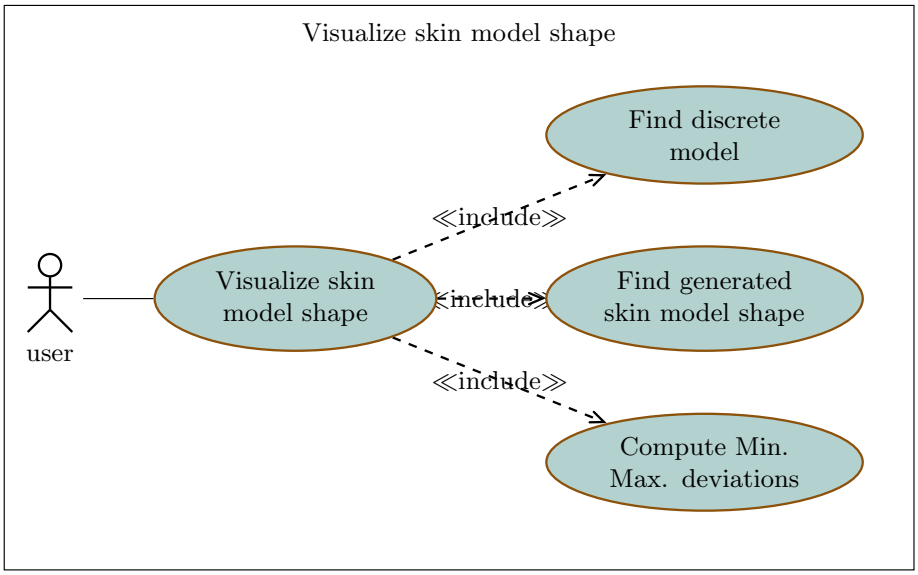

Fig. 4.10 Use case: visualize skin model shape

and the skin model shape, and compute the minimal and maximal deviation from them. Once that is done, a color map visualization can take place.

e Class diagrams

For the simulation of geometric deviation in individual parts, the skin model shape paradigm was implemented in PolitoCAT. In Fig.4.11, a UML class diagram presents the general data structure of the software before the implementation of the SMS generator.

The departing point is an assembly or a part. An assembly can be composed of one or more sub-assemblies and two or more parts. The parts are part of one assembly and they can have one or more tolerance features. A single tolerance feature object has as attributes: a name, the nature of the feature, the nominal geometry, the invariance class and the situation elements. The discretization of the feature in the previous architecture occur only in PolitoCAT using the OpenCascade meshing tools. The tolerance data consist on the type of contact or feature, and the tolerancing limits.

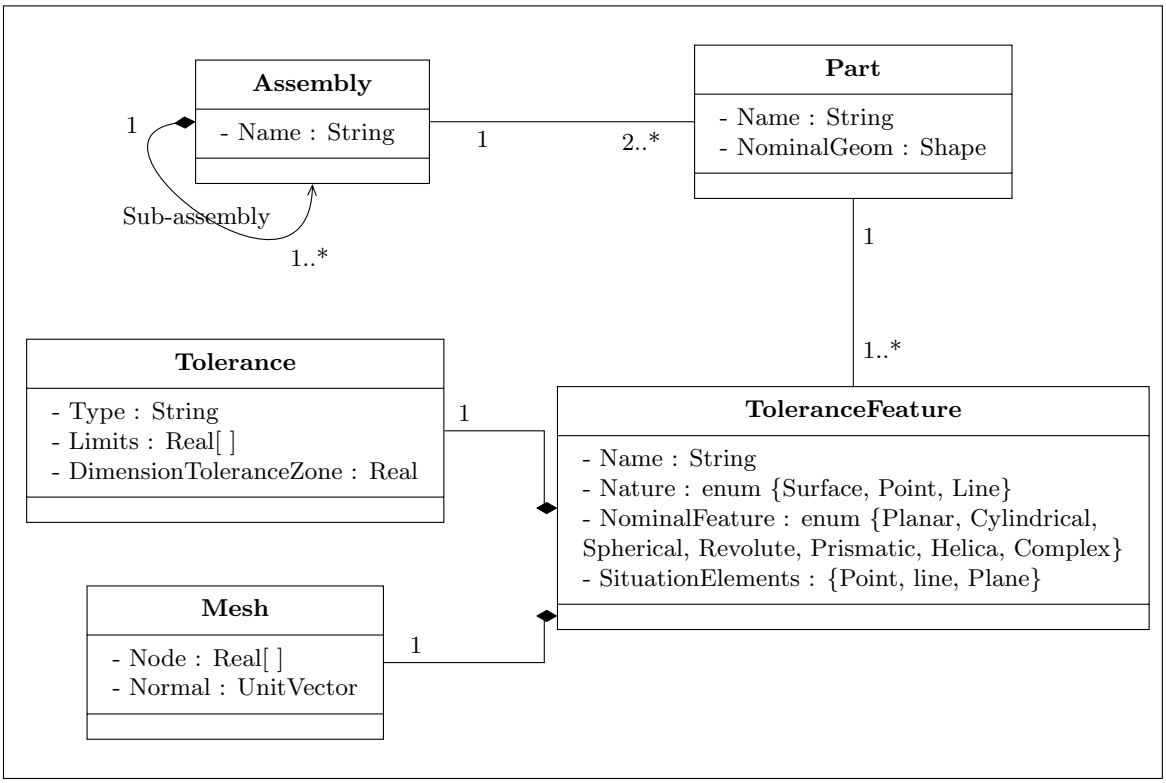

Fig. 4.11 General class diagram of PolitoCAT without including the Skin Model paradigm

The new structure that implements the Skin Model paradigm is build around the existing one as it can be seen in Fig.4.12. In this case, a single tolerance feature object has the same attributes as before plus: the feature representation (i.e.ideal, non-ideal), and a label

concerning the source of the discrete data. In the previous structure, the discrete model could only be generated in PolitoCAT; in the new one, the discrete model can come from measurements, simulations, or from a tessellating or meshing tool.

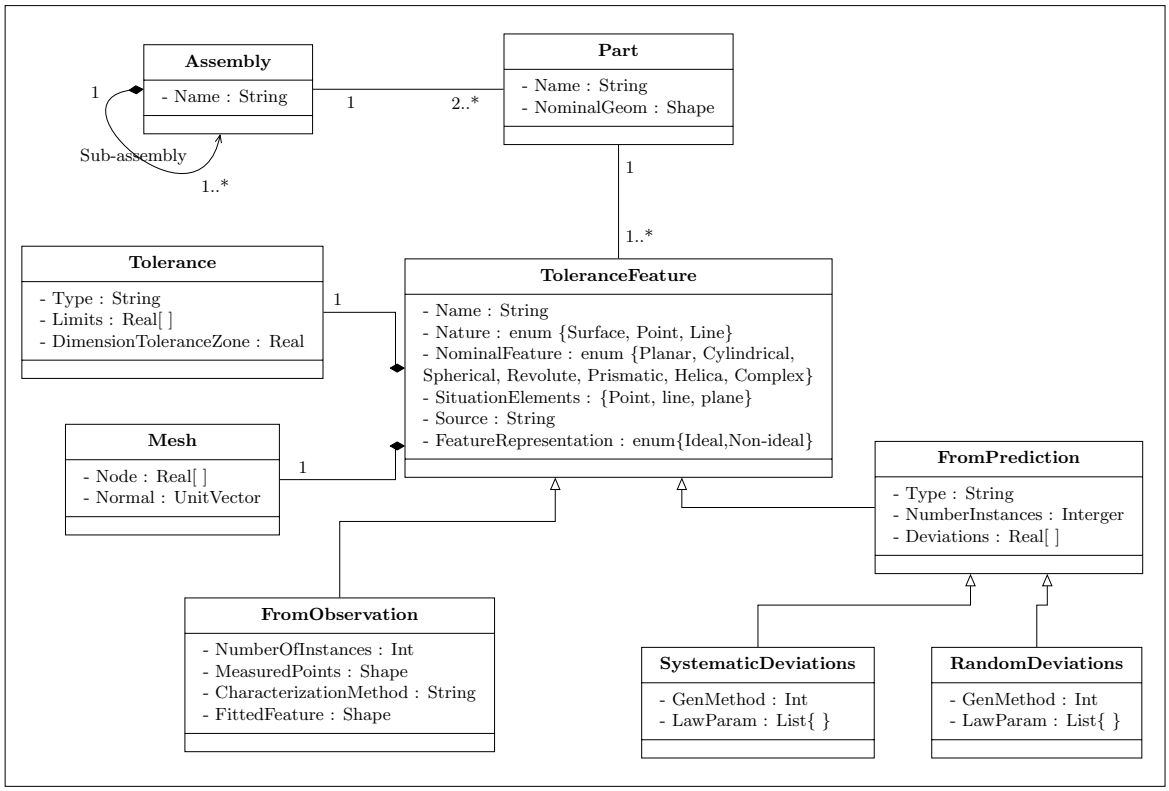

Fig. 4.12 General class diagram of PolitoCAT including the Skin Model paradigm

The Skin Model instances can be generated from both ideal and non-ideal features (i.e. a previous SMS). The deviation method to use depends on the type of feature and the and for the prediction case, on the type of deviations to generate (systematic or random). Each deviation method needs different parameters, and each deviation modeling method has a numerical identification

The deviation generator module has been programmed using C++ and is part of the PolitoCAT environment. It uses OpenCascade classes for the manipulation of the geometry. It allows the user to choose the type of deviation method to use, and set the parameters of the desired law for the deviation modeling. The advantage of having the deviation modeling process inside the PolitoCAT is that the topology and geometry of the CAD parts are directly exploitable.

f Example

The first part of the process takes place in Salome, the 3D modeling of the part and the partitioning and meshing process are carried out. Then, the deviation modeling and operand creation in PolitoCAT. The part taken as an example is a part with different types of features as it can be seen in Fig.4.13. The nominal model is exported in STEP to use it later in PolitoCAT.

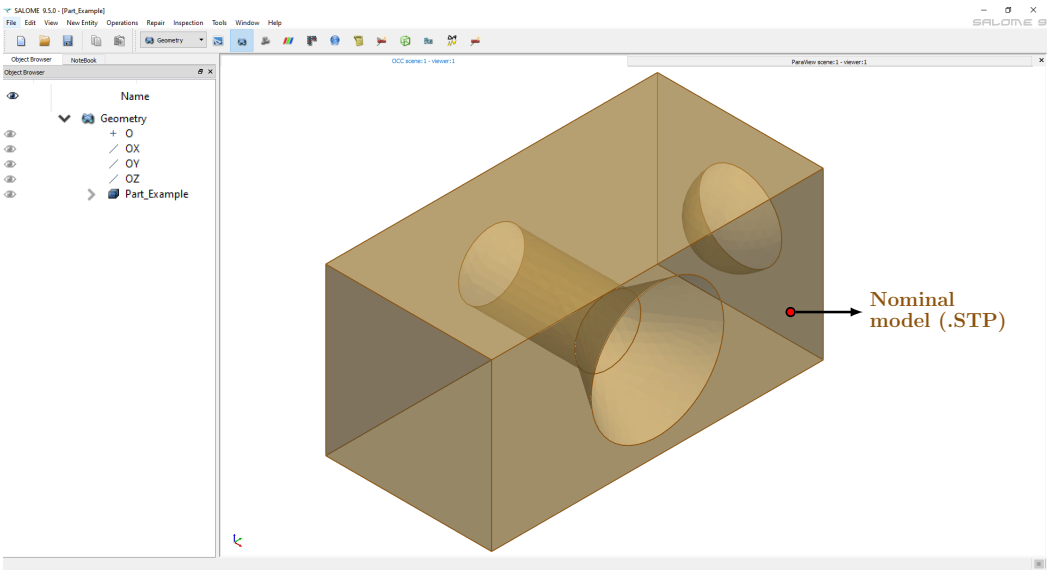

Fig. 4.13 CAD model created in Salome.

Partitioning

Inside Salome platform, the partition operation is performed in the part to identify the geometrical features belonging to the part. In this case, there are nine features identified as it can be seen in Fig.4.14.

There are six planar features, a cylindrical, a conical and a spherical feature. It is necessary to identify the features that play a role in the functional chain of a system. For the sake of this example, all of the features from the part were partitioned.

Discretization

The discretization step takes place in Salome. Salome has a wide range of mesh algorithms. For modeling deviations in a surface, it is important for the the mesh to be homogeneous

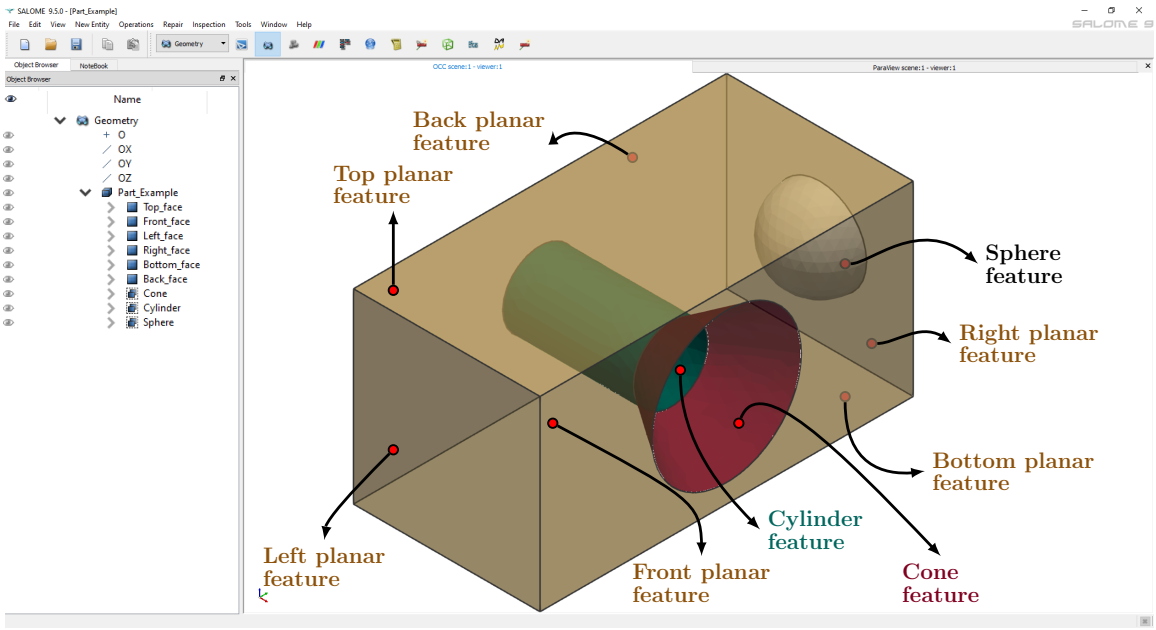

Fig. 4.14 Partitioning of the nine the tolerance features.

in density and globally consistent. When the mesh is not globally consistent, issues at the boundaries between features must be addressed. The meshing options in Salome include the wire discretization algorithms to control the density of points in the edges.

All of the features in the part were meshed independently but guaranteeing the global consistency as it can be seen in Fig.4.15. The features can be exported in many formats including STL, which is the one currently supported by PolitoCAT. The step part, and the nine meshes are the data input for the next steps.

Mesh association and operand creation from ideal features

Once the data has been gathered, it can be imported into PolitoCAT. The next step consists in linking the discrete features to the nominal model. It is necessary to input some geometric data at this stage as it is shown in Fig.4.16.a and Fig.4.16.b: the tolerance for a geometric feature in a zone or the clearance value, the number of tolerance features, whether there are any specific restrictions, the name of the discrete model and if it is a bilateral tolerance zone, or a unilateral or bilateral contact.

The feature that has been associated is presented in Fig.4.16.c, the user must select the outward direction. During this operation, all the edges are identified and the internal ones are suppressed for next operations. An internal edge limits a face that is inside a tolerance

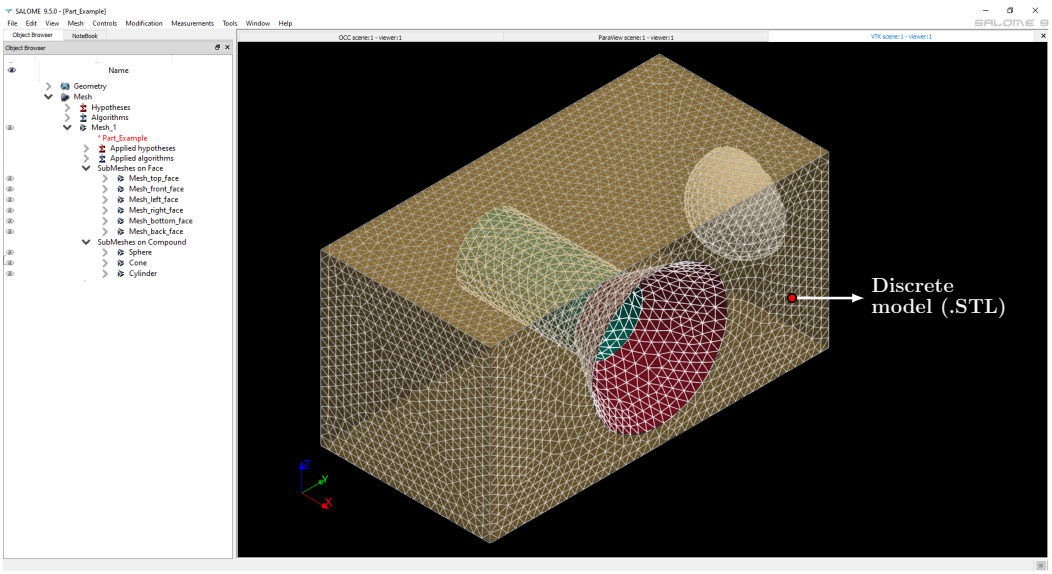

Fig. 4.15 Discretization step in Salome platform

element (i.e, edges created in CAD for solids of revolution).

The polytope that characterizes all the possible positions of the feature inside the tolerance zone is presented in Fig.4.16.d. When there are no form defects, the polytope correspond to a regular octahedron.

For the deviation modeling, the user needs to parametrize a text file with the geometric information about the part and feature, and the specific parameters for the deviation method chosen. An example of such text file can be found in the Annex.I.

In this case, only random deviations were generated to exemplify the use of the system in the prediction stage. Among the deviation methods for generating random deviations, the random Gaussian fields was chosen for implementation as the method is capable of generating deviations on any type of surface.

Random fields are a type of generalized stochastic process and are popular for modeling spatially varying uncertainties. The 3D random Gaussian method can be seen as a specific case of a random field. It is widely used in geology, hydrology and image processing. The random fields [3] take into account the spatial correlation among the elements of the mesh which translates into a more realistic modelization and visualization of the results. Gaussian fields are completely characterized by a mean function and a covariance matrix. The field

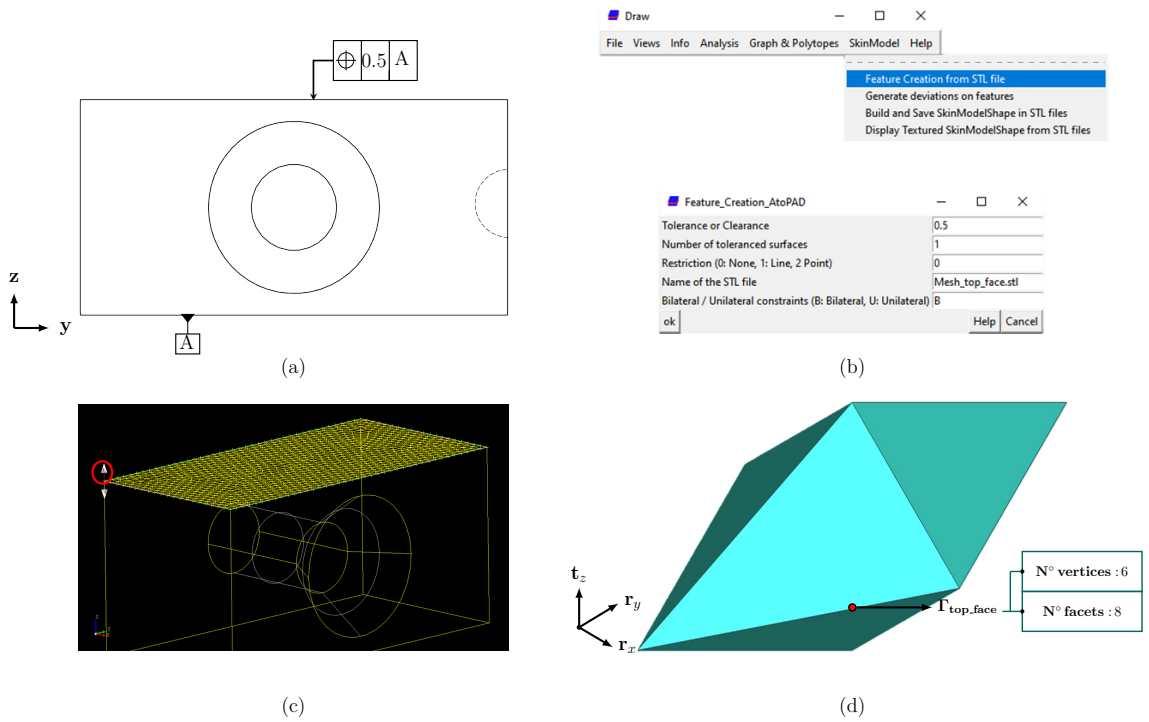

Fig. 4.16 a) Specification of a geometric tolerance feature. b) Parameters in PolitoCAT at the moment of the association of the discrete feature to the CAD model. c) The discrete model has been associated to the CAD part and the normal direction specified. d) Polytope of the top planar feature with no form defects.

is homogeneous if the mean and the variance are constant. A discrete approximation of a random field can be expressed as [117, 118]:

- Obtain auto correlation matrix $\boldsymbol{\rho}$, also known as kernel function, which is commonly calculated using the square exponential function:

$$\boldsymbol{\rho} = e^{\frac{||\mathbf{x}_i - \mathbf{x}_j||^2}{l_p}} \tag{4.1}$$

- The distance l_p corresponds to the correlation length that helps to the adjustment of correlation strength between two random variables in two points $\mathbf{x_i}$, $\mathbf{x_j}$ and it could be calibrated through the analysis of experimental data. If l_p is small, the two random variables are strongly correlated if the distance between $\mathbf{x_i}$ and $\mathbf{x_j}$ is small. Inversely if l_p is large, the random variables are strongly correlated if the distance between $\mathbf{x_i}$ and $\mathbf{x_j}$ is large.

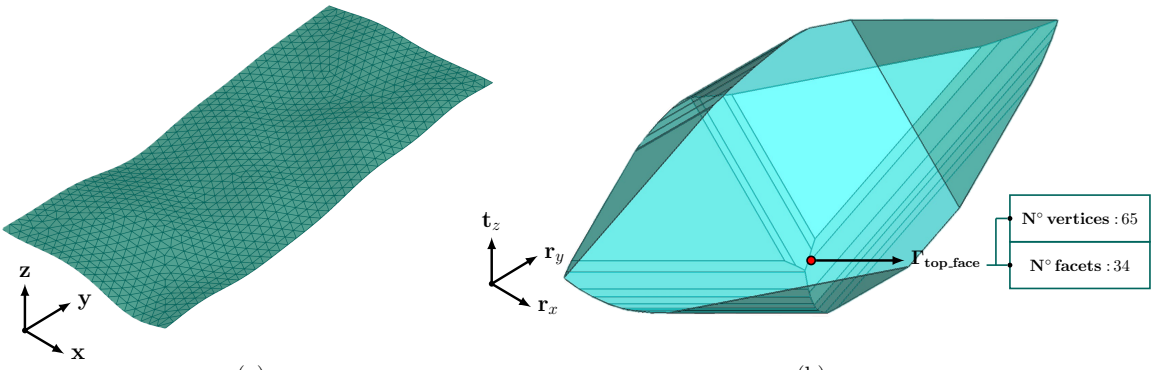

(a) (b)

Fig. 4.17 a) Skin model shape of the top feature. b) the polytope of the feature in the specified tolerance zone with form defects

- Calculate **B**, the largest eigenvalues of the auto correlation matrix in the principal diagonal, and **C**, the corresponding eigenvectors to compute the transformation matrix **A** as:

$$\mathbf{A} = \mathbf{B}\mathbf{C}^{(\mathbf{1}/\mathbf{2})} \tag{4.2}$$

- The vector of random values $\boldsymbol{\delta}$ can be calculated as follows:

$$\boldsymbol{\delta} = \boldsymbol{\mu} + \boldsymbol{\sigma}\mathbf{A}\boldsymbol{\varepsilon} \tag{4.3}$$

- $\boldsymbol{\mu}$ and $\boldsymbol{\sigma}$ are the mean and the standard variation respectively, and $\boldsymbol{\varepsilon}$ is the vector containing n independent Gaussian random variables with zero mean and unit variance.

The algorithm for obtaining the random fields was programmed in C++ and it makes part of the deviation feature generator module. This method has as modifiable parameters: the standard deviation ($\boldsymbol{\sigma}$), correlation length (l_p), initial mean vector ($\boldsymbol{\mu}$) and the kernel estimation. This can lead to achieving a more realistic distribution and level of the defects. For the specific case, the non-ideal part corresponds to the value of the correlation length of 10, a mean and standard deviation of zero and one respectively.

The deviated feature is presented in Fig.4.17.a, and the corresponding polytope in Fig.4.17.b. Notice that adding the form defects produces a more complex irregular polytope. The volume of the operand with 34 faces and the 65 vertices characterizes the translation and rotations of the planar feature with form defects inside a tolerance zone.

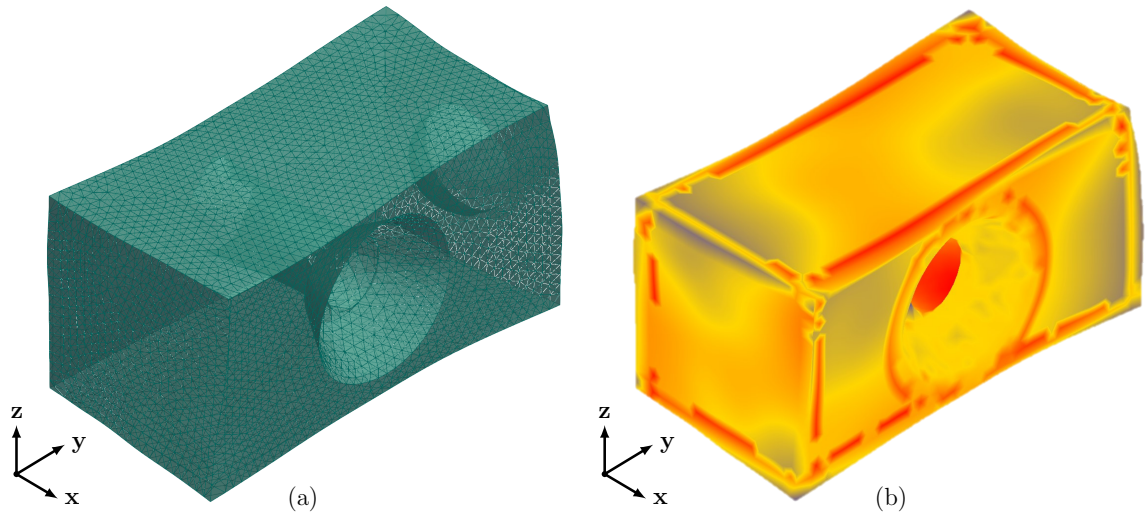

Fig. 4.18 a) Skin model shape of all the features in a part. b) Color map view of the same skin model shape

Lastly, we can repeat this procedure for all the features in the tolerance parts and reconstruct a deviated shape. In Fig.4.17.a, the skin model shape with defects in all of the feature is presented. Next to it, the same deviated part with a color map applied.

IV Contact modeling integration

For the contact modeling integration, it is necessary to differentiate between the contact modeling under rigid bodies hypothesis and the local deformation. In the contact modeling with the rigid bodies assumption, the idea is to solve the contact between two or more matting features, with or without form defects by including the external loads acting on the system. The local deformation process uses the rigid contact configuration to initiate the deformation process.

The contact modeling process is included in the system as an additional module, just as the SMS generator presented above. This module is composed of the rigid contact modeling and local deformation simulation. The general structure of the system does not change as it can be seen in Fig.4.19.

The data needed for the contact simulation consists on the geometric, specification and mechanical data. The contact modeling uses specially the polyhedral data of the studied contact as it is from the deviation space that the contact is resolved. The mechanical data consists in the external loading data (magnitude, direction and point of application) for the

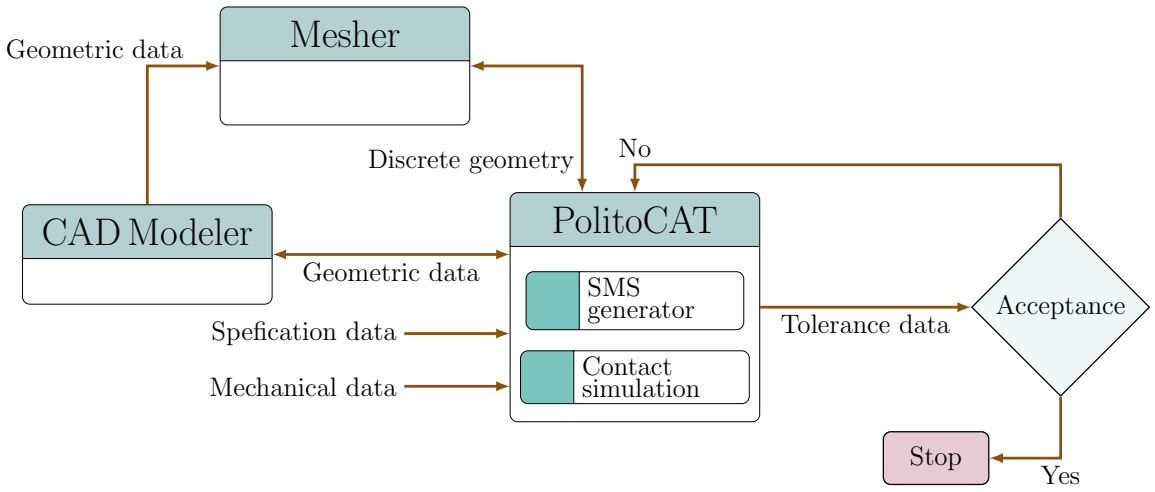

Fig. 4.19 General architecture PolitoCAT. The modules developed in this work shown inside PolitoCAT: SMS generator and Contact simulation

rigid contact configuration, and on the material properties for the local deformation process.

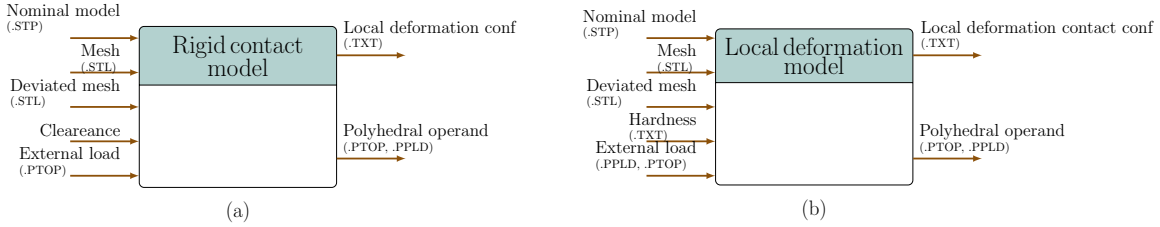

Fig. 4.20 a) View rigid contact model. b) View local deformation view

In Fig.4.20 the inputs and outputs of both models composing the contact simulation module are shown. On the left (a), the rigid contact model needs the geometric information coming from the nominal and discrete models. The rigid contact configuration can be found for ideal or non-ideal features potentially in contact. For doing so, the clearance value and the external load's direction, magnitude and point of application must be specified. The outputs are the contact polyhedron and contact configuration in the rigid case, consisting on the information about the vertex and half-spaces from the polyhedron, and the ID's and coordinates of contact points from the discrete geometry. On the right (b), the inputs are the same as in the rigid case (a) (except for the clearance assumed to be 0) plus the result of the rigid contact configuration and the material's hardness. The outputs for this model are the number and localization of the points that were deformed, the polyhedral operand after the

deformation process.

a Contact modeling classes

Two new classes are part of the system as it can be seen in Fig.4.21: contact feature and local deformation. The contact feature class is associated to the tolerance feature class. One tolerance feature can be part of zero or more contact features. The contact feature class represents the physical interaction between mating features modeled with or without form defects. This class resolves the contact between two or more features in contact. The class has a parameters the force magnitude, the point of application of the external loading and the wrench. The wrench parameter represents the combination of force and torque written at the calculation point.

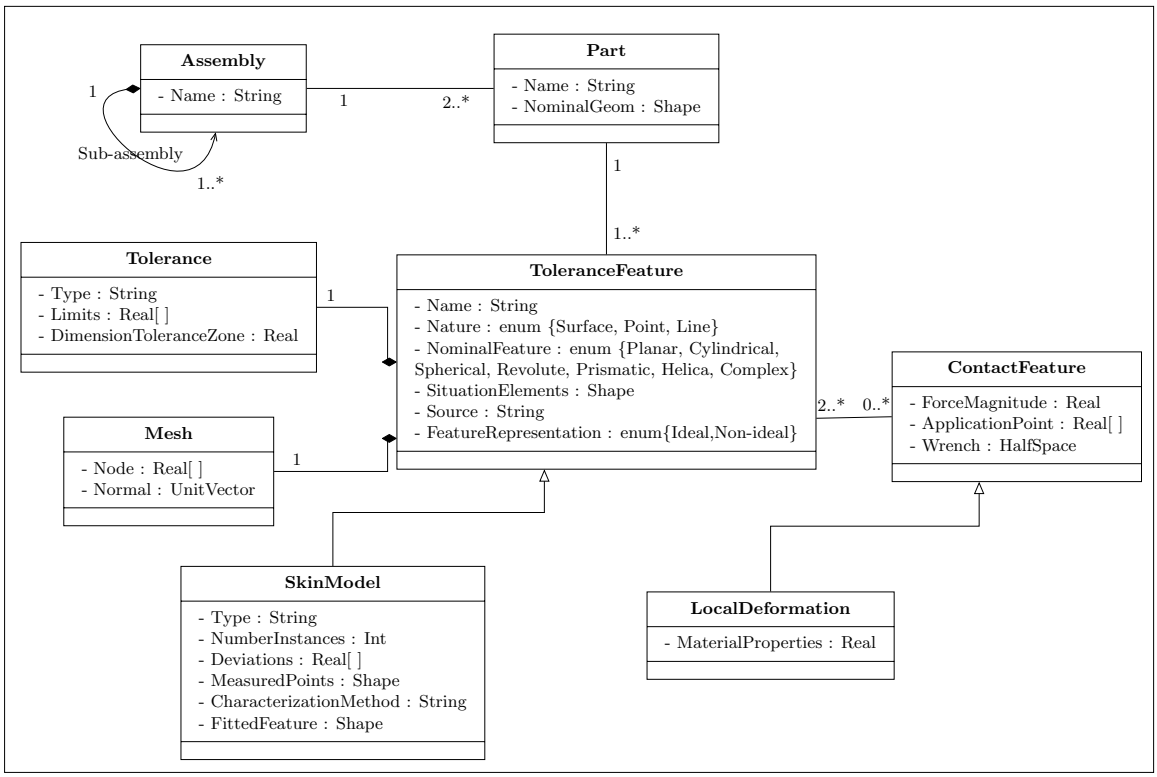

Fig. 4.21 Class diagram including the contact modeling

The local deformation class is inherited from the contact feature and resolves the contact when local deformation is modeled in the system. The material properties define the material characteristics that affect how the object deforms under the applied forces. The new classes

in the class diagram in Section e are represented In Fig.4.21 as the skin model class, it groups the classes depicted in the previous diagram (Fig.4.12).

The next section presents an example of the contact simulation in the rigid case and the algorithm to find the vertex that minimizes the volume of the contact polyhedron.

b Implementation example

To illustrate the functioning of the integrated system, specially of the contact simulation module, let us take the example of the assembly of the parts showed in Fig.4.22.a. The ring (in green, at the left) is connected to a pipe (in brown, at the right) by three bolts, not shown, spaced 120 °between them. Fig.4.22.b discretized contact element. It is obtained by intersecting the two features potentially in contact.

The difference surface shown in Fig.4.22.c comes from the deviations generated in both of the features potentially in contact. These features were generated using a modal decomposition method that models the systematic deviations of both features. The files used for the generation of both features are shown in Appendix I. The modal decomposition method uses a different base for planar and cylindrical surfaces, and a modal signature that composes the modes in the base. The user can define their own modal bases and signatures as long they respect the following requirements:

For planar features:

1. The sample plane for the base is a 50 mm x 50 mm square
2. The origin is the barycenter of the square
3. The plane normal is set along the $\hat{z}$ direction

For cylindrical features:

1. The radius from the sample cylinder is $14.08\,mm$
2. The length of the cylinder is $12.02\,mm$
3. The axis of the cylinder must be in the $\hat{z}$ direction

4. The origin has to be defined in the mid-point of the length coincident with the axis $\hat{z}$ of the cylinder. So half of the distance lays in the positive direction and half in the negative direction of the axis.

The feature coming from the ring becomes the difference surface. Fig.4.22.c also shows the feature whose deviations have been transferred to the difference surface.

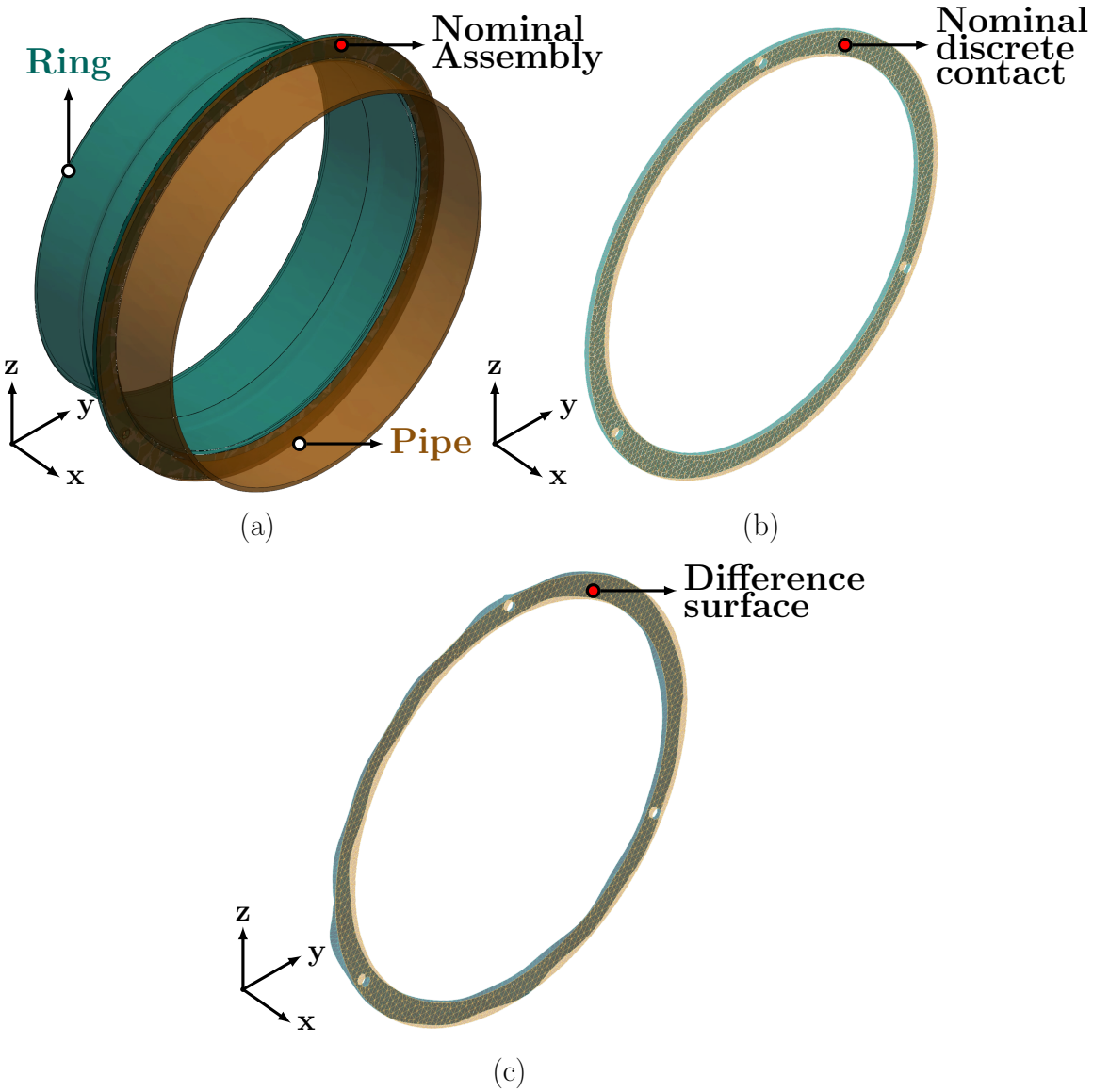

Fig. 4.22 a) Nominal assembly of two parts: a ring and a pipe. b) Discretized contact element coming from the intersection of the features potentially in contact. c) Difference and equivalent surfaces.

The operations executed on the assembly correspond to the identification stage (nominal model of the assembly, key mating features identification and partitioning), and the devia-

tion modeling stage (discretization, SMS generation and difference surface computation) described in the framework shown Chapter 1. All of the contact simulation operations happen between the different surface and an ideal feature.

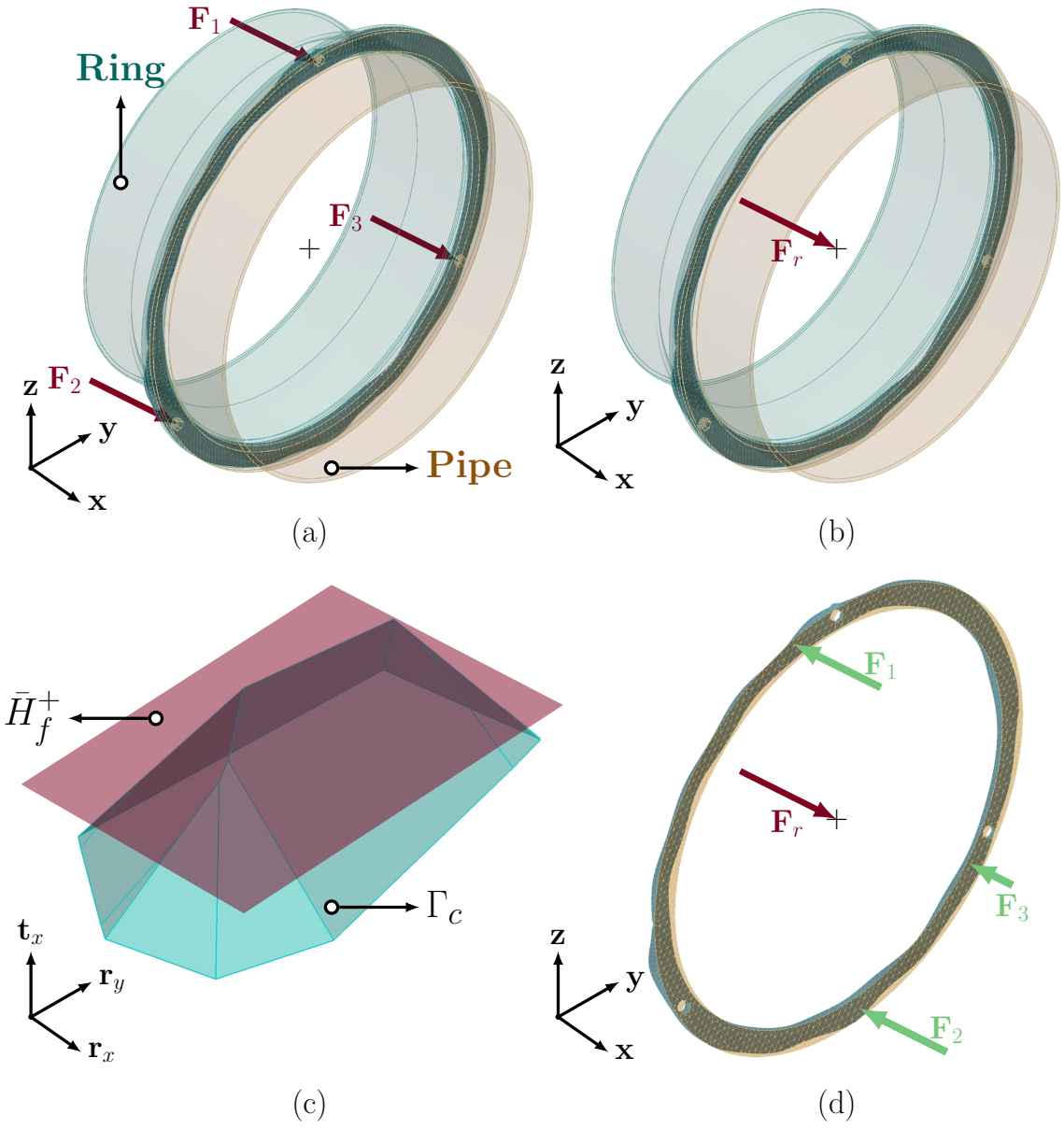

Fig. 4.23 a) Forces acting on planar contact between the difference surface (pipe) and equivalent surface (ring). b) Resultant force acting at the origin. c) Contact polyhedron with force half-space. d) Reaction forces (green) acting on the contact points

Once that the skin model instances of the contact have been generated, we can incorporate the external loading conditions as shown in Fig.4.23.a .The three forces represent the action

of the three bolts that maintain the contact between the two parts. These three forces can be expressed at the center of the contact between the two parts as shown in Fig.4.23.b, $\mathbf{F}_r$ represents the action of the three bolts.

Algorithm: volume minimization

The polyhedron shown in Fig.4.23.c results from the difference surface. The bottom part of the polyhedron is actually non-bounded since the contact is an unilateral one. As it was explained in Chapter 2 the action of an external load acting on the contact keeps it from moving, this load is represented as the half-space in red

.

Algorithm 1 Minimization of contact polyhedron

Require: $\Gamma_c, \bar{H}_f^+$
  Let $\{\Delta_i\}$ be the straight lines of Γ_c
  Let $\{\bar{H}_i^+\}$ be the half-spaces of Γ_c
  Let $\{V_i\}$ be the set of vertices composing Γ_c
  if $\{\sum_i \Delta_i\} \perp \{\bar{H}_f^+\}$ **then** ▷ Kinematic compliance is verified
    if $Vol(\{(\cap \bar{H}_i^+) \cap (\bar{H}_f^+)) > 0$ **then** ▷ The intersection generates a volume
      Compute the distance (D_i)
      (D_i) distance between V_i and $\bar{H}_f^+$
      for $i = 1; i <$ size of V_i; i++ **do**
        Compute the distance (D_{i+1})
        (D_{i+1}) distance between V_{i+1} and $\bar{H}_f^+$
        if $(D_{i+1}) > (D_i)$ **then**
          Reset (D_{max})
          $(D_{max}) = (D_i)$
          $(D_i) = (D_{i+1})$
        else if $(D_{i+1}) == (D_i)$ **then**
          $(D_{max}) = [(D_i), (D_{i+1})$
        end if
      end for
    else ▷ The wrench does not bound the polyhedron
      Stop
    end if
  else ▷ The wrench is not included in the subspace of bounded displacements
    Stop
  end if

The search of the vertex that minimizes the volume of the polyhedron can be simply be written as the search for the maximal distance between the force half-space and each of the vertices that conforms the polyhedron as in the Algorithm 1. The algorithm requires the contact polyhedron Γ_c and the load wrench represented as the half-space $\bar{H}_f^+$. The first thing is to verify if the kinematic compliance is respected. This can be done by assuring that the straight lines of the contact polyhedron (Δ_i) are perpendicular to the force half-space itself. If it is not respected, then the procedure stops. If it is respected, then it is necessary to verify if the external load can actually turn the unbounded operand into a bounded one. This can be done by checking if the intersection of the polyhedron and force restriction gives a positive volume. If the operand cannot be bounded by the additional force half-space, then the procedure stops; otherwise, the algorithm searches for the furthest vertex by calculating and comparing the distance from each vertex to the force half-space. It can sometimes happen than more than one vertex have the same distance value to the half-space which generally translates in a instability on the contact.

The resolution of the contact gives back as the result the contact points. By having the contact points and the external load, the static solution of the contact be found. In Fig.4.23.d a small displacement torsor has been applied to the ring so the green arrows indicate the nodes in contact. These arrows represent the direction and magnitude of the reaction forces at each point. This image represents the way PolitoCAT actually shows the reaction forces in the system.

In Fig.4.24 the politoCAT interface with example is shown. On the left part, the console shows the parameters needed for the resolution of the contact in rigid configuration. These parameters are:

1. The HV-description of the contact feature
2. The wrench of the external load in .PTOP format
3. The H-description of the contact feature
4. The coordinates of the calculation point
5. The direction of the external load
6. The magnitude of load

The result is shown on the viewer with the green arrows pointing at the contact points. A text file is generated as an output every time this command is executed. The text file contains

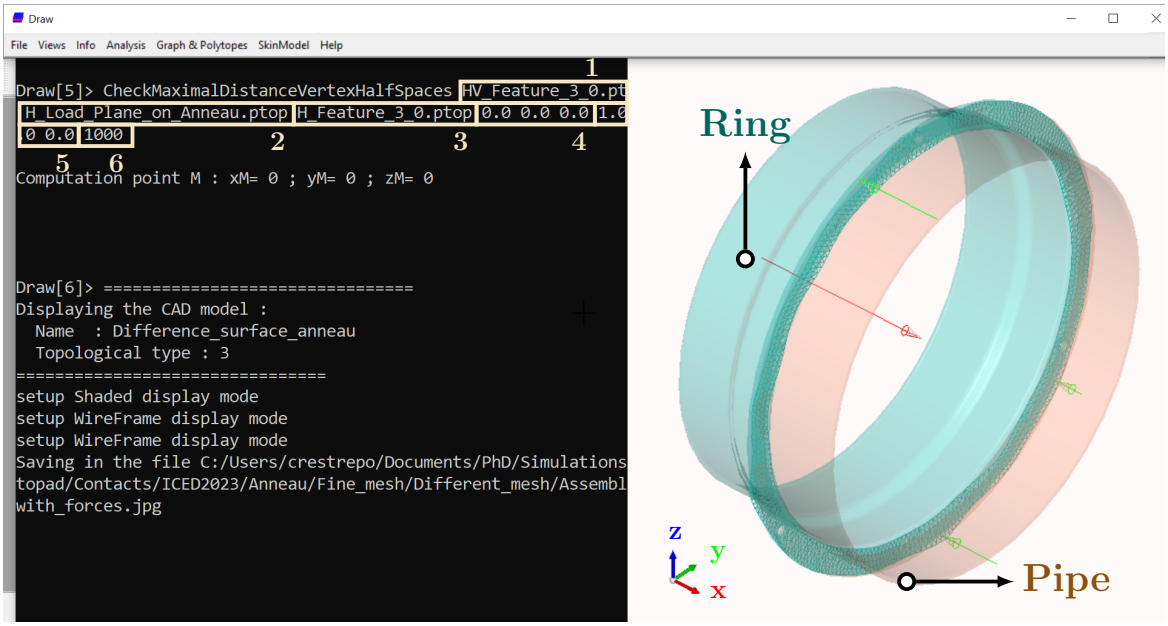

Fig. 4.24 The list of parameters in the console (left part of the image): 1) The HV-description of the contact element. 2) The wrench of the external load in .PTOP format. 3) The H-description of the contact feature. 4) The calculation point. 5) The direction of the external load. 6) The magnitude of load.

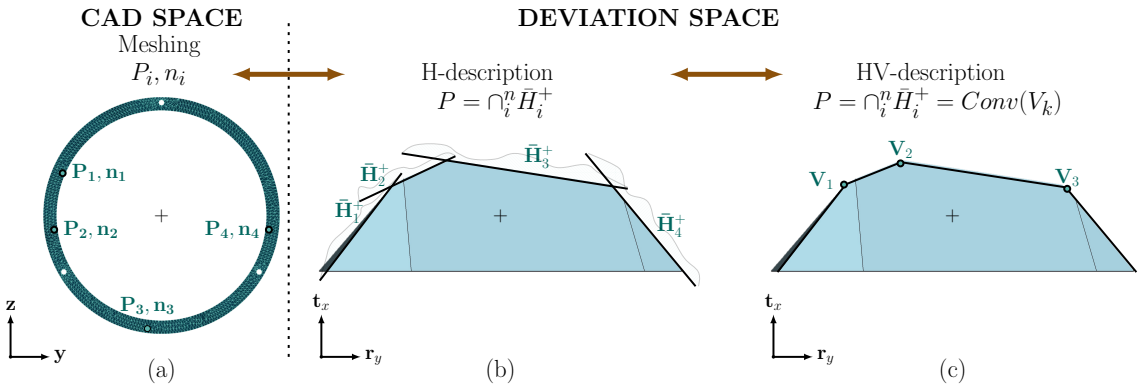

Fig. 4.25 Data tracking between the CAD and deviation space. a) Planar contact feature in the CAD space. b) Schematic 2D view of the contact polyhedron showing the H-description. c) Schematic 2D view of the contact polyhedron showing the HV-description.

the static solution of the system, the ID and coordinates of the contact points in the mesh and the topological information of the vertex (or vertices) from the polyhedron that generated the result.

Tracing back the contact points from the HV-description is possible because the half-spaces are written for specific points on the mesh. In Fig.4.25.a, a planar contact feature

is shown in the CAD space. This feature is meshed with a given number of points $\mathbf{P}_i$ that have normals $\mathbf{n}_i$. Half-spaces are expressed on each one of these nodes and they result in the H-description of the contact polyhedron shown in Fig.4.25.b. When these half-spaces are intersected, then the vertices of the polyhedron can be found. This results in the HV-description shown in Fig.4.25.c. For any given vertex in the HV-description it is possible to find the half-spaces that generates it, therefore, the point in the CAD space where the half-spaces were written.

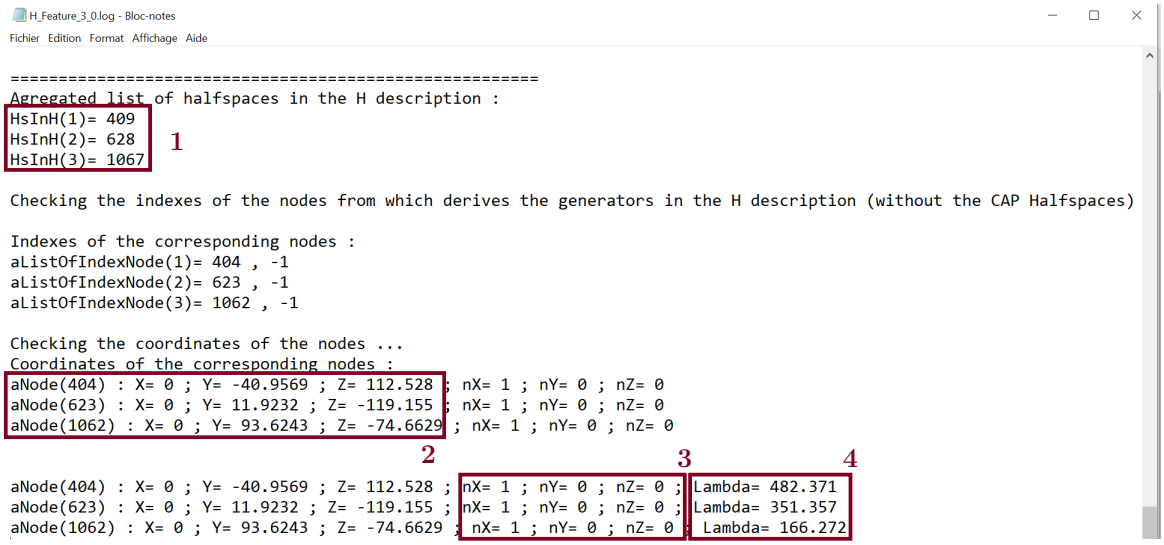

Fig. 4.26 The information in the text file: 1) The index of the half-space in the H-description that generate vertex that minimizes the volume. 2) The corresponding nodes' coordinates of the difference surface mesh. 3) The direction of the external load. 4) The magnitude of the reaction forces on the contact points.

In Fig.4.26 the text file is shown. The information presented in the text file corresponds to:

1. The index of the half-space in the H-description that generate vertex that minimizes the volume
2. The corresponding nodes' coordinates of the difference surface mesh
3. The direction of the external load.
4. The magnitude of the reaction forces on the contact points

The force reactions calculation is currently able to solve only the isostatic configurations. In this case, if there was one, or there were two or three reaction forces the system would be

able to find a solution. This is the first step for the local deformation process.

V Conclusions and future work: Implementation

The idea behind many CAT solutions is not only to allow tolerance analysis and synthesis, but doing it in a comprehensive manner that allows the inclusion of different sources of variation, and integration of other mechanical phenomena that impacts the final quality of a piece and/or assembly.

Most of the current CAT systems are integrated in complex software suites that are moving towards the goal of a holistic approach in engineering, it includes the design, simulation, manufacturing and inspection of complex systems. Because of the intricate network they are it is difficult to implement specific paradigms or workflows, specially the inclusion of form defects from the conception, and the impact of the local deformations in the conformity of the assemblies.

This first part of this chapter showed the implementation of the skin model paradigm in an open source CAT. A deviation modeler was implemented to take into account the geometric deviations from a prediction or observation perspective. From a prediction point of view, the system allows the modeling of systematic and random deviations, and since it is open source, an user could add their own geometric deviation laws if needed. From an observation point of view, the user could import a triangular mesh coming from measurements and with a given modal base the system can find the modal signature that produces such measured deviations.

The second part showed the implementation of the contact modeling module divided in two parts: rigid contact and local deformation configuration. Only the rigid configuration has been fully implemented. In the rigid case, the contact was solved by incorporating the external wrench as an additional half-space in the deviation space (contact polyhedron). The magnitude of the reaction forces is only possible for the isostatic case.

The inclusion of the aforementioned modules in PolitoCAT has the following advantages:

- The deviation modeling process for generating the skin model shapes can be used as standalone module

- The existing methods for deviation modeling can be easily parameterized and new ones can be added
- The deviation modeling is performed in a feature-based manner which allows to adapt the level of simulation detail
- The contact simulation with or without form errors can be simulated by incorporating the external loading conditions

There exists some disadvantages on the use of any CAT software, for PolitoCAT some of them concern:

- **Limited analysis:** Although analysis and synthesis can be performed using polyhedral operands, all stochastic analysis currently takes place outside of PolitoCAT.
- **Integration:** Even if it is fully compatible with platforms based on OpenCascade, the direct integration has not been fully achieved which necessary implies to switch from one software to another
- **Custom functionalities:** As any open source solution, adding new functionalities can result difficult due the familiarization with tool.

The perspective of this project is to be able to incorporate PolitoCAT as a deviation modeling and tolerancing module in Salome platform. Since both software are based in OpenCascade kernel and use $C++$ as programming languages the compatibility is assured. The algorithms for the calculation of contact points given the load boundary would also be available in the same environment.

The plastic local deformation algorithms are currently being developed and they will be also available in a future release of the software.The resources and how to obtain Skin model shapes, the contact simulation as well as the new version of PolitoCAT can be downloaded from the website of the project AToPAd.

Chapter 5

Conclusions and perspectives

The main interest of this work is to contribute to a more realistic behavior of complex mechanical systems. The work was carried out using prismatic polyhedra and it can be situated at the conjunction between purely geometrical and purely mechanical approaches in mechanics. The characterization of geometrical deviations and their incorporation in tolerancing process is one of the added-value of this work. The quantification of the contribution of the form defects in a contact chain under the hypothesis of rigid bodies allows to establish more realistic tolerance limits and could be use to suggest better capability indexes for the processes. The digital implementation plays an important role in this work. The motivation was to offer tools that allowed the modeling of complex architectures and there were open and free of use.

The first chapter presents the general framework for the incorporation of the skin model shapes and contact modeling using the polyhedral-based approach in tolerancing. The discrete framework is divided in three phases: model preparation, contact simulation and model evaluation. The framework allows the designer to adapt the level of detail that they need to use in the modeling of a mechanical system.

The main contribution of the second chapter is the enrichment of the mathematical definition of prismatic polyhedra for contact modeling. The inclusion of the external loads as additional constraints in the deviation space allows to solve the contact between any two ideal or non-ideal mating features. It was also shown that with the explicit description of the external loads in the polyhedral-based model the fixed and floating configurations in unilateral contacts can be fully modeled. The study case in Chapter 2 showed that the contact points in the geometry can be found even for sliding contacts whose degrees of freedom are constraint by a parallel contact (See Section V in Chapter 2). The main advantage of using the proposed method is that once the contact polyhedron has been computed, the rest of the process happens in the deviation space which makes it independent of the type of contact being modeled.

The approach presented in Chapter 3 allows to model the local deformation between two features in contact. The computation of the local deformation in the tolerancing context is generally done independently of the tolerancing model, the computed deformations are then

included in the tolerance model to validate a functional condition. The approach presented here iterates directly over the tolerancing model which allows to follow the state of the deformed feature at every step. Since it all happens in the wrench and deviation spaces, we can make abstraction of the type of contact being modeled.

The fourth chapter presented the implementation of the skin model shapes and the methods presented in the second and thirds chapter for contact modeling. It highlighted the importance of having integrated CAT solutions that allow a more realistic simulation of the geometrical and mechanical behavior of systems. With the developed algorithms and modules this work contributes to use open source integrated CAT solutions.

The development of open-source CAT systems, as exemplified by PolitoCAT, plays a critical role in democratizing access to advanced tools for tolerance allocation and analysis. By providing open and freely available software, the designers and researchers can model complex mechanical systems, incorporate non-ideal features, and perform detailed tolerance analysis without the barriers of proprietary software costs. This open access can lead to wider adoption and further innovation in the field of tolerance engineering.

The integration of local deformation modeling directly into the tolerance analysis process represents a significant advancement in the accuracy of mechanical simulations. By iterating over the tolerancing model and accounting for local deformations at every step, the approach enables a more detailed understanding of how these deformations impact the overall assembly. This detailed modeling can lead to more precise tolerance allocation, ensuring that products meet both functional and durability requirements under real-world conditions.

I Perspectives

This work responded to the research questions concerning the representation and integration of non-ideal features in the polyhedral-based approach, and the contact modeling aspect. The depth of given responses was variable, and in some cases, implied a significant limitation to the generality of the presented approaches. In Chapter 1, the presented framework focused on discrete features. As explained in the chapter, even if this type of features are the most common in the tolerancing context, the continuous representations (B-rep and NURBS) are also used in this context [105]. A framework to conduct tolerance analysis and synthesis using continuous representations models could be of interest to researches across different fields in engineering.

Concerning the contact modeling, the work presented here did not include any stabilization criteria for dealing with unstable contact cases. The obvious expansion of the presented approach for rigid contacts is to is to include such stabilization criteria. Both, the rigid contact modeling and local deformation assumed frictionless contacts. It could be interesting to explore how to include friction in the polyhedral-based model. Roboticians already do this

by incorporating a friction model and representing the acting forces by polyhedral cones [80]

For the local deformation case, the next step should be the inclusion of the elastic behavior of the contact. An elasto-plastic model represents better the behavior of parts in contact. It can also be interesting of finding a way to include the bulk deformation and not only the local one for some specific contact configurations.

This work highlights the importance of future developments in contact modeling within CAT systems, particularly the need to incorporate stabilization criteria, friction models, and elastic behavior. These enhancements will provide a more comprehensive understanding of contact interactions, particularly in non-ideal conditions, allowing for more realistic simulations. As these aspects are integrated, CAT systems will be better equipped to handle complex mechanical interactions, leading to more informed tolerance analysis and allocation, and improved product performance.

It is important to keep updating PolitoCAT and Politopix with the new methods and objects. The current version of PolitoCAT can be freely downloaded online. For more information see Appendix II. The following stage for PolitoCAT concerns the incorporation of stochastic tools for conducting statistical tolerance analysis and allocation within the software.

References

[OFF] Object File Format (.off).

[2] 10303-11, I. S. O. (2004). ISO 10303-11:2004 - Industrial automation systems and integration - Product data representation and exchange - Part 11: Description methods: The EXPRESS language reference manual.

[3] Ahmad, O. (2013). Stochastic representation and analysis of rough surface topography by random fields and integral geometry-Application to the UHMWPE cup involved in total hip arthroplasty.

[4] Alex, B., Antoine, J., and Philippe, D. (2010). Experimental evaluation of convex difference surface for planar joint study.

[5] Alhir, S. S. (1998). *UML in a nutshell*. OReilly & Associates, CA, first edit edition.

[6] Allen, J. (2006). The Unicode Standard / the Unicode Consortium. *Unicode, Inc.*, 5:42.

[7] Allex Ballu, Jean-Yves Dantan, L. M. (2010). Geometric Tolerancing Languages Language of Tolerancing : GeoSpelling. In Francois Villeneuve, L. M., editor, *Geometric Tolerancing of Products*, chapter Chapter 2, pages 23–53. ISTE Ltd.

[8] Ameta, G., Serge, S., and Giordano, M. (2011). Comparison of spatial math models for tolerance analysis: Tolerance-maps, deviation domain, and TTRS. *Journal of Computing and Information Science in Engineering*, 11(2).

[9] Anitescu, M. and Potra, F. A. (1997). Formulating Dynamic Multi-Rigid-Body Contact Problems with Friction as Solvable Linear Complementarity Problems. *Nonlinear Dynamics*, 14(3):231–247.

[10] Anselmetti, B. (2006). Generation of functional tolerancing based on positioning features. *CAD Computer Aided Design*, 38(8):902–919.

[11] Anselmetti, B., Chavanne, R., Yang, J. X., and Anwer, N. (2010). Quick GPS: A new CAT system for single-part tolerancing. *CAD Computer Aided Design*, 42(9):768–780.

[12] Anwer, N., Ballu, A., and Mathieu, L. (2013). The skin model, a comprehensive geometric model for engineering design. *CIRP Annals - Manufacturing Technology*, 62(1):143–146.

[13] Anwer, N., Schleich, B., Mathieu, L., and Wartzack, S. (2014). From solid modelling to skin model shapes: Shifting paradigms in computer-aided tolerancing. *CIRP Annals - Manufacturing Technology*, 63(1):137–140.

[14] Anwer, N. and Srinivasan, V. (2022). Towards a Mathematical Definition of Skin Model for Geometrical Product Specification and Verification and its Physical Interpretation. *Procedia CIRP*, 114:54–59.

[15] Armillotta, A. (2016). Tolerance Analysis Considering form Errors in Planar Datum Features. *Procedia CIRP*, 43:64–69.

[16] Arroyave-tobon, S. (2018). *Polyhedral models reduction in geometric tolerance analysis*. PhD thesis, Université de Bordeaux.

[17] Arroyave-Tobón, S., Teissandier, D., and Delos, V. (2017a). Tolerance Analysis with Polytopes in HV-Description. *Journal of Computing and Information Science in Engineering*, 17(4):1–9.

[18] Arroyave-Tobón, S., Teissandier, D., and Delos, V. (2017b). Tolerance Analysis with Polytopes in HV-Description. *Journal of Computing and Information Science in Engineering*, 17(4):1–9.

[19] ASME, A. S. M. E. (2019). ASME Y14.41 - Digital Product Definition Data Practices. *ASME Digital Standards*, page 128.

[20] Ballu, A., Mathieu, L., and Dantan, J. Y. (2015). Formal Language for GeoSpelling. *Journal of Computing and Information Science in Engineering*, 15(2):1–6.

[21] Baudin, M., Dutfoy, A., Looss, B., and Popelin, A. L. (2017). OpenTURNS: An industrial software for uncertainty quantification in simulation. *Handbook of Uncertainty Quantification*, pages 2001–2038.

[22] Bénière, R., Subsol, G., Gesquière, G., Le Breton, F., and Puech, W. (2011). Recovering primitives in 3D CAD meshes. *Three-Dimensional Imaging, Interaction, and Measurement*, 7864:78640R.

[23] Bénière, R., Subsol, G., Gesquière, G., Le Breton, F., and Puech, W. (2013). A comprehensive process of reverse engineering from 3D meshes to CAD models. *CAD Computer Aided Design*, 45(11):1382–1393.

[24] Biasotti, S., De Floriani, L., Falcidieno, B., Frosini, P., Giorgi, D., Landi, C., Papaleo, L., and Spagnuolo, M. (2008). Describing shapes by geometrical-topological properties of real functions. *ACM Computing Surveys*, 40(4).

[25] Bickel, S., Schleich, B., and Wartzack, S. (2023). A Novel Shape Retrieval Method for 3D Mechanical Components Based on Object Projection, Pre-Trained Deep Learning Models and Autoencoder. *CAD Computer Aided Design*, 154:103417.

[26] Borst, W. (1997). *Construction of Engineering Ontologies*. PhD thesis.

[27] Borsuk, K. and Dydak, J. (1980). What is the theory of shape? *Bulletin of the Australian Mathematical Society*, 22(2):161–198.

[28] Botsch, M. and Sorkine, O. (2008). On linear variational surface deformation methods. *IEEE Transactions on Visualization and Computer Graphics*, 14(1):213–230.

[29] Bourdet, P. (1987). *Contribution à la mesure tridimensionnelle : Modèle d ' identification géométrique des surfaces , Métrologie fonctionnelle des pièces mécaniques , Correction géométrique des machines à ...* PhD thesis, Université de Nancy.

[30] Boyer, M. and Stewart, N. F. (1991). Modeling spaces for toleranced objects. *International Journal of Robotics Research*, 10(5):570–582.

[31] Bruno Siciliano, O. K. (2008). *Springer Handbook of Robotics*. Springer Berlin Heidelberg.

[32] Cai, N. and Qiao, L. (2016). Rigid-compliant hybrid variation modeling of sheet metal assembly with 3D generic free surface. *Journal of Manufacturing Systems*, 41:45–64.

[33] Cammarata, A. (2017). A novel method to determine position and orientation errors in clearance-affected overconstrained mechanisms. *Mechanism and Machine Theory*, 118:247–264.

[34] Chen, H., Jin, S., Li, Z., and Lai, X. (2014). A comprehensive study of three dimensional tolerance analysis methods. *CAD Computer Aided Design*, 53:1–13.

[35] Clozel, P. and Rance, P. A. (2013). MECAmaster: A Tool for Assembly Simulation from Early Design, Industrial Approach. *Geometric Tolerancing of Products*, pages 241–273.

[36] Davidson, J. K., Mujezinović, A., and Shah, J. J. (2002). A new mathematical model for geometric tolerances as applied to round faces. *Journal of Mechanical Design, Transactions of the ASME*, 124(4):609–622.

[37] Delos, V. (2024). politopix - I2M - Institut de mécanique et d'ingénierie.

[38] Delos, V., Teissandier, D., Malyshev, A., Nuel, G., and García, S. C. (2021). Polyhedral-based Modeling and Algorithms for Tolerancing Analysis. *CAD Computer Aided Design*, 141:103071.

[39] Deng, J. and Deng, S. (2002). The adaptive branch and bound method of tolerance synthesis based on the reliability index. *International Journal of Advanced Manufacturing Technology*, 20(3):190–200.

[40] Desrochers, A. and Clément, A. (1994). A dimensioning and tolerancing assistance model for CAD/CAM systems. *The International Journal of Advanced Manufacturing Technology*, 9(6):352–361.

[41] Dumas, A. (2015). *Développement de méthodes probabilistes pour l ' analyse des tolérances des systèmes mécaniques sur-contraints To cite this version : HAL Id : tel-01177079*. PhD thesis, Ecole National Superieur d'Arts et Métiers.

[42] Falgarone, H., Thiébaut, F., Coloos, J., and Mathieu, L. (2016). Variation Simulation during Assembly of Non-rigid Components. Realistic Assembly Simulation with ANATOLEFLEX Software. *Procedia CIRP*, 43:202–207.

[43] Fenves, S. J. (2001). A Core Product Model for Representing Design Information, NISTIR 6736. *NISTIR 6736*, (January 2001).

[44] Fenves, S. J., Foufou, S., Bock, C., and Sriram, R. D. (2008). CPM2: A core model for product data. *Journal of Computing and Information Science in Engineering*, 8(1):0145011–0145016.

[45] Fiorentini, X., Gambino, I., Liang, V.-C., Sudarsan, R., Mani, M., and Bock, C. (2007). An Ontology for Assembly Representation. *Nistir 7436*, page 76.

[46] Fischer, B. R. (2011). Mechanical Tolerance Stackup and Analysis. *Mechanical Tolerance Stackup and Analysis*.

[47] Franciosa, P., Gerbino, S., and Patalano, S. (2011). Simulation of variational compliant assemblies with shape errors based on morphing mesh approach. *International Journal of Advanced Manufacturing Technology*, 53(1-4):47–61.

[48] Frère, L., Royer, M., and J., F. (2018). Tolerance analysis using a Computer Aided Tolerancing Software:ANATOLE 3D. In *Procedia CIRP*, volume 72, pages 622–628.

[49] Gain, J. and Bechmann, D. (2008). A survey of spatial deformation from a user-centered perspective. *ACM Transactions on Graphics*, 27(4):1–36.

[50] Gallucci, A., Znamenskiy, D., Long, Y., Pezzotti, N., and Petkovic, M. (2023). Generating High-Resolution 3D Faces and Bodies Using VQ-VAE-2 with PixelSNAIL Networks on 2D Representations. *Sensors*, 23(3).

[51] Gao, J., Chase, K. W., and Magleby, S. P. (1998). Generalized 3-D tolerance analysis of mechanical assemblies with small kinematic adjustments. *IIE Transactions (Institute of Industrial Engineers)*, 30(4):367–377.

[52] Gaunet, D. (2003). 3D Functional Tolerancing & Annotation: CATIA tools for Geometrical Product Specification. *Geometric Product Specification and Verification: Integration of Functionality*, pages 25–33.

[53] Geo-Ry Tang, Fuh, Y. M., and Kung, R. (1993). A list approach to tolerance charting. *Computers in Industry*, 22(3):291–302.

[54] Giordano, M., Samper, S., and Petit, J. P. (2007). Tolerance analysis and synthesis by means of deviation domains, axi-symmetric cases. *Models for Computer Aided Tolerancing in Design and Manufacturing - Selected Conference Papers from the 9th CIRP International Seminar on Computer-Aided Tolerancing, CAT 2005*, pages 85–94.

[55] Goka, E. (2019). *Analyse des tolérances des systèmes complexes*. PhD thesis, Ecole National Supérieur d'Arts et Métiers.

[56] Gómez, S. C. G. (2024). *Geometrical tolerance allocation and optimization using the prismatic polyhedral approach To cite this version : HAL Id : tel-04501194*. PhD thesis, University of Bordeaux.

[57] Gouyou, D., Teissandier, D., Delos, V., and Ledoux, Y. (2020). Statistical tolerance analysis applied on overconstrained mechanisms with form deviations. *Journal of Computational Design and Engineering*, 7(3):308–322.

[58] Grandjean, J. (2014). Influence des défauts de forme sur les performances d ' assemblages : application aux prothèses totales de hanche To cite this version : HAL Id : tel-00944735 Influence des défauts de forme sur les performances d ' assemblages Application aux prothèses to.

[59] Grandjean, J., Ledoux, Y., and Samper, S. (2013). On the role of form defects in assemblies subject to local deformations and mechanical loads. *International Journal of Advanced Manufacturing Technology*, 65(9-12):1769–1778.

[60] Gupta, S. and Turner, J. U. (1993). Variational Solid Modeling. *IEEE Computer Graphics and Applications*, pages 64–74.

[61] Hallmann, M., Schleich, B., and Wartzack, S. (2020). *From tolerance allocation to tolerance-cost optimization: a comprehensive literature review*, volume 107. The International Journal of Advanced Manufacturing Technology.

[62] Hibbeler, R. (2011). *Mechanics of Materials*, volume 8.

[63] Homri, L., Goka, E., Levasseur, G., and Dantan, J. Y. (2017). Tolerance analysis - Form defects modeling and simulation by modal decomposition and optimization. *CAD Computer Aided Design*, 91:46–59.

[64] Homri, L., Teissandier, D., and Ballu, A. (2015). Tolerance analysis by polytopes: Taking into account degrees of freedom with cap half-spaces. *CAD Computer Aided Design*, 62:112–130.

[65] Huang, W. and Ceglarek, D. (2002). Mode-based Decomposition of Part Form Error by Discrete-Cosine-Transform with. *CIRP Annals - Manufacturing Technology*, 51(1).

[66] ISO-17450-1 (2011). BSI Standards Publication Geometrical product specifications (GPS). General concepts Part 1: Model for geometrical specification.

[67] ISO-17450-2 (2012). BSI Standards Publication Geometrical product specifications (GPS) - General concepts. *ISO*.

[68] ISO14638:2015 (2015). Geoemtrical product specification (GPS) - Matrix model. *ISO*.

[69] ISO/IEC (1998). ISO/IEC JTC 1/SC 34 - Document description and processing languages. Technical report, ISO.

[70] Kendall, D. G. (1984). Shape manifolds, procrustean metrics, and complex projective spaces. *Bulletin of the London Mathematical Society*, 16(2):81–121.

[71] Kettner, L. (1999). Using generic programming for designing a data structure for polyhedral surfaces. *Computational Geometry: Theory and Applications*, 13(1):65–90.

[72] Konkar, R. and Cutkosky, M. (1995). Incremental Kinematic Analysis of Mechanisms. *Journal of Mechanical Design*, 117(4):589–596.

[73] Lan, H. and Venkatesh, T. A. (2014). On the relationships between hardness and the elastic and plastic properties of isotropic power-law hardening materials. *Philosophical Magazine*, 94(1):35–55.

[74] Landon, Y., Lacombe, A., Kamgaing Souop, L. A., Daidié, A., Paredes, M., Benaben, A., and Chirol, C. (2023). Correlations Between the Hole Surface Integrity and Fatigue Life for Drilled 2024-T351 Aluminum Alloy. *Lecture Notes in Mechanical Engineering*, pages 1103–1114.

[75] Lê, H. N., Ledoux, Y., and Ballu, A. (2014). Experimental and theoretical investigations of mechanical joints with form defects. *Journal of Computing and Information Science in Engineering*, 14(4):1–10.

[76] Ledoux, Y., Samper, S., Grandjean, J., Talence, F., Savoie, P., Le, A., and Cedex, V. (2016). Integrating form defects of mechanical joints into the tolerance studies 2 Tolerancing And Form Surface Defects 3 Local Defect Characterization 4 Influence of Form Defects into relative position of surfaces. In *Adavances in mathematics and computer science and their applications*, volume 3, pages 84–89, Venice, Italy. WSEAS.

[77] Leirmo, T. L., Semeniuta, O., Baturynska, I., and Martinsen, K. (2020). Extracting shape features from a surface mesh using geometric reasoning. *Procedia CIRP*, 93:544–549.

[78] Liao, X. and Wang, G. G. (2007). Non-linear dimensional variation analysis for sheet metal assemblies by contact modeling. *Finite Elements in Analysis and Design*, 44(1-2):34–44.

[79] Liu, J., Zhang, Z., Ding, X., and Shao, N. (2018). Integrating form errors and local surface deformations into tolerance analysis based on skin model shapes and a boundary element method. *CAD Computer Aided Design*, 104:45–59.

[80] Lynch, Kevin; Park, F. (2017). *Modern Robotics: Mechanics, Planning, and Control*. Cambridge University Press.

[81] MacHado, M., Moreira, P., Flores, P., and Lankarani, H. M. (2012). Compliant contact force models in multibody dynamics: Evolution of the Hertz contact theory. *Mechanism and Machine Theory*, 53:99–121.

[82] Mansuy, M., Giordano, M., and Davidson, J. K. (2013). Comparison of two similar mathematical models for tolerance analysis: T-map and deviation domain. *Journal of Mechanical Design, Transactions of the ASME*, 135(10):1–7.

[83] Martinsen, K. and Kojima, T. (1997). EXPRESS definition of Vectorial Tolerancing in product modelling. *Information Infrastructure Systems for Manufacturing*, pages 313–324.

[84] Mawussi, K. and Anwer, N. (2004). Tolerance specification data model for design and manufacturing. *Integrated design and manufacturing in mechanical engineering (IDMME2004)*, (April).

[85] Mazur, M., Leary, M., and Subic, A. (2011). Computer Aided Tolerancing (CAT) platform for the design of assemblies under external and internal forces. *CAD Computer Aided Design*, 43(6):707–719.

[86] Mikael, R., Ann-Christine, F., Lars, L., and Rikard, S. (2016). Variation Analysis Considering Manual Assembly Complexity in a CAT Tool. *Procedia CIRP*, 43:94–99.

[87] Nackman, L. R. and Pizer, S. M. (1985). THREE-DIMENSIONAL SHAPE DESCRIPTION USING THE SYMMETRIC AXIS TRANSFORM I: THEORY. *IEEE Transactions on Pattern Analysis and Machine Intelligence*, PAMI-7(2):187–202.

[88] Niu, K. and Tian, C. (2022). Zernike polynomials and their applications. *Journal of Optics (United Kingdom)*, 24(12).

[89] OWL Working Group (2012). OWL - Semantic Web Standards.

[90] Pasupathy, T. M., Morse, E. P., and Wilhelm, R. G. (2003). A survey of mathematical methods for the construction of geometric tolerance zones. *Journal of Computing and Information Science in Engineering*, 3(1):64–75.

[91] Pichon, G., Daidié, A., Paroissien, E., and Benaben, A. (2023). Quasi-static strength and fatigue life of aerospace hole-to-hole bolted joints. *Engineering Failure Analysis*, 143(August 2022).

[92] Pierre, L., Rouetbi, O., and Anselmetti, B. (2018). Tolerance analysis of hyperstatic mechanical systems with deformations. *Procedia CIRP*, 75(March):244–249.

[93] Pierre, L., Teissandier, D., and Nadeau, J. P. (2014). Variational tolerancing analysis taking thermomechanical strains into account: Application to a high pressure turbine. *Mechanism and Machine Theory*, 74:82–101.

[94] Polini, W. (2011). Geometric Tolerance Analysis. In Colosimo, B. M. and Senin, N., editors, *Geometric Tolerances: Impact on Product Design, Quality Inspection and Statistical Process Monitoring*, pages 39–68. Springer London.

[95] Qie, Y. and Anwer, N. (2022). Geometric deviation modeling for single surface tolerancing using Laplace-Beltrami Operator. *Procedia CIRP*, 114(March):19–24.

[96] Qin, Y., Qi, Q., Lu, W., Liu, X., Scott, P. J., and Jiang, X. (2018). A review of representation models of tolerance information. *International Journal of Advanced Manufacturing Technology*, 95(5-8):2193–2206.

[97] Rabemananjara, L., Hernot, X., Mauvoisin, G., Gavrus, A., and Collin, J. M. (2015). Formulation of a representative plastic strain and representative plastic strain rate by using a conical indentation on a rigid visco-plastic material. *Materials and Design*, 68:207–214.

[98] Rachuri, S., Han, Y. H., Feng, S. C., Wang, F., Sriram, R. D., Lyons, K. W., and Roy, U. (2003). Object-oriented representation of electro-mechanical assemblies using UML. *Proceedings of the IEEE International Symposium on Assembly and Task Planning*, 2003-Janua(May 2014):228–234.

[99] Rameau, J. F., Serré, P., and Moinet, M. (2018). Clearance vs. tolerance for rigid overconstrained assemblies. *CAD Computer Aided Design*, 97:27–40.

[100] RDnT (2024). The tool RDnT - RDnT Technology.

[101] Requicha, A. A. (1983). Toward a Theory of Geometric Tolerancing. *The International Journal of Robotics Research*, 2(4):45–60.

[102] Requicha, A. A. and Chan, S. C. (1986). Representation of Geometric Features, Tolerances, and Attributes in Solid Modelers Based on Constructive Geometry. *IEEE Journal on Robotics and Automation*, 2(3):156–166.

[103] Requicha, A. G. (1980). Representations for Rigid Solids: Theory, Methods, and Systems. *ACM Computing Surveys (CSUR)*, 12(4):437–464.

[104] Restrepo Garcia, C. A., Teissandier, D., Anwer, N., Delos, V., Ledoux, Y., and Pierre, L. (2022). An integrated open source CAT based on Skin Model Shapes. In *17th CIRP Conference on Computer Aided Tolerancing*, volume 114, pages 1–6. Elsevier B.V.

[105] Reuter, M., Wolter, F. E., and Peinecke, N. (2006). Laplace-Beltrami spectra as 'Shape-DNA' of surfaces and solids. *CAD Computer Aided Design*, 38(4):342–366.

[106] Roman, D., Keller, U., Lausen, H., De Bruijn, J., Lara, R., Stollberg, M., Polleres, A., Feier, C., Bussler, C., and Fensel, D. (2011). Web Service Modeling Ontology. *Applied Ontology*, 1:107–129.

[107] Romero, F., Rosado, P., and Bruscas, G. M. (2015). Application Feature Model for Geometrical Specification of Assemblies. *Procedia Engineering*, 132(2):1128–1135.

[108] Rong, G., Cao, Y., and Guo, X. (2008). Spectral Surface Deformation with Dual Mesh. *Proceedings of International Conference on Computer Animation and Social Agents (CASA 2008)*, pages 17–24.

[109] Rossignac, J. R. and Requicha, A. A. (1986). Offsetting operations in solid modelling. *Computer Aided Geometric Design*, 3(2):129–148.

[110] Rossignac, J. R. and Requicha, A. A. G. (1991). Constructive Non-Regularized Geometry. *Computer Aided Geometric Design*, 23(1):21–32.

[111] Roux, J., Samadi, S., Kuroiwa, E., Yoshiike, T., and Kheddar, A. (2021). Control of Humanoid in Multiple Fixed and Moving Unilateral Contacts. *2021 20th International Conference on Advanced Robotics, ICAR 2021*, pages 793–799.

[112] Roy, U., Liu, C. R., and Woo, T. C. (1991). Review of dimensioning and tolerancing: representation and processing. *Computer-Aided Design*, 23(7):466–483.

[113] Sa, G., Bai, H., Liu, Z., Liu, X., and Tan, J. (2023). A tolerance analysis method based on assembly deformation simulation with stable contact. *Robotic Intelligence and Automation*, (January).

[114] Salome, A. (2012). About SALOME Platform.

[115] Samper, S., Adragna, P. A., Favreliere, H., and Pillet, M. (2009). Modeling of 2D and 3D assemblies taking into account form errors of plane surfaces. *Journal of Computing and Information Science in Engineering*, 9(4):1–12.

[116] Samper, S. and Formosa, F. (2007). Form defects tolerancing by natural modes analysis. *Journal of Computing and Information Science in Engineering*, 7(1):44–51.

[117] Scarth, C., Adhikari, S., Cabral, P. H., Silva, G. H., and do Prado, A. P. (2019). Random field simulation over curved surfaces: Applications to computational structural mechanics. *Computer Methods in Applied Mechanics and Engineering*, 345:283–301.

[118] Schleich, B., Anwer, N., Mathieu, L., and Wartzack, S. (2014). Skin Model Shapes: A new paradigm shift for geometric variations modelling in mechanical engineering. *CAD Computer Aided Design*, 50:1–15.

[119] Schleich, B., Qie, Y., Wartzack, S., and Anwer, N. (2022). Generative adversarial networks for tolerance analysis. *CIRP Annals*, 71(1):133–136.

[120] Schleich, B., Walter, M., Wartzack, S., Anwer, N., and Mathieu, L. (2012). A comprehensive framework for Skin Model Simulation. In *Proceedings of the ASME 2012 11th Biennial Conference on Engineering Systems Design and Analysis ESDA2012*, Nantes.

[121] Schleich, B. and Wartzack, S. (2015). Approaches for the assembly simulation of skin model shapes. *CAD Computer Aided Design*, 65:18–33.

[122] Sethi, M., Banerjee, A., and Manna, B. (2023). Unilateral frictional contact between a rigid wheel traversing on a flexible beam: An analytical investigation. *Applied Mathematical Modelling*, 120:612–635.

[123] Shah, J. J., Ameta, G., Shen, Z., and Davidson, J. (2007). Navigating the Tolerance Analysis Maze. *Computer-Aided Design and Applications*, 4(5):705–718.

[124] Shao, N., Ding, X., and Liu, J. (2020a). Tolerance analysis of spur gears based on skin model shapes and a boundary element method. *Mechanism and Machine Theory*, 144.

[125] Shao, N., Liu., J., and Xiaoyu, D. (2020b). Effects of contact behaviors on tolerance analysis of mechanism based on skin model shapes and a boundary element method. In *CIRP CAT*. Elsevier B.V.

[126] Shen, Z., Ameta, G., Shah, J. J., and Davidson, J. K. (2005). A comparative study of tolerance analysis methods. *Journal of Computing and Information Science in Engineering*, 5(3):247–256.

[127] Siciliano, B. and Khatib, O. (2016). *Springer handbook of robotics*. Springer Berlin Heidelberg.

[128] Sigmund (2024). Sigmund Tolerance Analysis Software for SOLIDWORKS.

[129] Söderberg, R., Wärmefjord, K., and Lindkvist, L. (2015). Variation simulation of stress during assembly of composite parts. *CIRP Annals - Manufacturing Technology*, 64(1):17–20.

[130] Spyns, P., Meersman, R., and Jarrar, M. (2000). STAR Lab Technical Report Data Modelling versus Ontology Engineering Data modelling versus Ontology engineering. *Building*, 31(4).

[131] Srinivasan, V. and O'Connor, M. A. (1996). Towards an ISO Standard for Statistical Tolerancing. In *Computer-aided Tolerancing*, pages 159–172. Springer, Dordrecht.

[132] Strang, G. (1999). The discrete cosine transform. *SIAM Review*, 41(1):135–147.

[133] Stuppy, J. and Meerkamm, H. (2009). Tolerance Analysis of mechanism taking into account joints with clearance and elastic deformormations. *International conference on egineering design, ICED 2009*, pages 489–500.

[134] Systems Dassault (2024). 3DCS Variation Analyst | SOLIDWORKS.

[135] Teissandier, D., Couetard, Y., and Delos, V. (1999). Operations on polytopes: application to tolerance analysis. *Global Consistency of Tolerances*, pages 425–434.

[136] Vallet, C., Lasseux, D., Sainsot, P., and Zahouani, H. (2008). Numerical determination of sealing performance of a rough contact: Real versus synthetic fractal surfaces. *American Society of Mechanical Engineers, Pressure Vessels and Piping Division (Publication) PVP*, 2:91–100.

[137] Wirtz, A. (1988). Vektorielle Tolerierung zur Qualitätssteuerung in der mechanischen Fertigung. *CIRP Annals - Manufacturing Technology*, 37(1):493–498.

[138] Xu, X. and Nee, A. Y. C. (2009). *Advanced Design and Manufacturing Based on STEP*.

[139] Yan, X. and Ballu, A. (2018). Tolerance analysis using skin model shapes and linear complementarity conditions. *Journal of Manufacturing Systems*, 48(July):140–156.

[140] Yang, L., Cormican, K., and Yu, M. (2019). *Ontology-based systems engineering : A state-of-the-art review Computers in Industry Ontology-based systems engineering : A state-of-the-art review*. PhD thesis.

[141] Yang, T. H. and Jackman, J. (2000). Form error estimation using spatial statistics. *Journal of Manufacturing Science and Engineering, Transactions of the ASME*, 122(1):262–272.

[142] Yates, K. M. and Untaroiu, C. D. (2018). Finite element modeling of the human kidney for probabilistic occupant models: Statistical shape analysis and mesh morphing. *Journal of Biomechanics*, 74:50–56.

[143] Zhang, M. (2012). *Discrete shape modeling for geometrical product specification : contributions and applications to skin model simulation*. PhD thesis, ENS Paris-Saclay.

[144] Zhang, M., Anwer, N., Mathieu, L., and Zhao, H. B. (2011). A discrete geometry framework for geometrical product specifications. In *Proceedings of the 21st CIRP Design Conference, Korea 2011: Interdisciplinary Design*, volume 2, pages 142–148.

[145] Zhang, Z., Liu, J., Anwer, N., Pierre, L., and Shao, N. (2020). Integration of surface deformations into polytope-based tolerance analysis: Application to an over-constrained mechanism. *Procedia CIRP*, 92:21–26.

[146] Zhang, Z., Liu, J., Ding, X., and Shao, N. (2018). Tolerance analysis of annular surfaces considering form errors and local surface deformations. In *Procedia CIRP*, volume 75, pages 291–296. Elsevier B.V.

[147] Zhao, X., Kethara Pasupathy, T. M., and Wilhelm, R. G. (2006). Modeling and representation of geometric tolerances information in integrated measurement processes. *Computers in Industry*, 57(4):319–330.

[148] Ziegler, G. M. (2014). *Lectures on Polytopes*. Number 1.

Appendix A

Appendix A

Deviation modeling table

Type of method	Deviation method	Type of deviations	Stage	Advantages	Disadvantages	Ref
Morphing	Statistical Shape Analysis, Principal Component Analysis (PCA) and Mesh morphing	Systematic and random	Observation	It assumes the linearity in the reduction as it is based on PCA	Fast to find correspondence between a template and a target discrete geometries. The model can incoporate material properties	[142]
Morphing	Spectral mesh deformation linear variational methods	Systematic and random	Prediction	Robustness and ease of implementation; Great variety of methods	The linearization of nonlinear deformation problem might cause underestimation when large deformations occur	[108, 28, 47]
Morphing	Free-form deviation	Systematic and random	Both	Versatility, ease-of-use and efficiency; Use of continuous or discrete models	Closest point point parametrization, continuity surfaces issues; lacks of control over individual object vertices	[49]
Spectral	Laplace-beltrami operator (LBO)	Systematic and random	Both	It is isometry invariant; It is independent of the object's representation	Sensible to data noise	[95, 105]]
Spectral	Discrete Cosine Transformation	Systematic	Prediction	Deviations can be represented with only a subset of deviation modes; Independence of its coefficients	It defines a priori shape bases; it is not straightforward to use it on non-planar surfaces	[65, 132]

Type of method	Deviation method	Type of deviations	Stage	Advantages	Disadvantages	Ref
Spectral	Zernike polynomials	Systematic	Prediction	The polynomials are orthogonal over a unit circle; they have great correspondence relationships with optical aberrations	The shapes bases are adapted for disks (unit circle), it is not directly adapted for the other type of surfaces	[88, 146]
Spectral	Discrete Modal Decomposition of vibrating modes	Systematic	Both	For many cases it is possible to link the modes to technological process that generate the defects	It is dependant on the geometry; very sensible to discretization and boundary conditions; complex surfaces need specific bases	[116, 59, 63]
Machine Learning	Generative Adversial Networks	Both	AI	Low modelling effort; it is shape agnostic	The initial training time can high; many synthetic or real deviation patterns need to be fed to the model	[119]
Machine Learning	Variational Autoeconder (VAE)	Both	AI	Ability to generate new and diverse samples of geometric deviations based on the learned latent space. It can be directly applied on registered templates	They can sometimes generate shapes that are not physically feasible or that violate design constraints	[25, 50]

Table A.1 Deviation modeling methods for Skin Model Shapes - Advanatges and Disadvanatages

Appendix B

Appendix B

I Text file with parameters for deviation modeling in PolitoCAT: Example in Section f

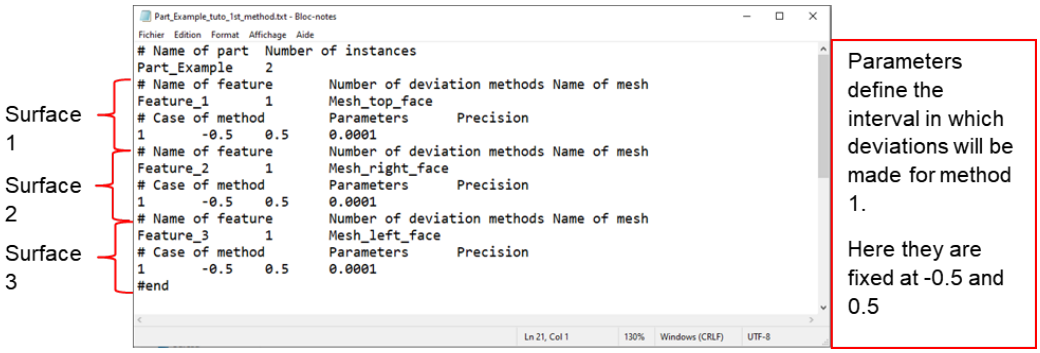

Fig. B.1 Example of text file with parameters

Text file with parameters for deviation modeling in PolitoCAT: Example contact modeling in Section b

Parameters planar feature modal decomposition:

1. Method number
2. The nodes of the planar square feature
3. The triangles of the planar square feature

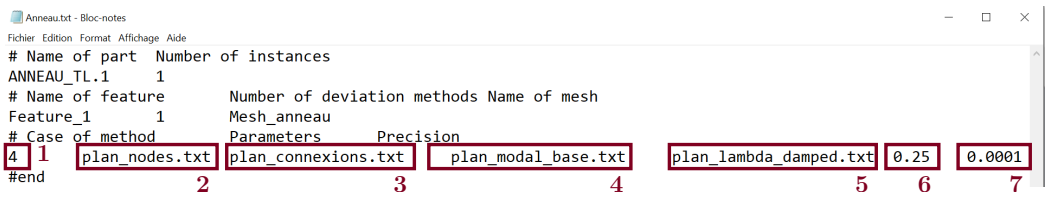

Fig. B.2 Example of text file with parameters

4. The modal base
5. The modal signature
6. An scaling factor for the generated deviations
7. Value for numerical precision

II PolitoCAT and project website

The website to download PolitoCAT v2.0.2 is accessible from the link below:

PolitoCAT and Politopix

The project's website can be accessible from the link below. It includes a summary of the project, the publications and its members.

AToPAd project